



NTNU – Trondheim
Norwegian University of
Science and Technology

Dynamic Analysis of the Bergsøysund Bridge in the Time Domain

Sindre Martin Hermstad

Civil and Environmental Engineering (2 year)

Submission date: June 2013

Supervisor: Ole Andre Øiseth, KT

Norwegian University of Science and Technology
Department of Structural Engineering



MASTER THESIS 2013

SUBJECT AREA: Structural Dynamics	DATE:10.06.2013	NO. OF PAGES: 160 20+110+30
--------------------------------------	-----------------	--------------------------------

TITLE:

Dynamic Analysis of the Bergsøysund Bridge in the Time Domain

Dynamisk analyse av Bergsøysundbrua i tidsplanet

BY:

Sindre Martin Hermstad



SUMMARY:The work has contributed to the assessment of the implementation of hydrodynamic effects in a nonlinear time domain analysis. Critical mechanisms like "snap through" can only emerge in analyses that consider geometric nonlinearities or the actual structure after completion, and are therefore essential for the development of new floating bridge concepts that ultimately can carry traffic over the Sognefjord. This master thesis considers the dynamic response in the time domain on the Bergsøysund Bridge, a 900 meters long pontoon bridge where the hydrodynamic wave action is the external force contributor, and where geometric nonlinearities and frequency dependent hydrodynamics can be studied.

The finite element model was firstly constructed in the Abaqus software interface as a part of my project assignment in my ninth semester, and is further developed in this thesis. The applied changes to the model are made to reduce computational time without reducing the credibility of the results; creating an effective and manageable model. The waterborne pontoons are modeled and simulated in DNV's software so hydrodynamic effects can be implemented in the comprehensive Abaqus time domain analysis.

A broad banded sea state is developed by estimating the spectral densities for a two dimensional space. The statistical waves are developed according to the recommended sea spectra from ITTC (International Towing Tank Conference). By combining a time domain wave pattern with transfer functions developed in Wadam, sea loads are extracted and considered in the Abaqus time series analysis. Hydrodynamic response is also evaluated incrementally in Abaqus by implementing software developed at NTNU.

The bridge response in time domain is then evaluated in the auto spectral domain. The results from the analysis in Abaqus suggest that the hydrodynamics caused by dynamic response are included and that the augmented FE-model is an effective and accurate representation of the real bridge. The combination of transfer function and sea spectra is also successfully implemented. Results from linear analyses are compared to Knut Andreas Kvåle's master thesis; Dynamic Analysis of the Bergsøysund Bridge in the Frequency Domain (Kut:2013:MasterJ). He has evaluated dynamic response in the frequency domain. The results were corresponding adequately and the use of the two methods together can be further investigated.

Keywords: Structural Dynamics, Time Domain, Floating Bridge, Pontoons, Hydrodynamics

RESPONSIBLE TEACHER: Ole Andre Øiseth

SUPERVISOR(S): Ole Andre Øiseth

CARRIED OUT AT: Department of Structural Engineering, NTNU

Institutt for konstruksjonsteknikk

FAKULTET FOR INGENIØRVITENSKAP OG TEKNOLOGI
NTNU – Norges teknisk-naturvitenskapelige universitet

MASTEROPPGAVE 2013

for

Sindre M Hermstad

Dynamisk analyse av Bergsøysundbrua i tidsplanet

Assessment of the dynamic response of the Bergsøysund Bridge in the time domain

I forbindelse med prosjektet ferjefri E39 skal Bergsøysundbrua instrumenteres for å kartlegge nøyaktigheten til de metodene som benyttes til å beregne dynamisk respons av slike konstruksjoner utsatt for naturlaster. Denne oppgaven dreier seg om å beregne responsen til brua i tidsplanet.

Oppgaven bør inneholde følgende temaer:

- Beregning av hydrodynamisk bolgelastlast, masse, demping og stivhet i DNV programmet Wadam.
- Videreutvikling av Abaqusmodellen som ble laget i prosjektoppgaven.
- Beregne systemets egenfrekvenser, svingeformer og dempingsforhold når hydrodynamiske effekter er tatt hensyn til.
- Simulering av bolgelaster.
- Beregning av respons i tidsplanet.

Besvarelsen organiseres i henhold til gjeldende retningslinjer.

Veilederte): Ole Andre Oiseth

Besvarelsen skal leveres til Institutt for konstruksjonsteknikk innen 10. juni 2013.

NTNU, 14. januar, 2013

Ole Andre Oiseth
faglærer

Abstract

The work has contributed to the assessment of the implementation of hydrodynamic effects in a nonlinear time domain analysis. Critical mechanisms like “snap through” can only emerge in analyses that consider geometric nonlinearities or the actual structure after completion, and are therefore essential for the development of new floating bridge concepts that ultimately can carry traffic over the Sognefjord. This master thesis considers the dynamic response in the time domain on the Bergsøysund Bridge, a 900 meters long pontoon bridge where the hydrodynamic wave action is the external force contributor, and where geometric nonlinearities and frequency dependent hydrodynamics can be studied.

The finite element model was firstly constructed in the Abaqus software interface as a part of my project assignment in my ninth semester, and is further developed in this thesis. The applied changes to the model are made to reduce computational time without reducing the credibility of the results; creating an effective and manageable model. The waterborne pontoons are modeled and simulated in DNV’s software so hydrodynamic effects can be implemented in the comprehensive Abaqus time domain analysis.

A broad banded sea state is developed by estimating the spectral densities for a two dimensional space. The statistical waves are developed according to the recommended sea spectra from ITTC (International Towing Tank Conference). By combining a time domain wave pattern with transfer functions developed in Wadam, sea loads are extracted and considered in the Abaqus time series analysis. Hydrodynamic response is also evaluated incrementally in Abaqus by implementing software developed at NTNU.

The bridge response in time domain is then evaluated in the auto spectral domain. The results from the analysis in Abaqus suggest that the hydrodynamics caused by dynamic response are included and that the augmented FE-model is an effective and accurate representation of the real bridge. The combination of transfer function and sea spectra is also successfully implemented. Results from linear analyses are compared to Knut Andreas Kvåle’s master thesis; Dynamic Analysis of the Bergsøysund Bridge

in the Frequency Domain [11]. He has evaluated dynamic response in the frequency domain. The results were corresponding adequately and the use of the two methods together can be further investigated.

Sammendrag

Masteroppgaven tar for seg den dynamiske responsen i tidsdomenet og frekvensdomenet på Bergsøysundsbrua, en 932 meter lang flytebro, hvor sjølastene er den eksterne lastbidragsyteren. Elementmodellen som er brukt, ble først utviklet i det omfattende elementprogrammet Abaqus som en del av prosjektoppgaven i mitt 9. semester ved NTNU.

I oppstartsfasen av masteroppgaven ble den tidligere modellen videreutviklet. Endringene som ble tilført modellen var for å oppnå en beregningseffektiv modell som fortsatt gir nøyaktige resultater. De viktigste endringene har vært å bytte ut pongtonggeometrien bestående av skallelementer, med enkeltelementer som kan ta for seg alle tregheter. Elementtettheten er blitt redusert, og skall-elementene som beskriver ståldekket har blitt erstattet med bjelke-elementer. Skrittlengdene i tidsdomeneanalysen er også blitt revudert. Ved å gjennomføre disse endringene har modellen blitt beregningsmessig effektiv, og dynamisk implisitte tidsdomeneanalyser har utviklet seg til å bli en effektiv måte å studere den dynamiske responsen i systemet.

Pongtonggeometrien som er utviklet i Abaqus har blitt konvertert til panel -element -modeller i Genie programvare, og videre blitt analysert i Wadam-program-varen som er en del av Det Norske Veritas' HydroD programvarepakke. Fra Wadam har frekvensavhengige effekter blitt hentet ut og senere implementert i Abaqus-analysen. Effekter grunnet struktur-vann-interaksjon som er tatt stilling til er tilleggsmasse og tilleggsdempning, samt opprettholdende stivheter. Overføringsfunksjoner som brukes for å utvikle lasttidsserier er utviklet fra de samme Wadam-resultatene.

Bredbåndet sjøtilstand er blitt utviklet ved å beregne spektraltetthetene for et todimensjonalt rom. De stokastiske bølgene er utviklet i henhold til sjøspektra fra IITC (International Towing Tank Conference). Ved å kombinere bølgestrukturen med transferfunksjoner generert fra utdata fra Wadam kan sjølaster utvikles ved hjelp av en Monte Carlo simulering. Tidsavhengige lastserier kan videre implementeres i Abaqus sin tidsdomeneanalyse. Tidsdomeneanalysen var vellykket og aspekter ved hydrody-

namikken som er nevnt over ble inkludert. Det er også blitt utført enkelte sammenligninger med Knut Andreas Kvåles resultater. Han har utført frekvensdomeneanalyse av den samme brua med like forutsetninger i sin masteroppgave; Dynamisk analyse av Bergsøysundsbrua i frekvensdomenet [11]. Hvit støy ble brukt og resultatene samsvarte.

Preface

This thesis is written as my concluding assignment for my masters education at NTNU for the department of Structural Mechanics. The thesis counts for 30 credits, and is finalized at the end of the spring semester, before the 10th of June 2013.

An understanding of the hydrodynamic aspects of a floating bridge analysis has been developed personally. Both the development of a relevant and realistic sea state, and the approximation of frequency dependent effects caused by the interaction between vessel and liquid have been implemented in a finite element model, where a time domain solution has been extracted and commented on.

I want to thank Associate Professor Ole Andre Øiseth for excellent guidance throughout both my project assignment and my master thesis. Professor Ragnar Sigbjörnsson has also been a tremendous help and inspiration when helping me with the development of a proper sea state and helping me to grasp basic concepts in Marine Engineering. Support from Abdillah Suyuthi regarding the Wadam analysis has also been helpful. I finally want to thank Knut Andreas Kvåle for the collaboration and the like-minded optimistic and persistent attitude towards our work all the way to the end.

Trondheim, June 2013

Sindre Martin Hermstad

Contents

I	Literature Review	3
1	Bridge description	5
1.1	The Bergsøysund Bridge	5
1.2	Structure Description	5
1.3	Assignment Description	8
2	Hydrodynamic and Hydrostatic Effects	9
2.1	Wave Action Simulation	12
2.2	Monte Carlo Simulation of the Sea State	17
2.3	White noise	20
2.4	Hydrostatic Properties	21
3	Analysis tools	23
3.1	Wadam	23
3.2	Abaqus CAE	27
3.3	Cross-X	36

4	Signal processing	37
4.1	Fast Fourier Transform	37
4.2	Welch's Method	38
4.3	Histogramical Presentation	38
II	Bridge Action Modeling	39
5	Pontoon Modeling	41
5.1	Genie	44
5.2	HydroD and Wadam	44
6	Wave Pattern and Stochastic Forces	47
7	Abaqus model	49
7.1	Earlier Model	49
7.2	Numerical Analysis	50
7.3	Structure	52
7.4	Pontoon Connectors	56
7.5	Boundary Conditions	58
7.6	Combination of Input Data	59
III	Experimental Design	61
8	Pre-analysis Considerations	63
8.1	Water Level	63
8.2	Cross-X	64

9	Analysis Considerations	67
9.1	Damping	68
9.2	Mesh Seeding	70
9.3	Time Domain Analysis	70
9.4	Nonlinearities	73
9.5	Differences in the Direct Implicit Method	74
IV	Computational Results, Discussion and Conclusion	77
10	Results	79
10.1	Wadam Results	81
10.2	Eigenfrequency and Eigenmode Results	85
10.3	Time Domain Results	88
11	Discussion	99
11.1	Wadam Discussion	99
11.2	Wave Action Discussion	100
11.3	Abaqus Time Domain Analysis Discussion	101
12	Conclusions	105
13	Further Work and Source of Error	107
	Bibliography	109

V	Appendix	111
A	Comparison of Sea Loads	113
B	Steel structure	115
C	Concrete structure	125
D	Matlab scripts	129
	D.1 AddedMassAndDampingAbaqus.m	129
E	Wadam extracts	132
	E.1 Scripts used in Abaqus	139

List of Figures

1.1	Pictures of location	6
1.2	Bridge geometry presented as a FE-model	7
1.3	Simplified conceptual illustration	7
2.1	Vessel motion description	9
2.2	ISSC wave spectra with directional distribution	15
2.3	Forces transferred to the global system	19
3.1	Two-dimensional panel model	25
3.2	Example of added mass plot	30
3.3	Bridge deck design	36
4.1	Complete FE-model of the Bergsøysund Bridge	40
5.1	Pontoon numbering	41
5.2	The development of the Panel model analysis	43
5.3	Loading conditions for Pontoon 2 to 6	44
6.1	Wave action for one point	48
7.1	Seeding, west end of bridge	51

7.2	Coordinate system	52
7.3	Profile illustration	53
7.4	Bridge assembly of floor beams	54
7.5	Wire tool	54
7.6	Frame work, x-y-plane	55
7.7	Pontoon connection	57
7.9	Boundary conditions in Abaqus	58
8.1	Cross-X example: σ_x due to M_y	64
8.2	Implementation of the simplified bridge deck	65
9.1	Illustrative presentation of α and β calculations	68
9.2	Demonstration of time step influenced results	72
9.3	Nonlinear effects and linear effects compared, time domain	73
9.4	Nonlinear effects and linear effects compared for pontoon five, spectral density	74
9.5	Direct implicit method with default and recommended setting	76
10.1	Pontoon numbering	80
10.2	Added Mass	82
10.3	Added Damping	83
10.4	Transfer function	84
10.5	Time series, pontoon 1, y-direction	89
10.6	Snapshots from time series animation in the x-y-plane. Color coding describes displacements	90
10.7	Histogram representation of displacements	91
10.8	Auto Spectral Densities, Pontoon four	93

10.9 Auto Spectral Densities, Pontoon two	94
10.10 All Auto Spectral Densities regarding displacement	95
10.11 Presentation of covariance, pontoon two and six	96
10.12 Auto Spectral Density of displacement	98
11.1 Spectral Density and Eigenfrequencies, Pontoon 4, sway	102

List of Tables

5.1	Pontoon properties	42
7.1	Steel Properties	53
7.2	Material and cross-sectional properties	56
8.1	Cross-sectional properties for the bridge deck	64
9.1	Rayleigh Damping Coefficients	68
9.2	Analysis description	71
9.3	Computational time	74
10.1	Eigenfrequencies and Eigenmodes	86
10.2	Additional Eigenfrequencies and Eigenmodes	87
10.3	Displacement variance for time series	92
10.4	Values used for white noise	97
10.5	Percentage difference between time domain and frequency domain analysis	97

Introduction

Even though the Bergsøysund Bridge was built more than 20 years ago, it's structure is of current interest. As of today there are only two pontoon bridges in Norway; the Bergsøysund Bridge and the Nordhordland Bridge. As Coastal Highway Route E39 is being planned, new pontoon bridges are considered. The longest span along E39 is the Sogne Fjord which might be crossed by a pontoon bridge in the future. The issues that need to be resolved regarding bridges over wide and deep fjords today was resolved with a pontoon bridge over the entrance to the Tingvoll Fjord. It is therefore interesting to study the credibility of a dynamic time series analysis for the Bergsøysund Bridge. The results can be of further interest when developing new bridge concepts in the near future. The process of obtaining time domain solutions is computationally demanding for big systems with a great number of degrees of freedom. This kind of analysis is made possible due to the recent development in computer calculation capacity.

This thesis considers the dynamic response in the time domain on the Bergsøysund Bridge, where the hydrodynamic wave action is the external force contributor. The finite element model was first developed as a part of my earlier project assignment with the Abaqus software interface, and is further developed in this assignment. The applied changes are made to reduce computational time, creating an effective and manageable model. The waterborne pontoons are modeled in DNV's genie software and simulated in the Wadam software so hydrodynamic frequency dependent effects are submitted.

The external forces are further improved from the project assignment. The stochastic waves are developed according to the recommended sea spectrum from ITTC (International Towing Tank Conference) [7]. The spacial solution for the wave action forces

creates a model where directional distribution in an angular spectrum and lagged coherence between forces applied to the pontoons yield more realistic results. The bridge excitation is evaluated in the time domain and auto spectral domain.

Part I

Literature Review

Chapter 1

Bridge description

1.1 The Bergsøysund Bridge

The Bergsøysund Bridge was built in 1992 as a part of the mainland connection for Kristiansund and is a part of state highway 70 and European highway 39. The bridge is located in Møre og Romsdal, between Aspøya and Bergsøya, which are two islands separated by the 900 meters wide Tynfjord. The bridge is 930 meters long, about 12 meters wide and has a horizontal radius of 1300 meters. The longest bridge span between pontoon bearings is 106 meters and the water clearance is about 6 meters.

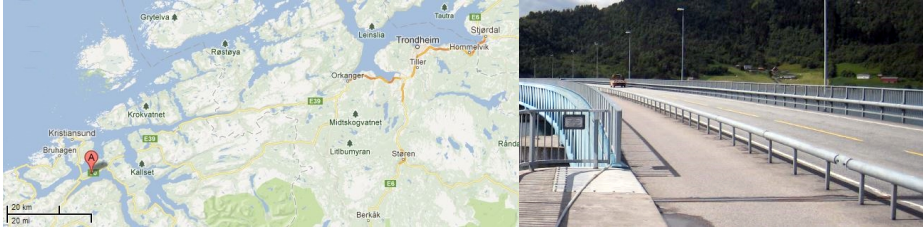
The daily bridge crossing traffic is traveling on a two lane road and on a sidewalk separated by a fence. The structure can be considered a truss work bridge that is lifted by seven light concrete pontoons. At the time it was built, it was the only floating bridge that was constructed without sideways anchorage. Because of the unique solution the bridge was scheduled as a historical monument which represents the progress of the Norwegian road network.

1.2 Structure Description

The Bergsøysund Bridge is a typical floating pontoon bridge which utilizes the buoyancy from the water beneath. The bridge was constructed in this way, because the



(a) Photo of the finished Bergsøysund Bridge



(b) Map of the position of the Bergsøysund Bridge

(c) Road lanes

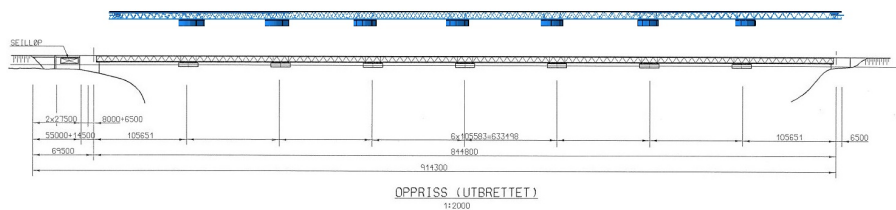
Figure 1.1: Pictures of location

fjord width was too wide for a suspension bridge, and too deep for multiple foundations.

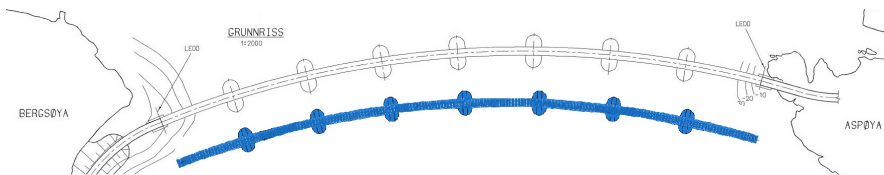
The required buoyancy can be achieved in a number of different ways, but the Bergsøysund Bridge is floating on seven light concrete pontoons. The cumulative force is sufficient for the bridge to be lifted in the vertical plane. Movement in the horizontal plane will be restricted by anchorage in the bridge endings, the stiffening bow shape and the restoring forces from the pontoons due to the water masses surrounding them.

The bridge is not anchored sideways along the bridge floor. Because of the lack of anchorage were snap through issues discussed in the initial bridge design phase. After 21 years at sea corrosion has been the main problem due to the constant presence of salt water inflection.

The bridge will experience movement along the bridge way due to the lack of sideways anchorage. The bow shaped bridge way stiffens and therefore lessen these effects, but effects will still be present. The bridge movement is possible and highly likely on the basis of hydro dynamic and wind dynamic loads. Traffic loads are also considerable due to the lack of sea bed infrastructure. The wind dynamic loads and traffic loads are neglected for this thesis.



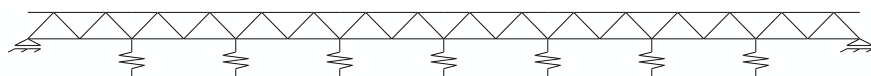
(a) Horizontal view



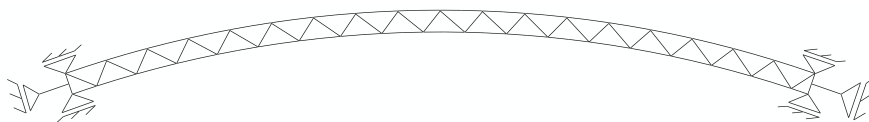
(b) Vertical view

Figure 1.2: Bridge geometry presented as a FE-model

The free spans between each of the seven pontoons and the anchorage are 106 meters at its most, and the truss work is required for the bridge to remain straight. Conceptually, the bridge is a freely supported beam with seven spring bearings and two stiff bearings in the horizontal plane and a fixed beam with two anchors in the vertical plane.



(a) vertical plane



(b) horizontal plane

Figure 1.3: Simplified conceptual illustration

1.3 Assignment Description

The thesis will explore the possibilities of simulating the dynamic response in the time domain for the Bergsøysund Bridge caused by a statistically generated wave field based on the Monte Carlo method and spectral representation of the sea.

For the analysis to be accurate, the Abaqus model is supplemented with hydrodynamic effects caused by the interaction between the sea and the water borne light concrete pontoons. Then an eigenfrequency analysis can be sufficiently accurate. By simulating a wave field can time series analysis also be carried out.

The FE-model describing the Bergsøysund Bridge, which was developed in my project assignment, will be reevaluated and improved for more accurate results and to obtain a faster analysis. Hydrodynamic effects will now be taken into account by submitting a FE-analysis in the Wadam software. Results from the analysis can be implemented in the Abaqus model.

After the modeling is satisfactory, an eigenfrequency analysis will be submitted. Wave loads will also be developed by combining transfer functions obtained from Wadam and wave spectra, so that a plausible time series analysis can be accomplished. Then there will be submitted a great number of time domain analysis in the Abaqus software.

The results were to be analyzed and compared to measured data gathered from five accelerometers deployed at Bergsøysund Bridge so that system identification procedures could be initiated. This was not done because of limits in terms of time.

Knut Andreas Kvåle has been working with a similar problem on the same bridge. He has been studying the frequency domain instead of a time domain problem. Our results have been compared and analyzed.

Chapter 2

Hydrodynamic and Hydrostatic Effects

In marine engineering the vessel movement is commonly described as a six degrees of freedom system. The six degrees describes displacement in x, y and z-axis, and rotation about the x, y and z-axis, where the x-axis is the longitudinal vessel direction. The names for these displacements and rotations are surge, sway, heave, pitch, roll and yaw, which is illustrated in the figure below [7]:

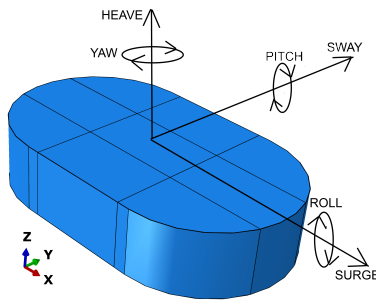


Figure 2.1: Vessel motion description

The project assignment done in the ninth semester did not include hydrodynamic contributions. When assuming harmonic response the equation of motion was presented and utilized on its commonly known form [6]:

$$[\mathbf{M}]\ddot{\mathbf{u}}(t) + [\mathbf{C}]\dot{\mathbf{u}}(t) + [\mathbf{K}]\mathbf{u}(t) = \mathbf{q}(t) \quad (2.1)$$

The following section is included as an introduction to the problems that are assessed in this master thesis. The formulas displayed here will be explained later in the literature review chapter and suitable solutions and explanation will be presented.

The seven pontoons are constantly influenced by the hydrodynamic and hydrostatic effects from the surrounding water masses. The water loads are the key forces present and are a necessity for a realistic time domain simulation of the response. The water masses contribute to restoring stiffness, added mass and added damping. On the other hand is the sea load the only external force accounted for. The equation of motion for one harmonic component can be rewritten to display hydrodynamic influences [13]:

$$[M + M_{hd}(\omega)]\ddot{u}(t) + [C + C_{hd}(\omega)]\dot{u}(t) + [K + K_{hd}]u = q(t) \quad (2.2)$$

$q(t)$ is the external force developed from the superposition of harmonic components from the sea elevation spectra, transfer functions developed in Wadam and presented in the time domain by creating a Monte Carlo simulation. Owing to this is the external load developed by both frequency and sea amplitude dependent aspects. The process of generating a three dimensional sea state is done in a separate simulation in Matlab, a numerical computation, visualization, and programming software. The internal motion induced forces are presented below to make it easier to grasp the new effects included in the master thesis:

$$q_{hd}(\omega, t) = M_{hd}(\omega)\ddot{u}(t) + C_{hd}(\omega)\dot{u} + K_{hd}u(t) \quad (2.3)$$

The external load does also consider the hydrodynamic effects and the general formulas are presented below in the frequency domain [8](the implications in the formula will be further assessed in chapter 2.2.3):

$$q(t) = \int_{-\infty}^{\infty} q(\omega)e^{i\omega t}dZ_{\eta} \quad (2.4)$$

Where the transfer function is the following [13]:

$$q(\omega, \beta) = [-(M_{hd}(\omega)\omega^2 + C_{hd}(\omega) i\omega + K_{hd})] \cdot X(\omega, \beta) \quad (2.5)$$

Where hd refers to hydrodynamic influences.

The hydrodynamic effects are prominent in both external force contributions and in the internal dynamic response, which will be explained and discussed in the following chapters.

2.1 Wave Action Simulation

When calculating and utilizing stochastic sea conditions in the time domain a spectral study of the sea qualities that will be included is appropriate. When assuming that the sea is a stationary random process over a limited period of time, sea spectra from ISSC can be used as an accurate model for the wave elevation. For a fully developed sea, the following formula is used [7]. Even though the bridge is not at open sea, the depths are large, and the fjord is wide, which can legitimate the use of the formula.

$$\frac{S_{\eta}(\omega)}{H_{\frac{1}{3}}^2 T_1} = \frac{0.11}{2\pi} \left(\frac{\omega T_1}{2\pi} \right)^{-5} e^{[0.44(\frac{\omega T_1}{2\pi})^{-4}]}$$
 (2.6)

$H_{\frac{1}{3}}$ is the value of one third of the highest waves and T_1 is the mean wave period. In this thesis T_1 and the standard deviation are fixed values so a simple iteration process can estimate $H_{\frac{1}{3}}$. The wave spectral density function does only describe one single point in space and time. For the bridge to have a coherent wave pattern, further assumptions must be deployed.

A wave amplitude is stochastically described with the autocorrelation function [9]:

$$R_{\eta}(\tau) = E[\eta(t + \tau) \eta(t)]$$
 (2.7)

Which describe the cross-correlation of the wave itself with a lagged time interval; τ . The coherence between the wave spectrum and the autocorrelation function is the following:

$$S_{\eta}(\omega) = \frac{1}{2\pi} \int_{-\infty}^{\infty} R_{\eta}(\tau) e^{-i\omega\tau} d\tau$$
 (2.8)

The cross-spectral density is then expressed as the density amplitude for two points in space.

$$S_{\eta_m \eta_n}(\omega) = \frac{1}{2\pi} \int_{-\infty}^{\infty} R_{\eta_m \eta_n}(\tau) e^{-i\omega\tau} d\tau$$
 (2.9)

As earlier, the wave spectrum is defined as the integral of the autocorrelation function over the time lag τ and the propagation ξ . The sea state is expanded to apply to point (x, t) and $(x + \xi, t + \tau)$. The autocorrelation function is then [9]:

$$R_{\eta_m \eta_n}(\tau) = R_\eta(\xi, \tau) = E[\eta(x + \xi, t + \tau) \eta(x, t)] \quad (2.10)$$

The autocorrelation function is expressed as the two dimensional wave spectra; where κ is the wave number:

$$R_\eta(\xi, \tau) = \int_{-\infty}^{\infty} \int_{-\infty}^{\infty} S_\eta(\kappa, \omega) e^{i(\omega\tau - \kappa\xi)} d\omega d\kappa \quad (2.11)$$

And the cross-spectrum

$$R_{\eta_m \eta_n}(\tau) = \int_{-\infty}^{\infty} S_{\eta_m \eta_n}(\omega) e^{i\omega\tau} d\omega \quad (2.12)$$

A general approach to the cross-spectral density for a multidimensional spectral density gives [9]:

$$S_{\eta_m \eta_n}(\omega, \kappa) = \int_{-\infty}^{\infty} S_\eta(\kappa, \omega) e^{-i\kappa\xi} d\kappa \quad (2.13)$$

Where ξ can be interpreted as $x_m - x_n$. By recognizing the dependence of the wave number and frequency as:

$$\omega^2 = g\kappa \tanh(\kappa h) \quad (2.14)$$

Where the gravitational acceleration is denoted as g and h is the ocean depth. By assuming that irregular waves are generated as a superpositional composition of harmonic waves the one dimensional wave spectrum can then be redefined by utilizing the Dirac's delta function [13]. The total cross-spectral density can then be expressed, with κ as a function instead of a variable:

$$S_{\eta_m \eta_n}(\omega) = \int_{-\infty}^{\infty} S_\eta(\omega) e^{-i \text{sign}(\omega) \kappa(\omega) \xi} d\kappa \quad (2.15)$$

Which also result in the following:

$$Co_{\eta_m \eta_n}(\omega) = S_\eta(\omega) \cos(\kappa(\omega)(x_m - x_n)) \quad (2.16)$$

$$Coh_{\eta_m \eta_n}(\omega) = 1$$

The directional distribution should also be included. The form which it is often presented, is a bell shaped function that peaks at its mean wave direction [13].

$$D(\theta) = \frac{\Gamma(s+1)}{2\sqrt{\pi}\Gamma(s+\frac{1}{2})} \cos^{2s} \left(\frac{\theta}{2} \right) \quad (2.17)$$

Where the gamma function, Γ is [12]:

$$\Gamma = (n-1)! \quad (2.18)$$

For the distribution that is used in the MATLAB scripts, a simpler form is proposed [9]:

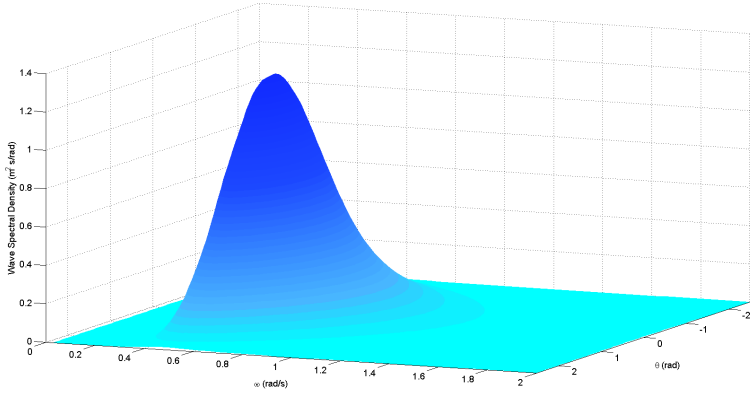
$$D(\theta) = C \cdot \cos^{2s}(\theta - \theta_{average}) \quad (2.19)$$

Where C is described as the normalization factor:

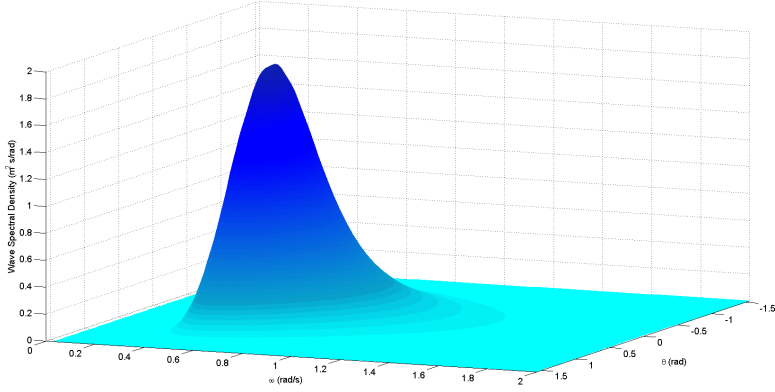
$$C = \int_{-\theta_{max}}^{\theta_{max}} \cos^{2s}(\theta) d\theta \quad (2.20)$$

The s determines the distribution width. Low values describes a short crested sea state, whereas high values indicates long crested waves. The value of s range typically between two and ten. The wave spectral density can then be expressed by a combination of (2.6) and a directional distribution.

$$S_{\eta}(\omega, \theta) = S_{\eta}(\omega) D(\omega, \theta) \quad (2.21)$$



(a) Bell shaped directional distribution



(b) Cosine directional distribution

Figure 2.2: ISSC wave spectra with directional distribution

The above picture is an illustrative plot of the wave spectral density from formula 2.21 used in this thesis with the spectra developed by ISSC, ($s=12$) and the cosine shaped spectra found in [8].

It is observed that the cosine directional distribution is much sharper over the directional distribution. With the directional distributions included a new description of the spectral densities are presented. For the lagged covariance between point n and m to be accounted for; the cross spectral density is prompted in the following way [13]:

$$S_{\eta_m \eta_n}(\omega) = S_{\eta}(\omega) \int_{-\theta}^{\theta} D(\omega, \theta) e^{(-i \frac{\text{sign}(\omega) \kappa(\omega)}{g} (\xi_x \cos(\theta) + \xi_y \cos(\theta)))} d\theta \quad (2.22)$$

The complex coherency may also be presented on a similar form

$$Coh_{\eta_m \eta_n}(\omega) = \int_{-\theta}^{\theta} D(\omega, \theta) e^{(-i \frac{\text{sign}(\omega) \kappa(\omega)}{g} (\xi_x \cos(\theta) + \xi_y \cos(\theta)))} d\theta \quad (2.23)$$

In this assignment, the coherency equals one, which means that randomly generated waves will not decay as they travel in the two dimensional space and the sea spectra is equal for the whole sea.

$$S_{\eta_n} \equiv S_{\eta_m} \quad (2.24)$$

2.2 Monte Carlo Simulation of the Sea State

2.2.1 One dimensional Time Series with Single Angular Wave Composition

It is possible to present and derive the Monte Carlo Simulation on Euler form:

$$\eta(x, t) = \int e^{i(\kappa \cdot x - \omega t)} d\mathbf{Z}_\eta(\kappa, \omega) \quad (2.25)$$

Where

$$dZ_\eta(\kappa, \omega) \sim \sqrt{2S_\eta(\kappa, \omega)} \delta\kappa \delta\omega e^{i\epsilon} \quad (2.26)$$

Using $x = \{x \ y\}$ and $\kappa = \{\kappa_x \ \kappa_y\} = \kappa \{\cos \theta \ \sin \theta\}$ denotes a two dimensional space.

The sinusoidal presentation of the problem gives the same results and is therefore used in the presentation of Monte Carlo theory.

Linear theory is used to simulate irregular sea states, so that simulation of stochastic hydrodynamic loads on the bridge pontoons can be developed. O. M Faltinsen's book [7] has been used to describe the following example for a one entry angle problem. A wave elevation that evolves from one singular point can be expressed as a sum of N wave components.

$$\eta(t) = \sum_{j=1}^N dZ(\omega_j) \sin(\omega_j t + \epsilon_j) \quad (2.27)$$

dZ_η , ω_j and ϵ_j are respectively the spectral process of η , radial frequency and random phase lag. The phase lag; ϵ_j is a randomly generated value for each j between 0 and 2π . The spectral process can be developed further in a discrete wave spectrum.

$$dZ_j = \sqrt{2S(\omega_j)\Delta\omega} \quad (2.28)$$

Where $\Delta\omega$ is the incremental step width between each frequency. The variance for the wave spectrum is therefore the integral over the spectral density.

$$\sigma^2 = \int_0^\infty S_\eta(\omega) d\omega \approx \sum_{j=1}^N dZ_\eta(\omega_j)^2 / 2 \quad (2.29)$$

$S_\eta(\omega)$ is the sea spectra established in the former chapter 2.6. The sum of the frequency dependent wave amplitude function (2.27) can describe a randomly developed one dimensional sea state. On vector form, for a one dimensional space, the sum is the following:

$$\eta(x, t) = [\sin(\boldsymbol{\omega}_j \cdot t - \boldsymbol{\kappa}(\boldsymbol{\omega}_j)x + \boldsymbol{\epsilon}_j)] \cdot [d\mathbf{Z}_{\eta,j}]^T \quad (2.30)$$

Where $\kappa = \frac{\omega^2}{g}$ is used for deep sea conditions, where g denotes the gravity.

2.2.2 Two dimensional Crested Sea with Multiple Angular Wave Composition

Creating a two dimensional crested sea, a discrete direction distribution algorithm is proposed:

$$D(\theta_i) = C \cdot \cos^{2s}(\theta_i - \theta_{average}) \quad (2.31)$$

Where θ_i describes the incremental angular value.

For the directional distribution to give suitable weighted results over the angular range is C denoted as the normalization factor represented on the following form:

$$C = \sum_{i=1}^K \cos^{2s}(\theta_i) \cdot \Delta\theta \quad (2.32)$$

$\Delta\theta$ is the fixed angular incremental step. The combination gives of the discrete directional distribution and the Monte Carlo simulation of the sea specter results in [9]:

$$\eta(t) = \sum_{j=1}^N \sum_{i=1}^K (2S(\omega_j, \theta_i) \Delta\omega_j \Delta\theta_i)^{\frac{1}{2}} \times \sin(\omega_j t - k_j x \cos(\theta_k) - k_j y \sin(\theta_k) + \epsilon_{jk}) \quad (2.33)$$

2.2.3 Wave Force Spectrum

In the forgoing section the development of a wave spectrum was described in detail. To further obtain a wave force spectrum, transfer functions derived from the Wadam software must be combined with the wave spectrum. The Wadam output carries information regarding the moments and forces in the frequency domain and the angular domain. The forces are calculated for seven local coordinate systems and then transferred to each pontoon as arrays of six independent force and moments acting in the global Cartesian coordinate system.

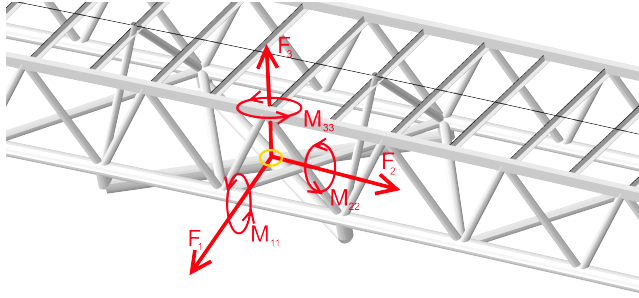


Figure 2.3: Forces transferred to the global system

The total hydrodynamic loading, $q_h(t)$, can be written on its simplest form by combining the transfer functions obtained by potential theory and the waves described as a Monte Carlo simulation. The sum of all the hydrodynamic effects is the following [8]:

$$q_h(t) = q(t) - q_{hm}(t) - q_{hc}(t) - q_{hr}(t) \quad (2.34)$$

Where $q_{hm}(t)$ is added mass, $q_{hc}(t)$ is added damping and $q_{hr}(t)$ are restoring forces. The wave excitation force, $q(t)$, can be expressed as the superpositioning of all the harmonic frequencies and amplitudes multiplied with their corresponding transfer functions:

$$q(t) = \int_{-\infty}^{\infty} q(\omega) e^{i\omega t} dZ_{\eta} \quad (2.35)$$

The wave spectra can be transferred over to the time domain through a Monte Carlo simulation, as can the external loads be transferred using the same tools as described in chapter 3.2.4.

2.3 White noise

A random wave spectrum was developed to confirm the coherence of Kvåle's results and the results presented in this thesis. To ensure a similar external load for the time and frequency domain, a constant load spectrum is assumed over the frequency range of interest. There are no cross spectral densities or directional distributions considered for the white noise.

$$q(\omega) = q \quad (2.36)$$

From formula (2.28) it is obtained that:

$$dZ_j = \sqrt{2S(\omega_j)\Delta\omega} = \sqrt{2q\Delta\omega} \quad (2.37)$$

And that the white noise time series is the following:

$$\eta(t) = \sum_{j=1}^N \sqrt{2q\Delta\omega} \sin(\omega_j t + \epsilon_j) \quad (2.38)$$

2.4 Hydrostatic Properties

2.4.1 Restoring Forces and Moments

The Restoring forces are caused by the hydrostatic qualities for a vessel submerged in a liquid. The effects can later be included in the final time domain analysis as springs.

A freely floating object that is symmetric in the z-x-plane and z-y-plane has nonzero values in heave, roll and pitch modes in the restoring force matrix. The force that is affecting the floating object owing to buoyancy can generally be described:

$$F_k = -C_{kj}\eta_j \quad (2.39)$$

here C_{kj} is the restoring coefficient. The relevant contributions for the submerged volume are then defined as the following [7]:

$$C_{33} = \rho g A_{WP} \quad (2.40)$$

$$C_{44} = \rho g V(z_B - z_G) + \rho g \iint_{A_{WP}} y^2 dA = \rho g V \overline{GM}_T \quad (2.41)$$

where A_{wp} is the submerged area, V is the displaced water volume, z_G is the z-coordinate for the center of gravity and z_B is the z-coordinate for the center of buoyancy, \overline{GM}_L is longitudinal meta-centric height and \overline{GM}_T is the transverse meta-centric height. The meta-centric height is defined as the distance between the center of gravity and its meta-center. The meta-center is the point which a structure submerged in liquid can be given a rotation about without generating angular moment.

2.4.2 Body Mass Matrix

When using the equations of linear and angular momentum, the steady-state sinusoidal motions can be generally expressed as [7]:

$$\sum_{k=1}^6 [(M_{jk} + M_{hd,jk})\ddot{\eta}_k + C_{hd,jk}\dot{\eta}_k + C_{jk}\eta_k] = F_j e^{-i\omega_e t} \quad (j = 1, \dots, 6) \quad (2.42)$$

Considering $j=1$, the linearized acceleration of the center of gravity in the x-direction is:

$$\frac{d^2\eta_1}{dt^2} + \frac{z_G d^2\eta_5}{dt^2} \quad (2.43)$$

This gives the following results:

$$M_{11} = M \quad M_{12} = 0 \quad M_{13} = 0 \quad M_{14} = 0 \quad M_{15} = Mz_G \quad M_{16} = 0$$

Doing the same procedure for $j=2$ and $j=3$ and computing the moment of inertia for each of the modes, a 6x6 mass matrix is developed:

$$M_{jk} = \begin{bmatrix} M & 0 & 0 & 0 & Mz_G & 0 \\ 0 & M & 0 & -Mz_G & 0 & 0 \\ 0 & 0 & M & 0 & 0 & 0 \\ 0 & -Mz_G & 0 & I_4 & 0 & -I_{46} \\ Mz_G & 0 & 0 & 0 & I_5 & 0 \\ 0 & 0 & 0 & -I_{46} & 0 & I_6 \end{bmatrix} \quad (2.44)$$

Where M is the mass of each pontoon, I is the product of inertia and z_G is the center of gravity.

Chapter 3

Analysis tools

3.1 Wadam

3.1.1 Frequency Dependent Hydrodynamic Properties

For the Abaqus time domain analysis to work realistically, hydrodynamic effects are included by implementing Wadam results. The hydrodynamic effects can simply be explained as the effects caused by oscillating impenetrable pontoons surrounded by liquid. As the pontoons move, water is forced around the geometry which then again causes pressure and pressure changes on the structure. The pressure depends on the acceleration of the geometry, which therefore creates a frequency dependent problem.

3.1.2 The Panel Method with Potential Theory

The Wadam analysis uses a combination of a panel model and a mass model when calculating the parameters of interest. The panel element method is based on a combination of potential theory, the source technique and a FE-model constructed from quadrilateral shell elements [3]. The source technique requires that the finite element model has a distribution of sources. The sources may be either sinks or sources all depending on the calculated strength parameter [7].

Throughout section is theory from the book “Sea loads on Ships and Offshore Structures” by O.M. Faltinsen [7] used throughout.

The total flux, over a surface due to a source is denoted as Q . In a 3D-system, the velocity potential is the following:

$$\phi = -Q/(4\pi R) \quad (3.1)$$

This can be seen from the integral of the velocity flux over a sphere’s surface:

$$\iint \frac{\delta\phi}{\delta R} ds = \frac{1}{4\pi} \frac{Q}{R^2} 4\pi R^2 = Q \quad (3.2)$$

For a two dimensional system, the velocity potential is presented as:

$$\phi = \frac{Q}{2\pi} \log r \quad (3.3)$$

Which holds for the integral of the velocity flux over a circle’s edge:

$$\int \frac{\delta\phi}{\delta R} dl = \frac{Q}{2\pi} \frac{2\pi}{R} R = Q \quad (3.4)$$

Because a two-dimensional formula basis is much simpler but still gives an adequate theoretical description, the two dimensional procedure is described instead of the three dimensional version. The following procedure will result in the computation of the added mass in heave. By arranging sources all over the body of a two dimensional edge, described as linear increments, the velocity potential is defined as:

$$\phi(y, z) = \int_S q(s) \log((y - \eta(s))^2 + (z - \xi(s))^2)^{1/2} ds \quad (3.5)$$

The integration is over the wetted surface where $\eta(s)$ and $\xi(s)$ are surface coordinates and y and z are fluid coordinates. The surface is a line since this is a two dimensional problem. 3.5 will gratify the Laplace equation:

$$\nabla^2 \phi = 0 \quad (3.6)$$

To compute (3.5) numerically, the surface is divided into N lines and the source density is assumed constant on each line segment. (3.5) can then be estimated as a sum:

$$\phi = \sum q_i \int_{S_i} \log((y - \eta(s))^2 + (z - \xi(s))^2)^{1/2} ds \quad (3.7)$$

The body boundary condition must be satisfied at the midpoint of each segment.

$$\frac{\delta \phi}{\delta r} = u_3 |\eta_3| \omega \cos(\omega t) \quad (3.8)$$

Where u_3 is the body velocity in heave. The formulation indicates that the velocity potential is reflected in the opposite direction so that the velocity potential is preserved over the surface. This can be achieved by normalizing the source density so that the time dependence and heave motion may be extracted.

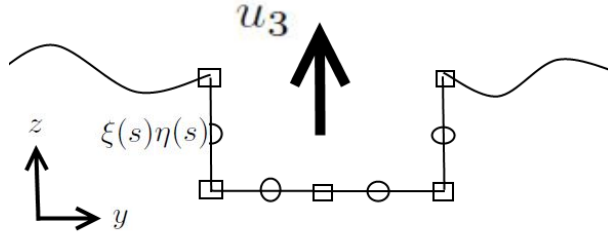


Figure 3.1: Two-dimensional panel model

By simplifying the problem at hand to a motion that is either in or out-of-phase the problem can be presented on matrix form where \bar{q}_i is the obtainable unknown.

$$q(s) = -\bar{q}(s) |\eta_3| \omega \cos(\omega t) \quad (3.9)$$

$$\begin{aligned} \sum_{i=1}^n \bar{q}_i \left[\frac{\delta}{\delta n} \int_{S_i} \log((y - \eta(s))^2 + (z - \xi(s))^2)^{1/2} ds \right]_{\bar{y}_1, \bar{z}_1} &= u_3 |_{\bar{y}_1, \bar{z}_1} \\ &\vdots \\ \sum_{i=1}^n \bar{q}_i \left[\frac{\delta}{\delta n} \int_{S_i} \log((y - \eta(s))^2 + (z - \xi(s))^2)^{1/2} ds \right]_{\bar{y}_n, \bar{z}_n} &= u_3 |_{\bar{y}_n, \bar{z}_n} \end{aligned} \quad (3.10)$$

The corresponding normalized velocity potential can now be found by combining formulas 3.10, 3.9 and 3.7, which is solved for in the equation above.

$$\phi = -\bar{\phi} |\eta_3| \omega \cos \omega t \quad (3.11)$$

The vertical force can now be found by utilizing the pressure over the structure:

$$p = -\rho \frac{\delta \phi}{\delta t} \quad (3.12)$$

$$F_3 = - \int_S p \, n_3 ds \approx -\{\rho \sum_{j=1}^n [\int_{S_j} \bar{\phi} \, u_3 \, ds]\} \omega^2 |\eta_3| \sin \omega t \quad (3.13)$$

The relation between forces in heave, added mass and heave damping is:

$$F_3 = -A_{33} \frac{d^2 \eta_3}{dt^2} - B_{33} \frac{d\eta_3}{dt} \quad (3.14)$$

For the purpose of an example a high frequency sea is studied. Damping is being neglected and the added mass can be presented as:

$$A_{33} = -\rho \sum_{j=1}^n [\int_{S_j} \bar{\phi} n_3 \, ds] \quad (3.15)$$

3.2 Abaqus CAE

The most utilized software in this thesis is the Abaqus CAE, which is a comprehensive finite element modeling software. The software can do both eigenfrequency and time domain analyses. The time domain analysis that was used is a dynamic implicit method where time increments that have been used have been varying between 0.02 and 0.1 second.

3.2.1 Dynamic Implicit Method

The time step maximum was set as 0.1 second, but the time step is not fixed, and can be reduced if it is necessary for convergence. The theory presented here is from the Abaqus theory manual [1].

The virtual work equation with the d’Lambert’s part included is presented below:

$$\int_V \mathbf{f} \delta \mathbf{v} dV = \int_V \mathbf{F} \cdot \delta \mathbf{v} dV - \int_V \rho \ddot{\mathbf{u}} \cdot \delta \mathbf{v} dV \quad (3.16)$$

Where ρ is the material density, \mathbf{b} is the displacement, \mathbf{F} is the external body force and \mathbf{f} is the body force at a point.

The d’Alembert term is more effectively described as reference values

$$\int_{V_0} \rho_0 \ddot{\mathbf{u}} \cdot \delta \mathbf{v} dV_0 \quad (3.17)$$

The finite element approximation of the integrals Abaqus utilizes is the following:

$$M^{NM} \ddot{u}^M + I^N - P^N = 0 \quad (3.18)$$

Where M^{NM} is the consistent mass matrix, I^N is the internal force vector and P^N is the internal force vector. The N implies an interpolation function basis, where N^N is displacement independent.

A balance of d’Lambert forces weighted average of static forces is displayed below:

$$M^{NM} \ddot{u}^M|_{t+\Delta t} + (1 + \alpha)(I^N|_{t+\Delta t} - P^N|_{t+\Delta t}) - \alpha(I^N|_t - P^N|_t) + L^N|_{t+\Delta t} = 0 \quad (3.19)$$

Where $L^N|_{t+\Delta t}$ is the sum of the Lagrange multiplier forces. The Newmark formula is used to obtain the displacements and velocity vectors.

$$u|_{t+\Delta t} = u|_t + \Delta t \dot{u}|_t + \Delta t^2((1/2 - \beta)\ddot{u}|_t + \beta\ddot{u}|_{t+\Delta t}) \quad (3.20)$$

$$\dot{u}|_{t+\Delta t} = \dot{u}|_t + \Delta t((1 - \gamma)\ddot{u}|_t + \gamma\ddot{u}|_{t+\Delta t}) \quad (3.21)$$

Where:

$$\beta = \frac{1}{4}(1 - \alpha)^2, \quad \gamma = \frac{1}{2}\alpha \quad \text{and} \quad -\frac{1}{3} \leq \alpha \leq 0 \quad (3.22)$$

When the automatic time increment method is used, some noise might occur if no damping is used. Numerical damping values around -0.05, ($\alpha = -0.05$) will efficiently remove noise, and at the same time keep the responses of interest unaffected.

For the analysis to work efficiently, time steps should to some extent be automatically altered. The half-step residual method [6] finds the residual error in 3.18 at time step $t + \frac{\Delta t}{2}$. The accelerations are assumed to be linearly varying, which gives:

$$\ddot{u}|_\tau = (1 - \tau)\ddot{u}|_t + \tau\ddot{u}|_{t+\Delta t}, \quad 0 \leq \tau \leq 1 \quad (3.23)$$

Since $t + \Delta t$ is already solved for, the current step must fulfill:

$$\begin{aligned} -\Delta u|_t &= \tau^3 \Delta u|_{t+\Delta t} + \tau(1 - \tau^2)\Delta t \dot{u}|_t + \tau^2(1 - \tau)\frac{\Delta t^2}{2}\ddot{u}|_t \\ &, \\ \dot{u}|_\tau &= \frac{\gamma}{\beta\tau\Delta t}\Delta u|_\tau + (1 - \gamma/\beta)\dot{u}|_t(1 - \frac{\gamma}{2\beta})\tau\Delta t\ddot{u}|_t \\ &\text{and} \\ \ddot{u}|_\tau &= \frac{1}{\beta\tau^2\Delta t^2}\Delta u|_\tau - \frac{1}{\beta\tau\Delta t}\dot{u}|_t + (1 - \frac{1}{2\beta})\ddot{u}|_t \end{aligned} \quad (3.24)$$

And the equilibrium residual magnitude is obtainable at any instance within a time step. The residual at the half step is obtained by combining 3.24 and 3.18

$$R^N|_{t+\Delta t/2} \stackrel{def}{=} M^{NM}\ddot{u}^M|_{t+\Delta t/2} + (1 + \alpha)(I^N|_{t+\Delta t/2} - P^N|_{t+\Delta t/2}) - \frac{1}{2}\alpha(I^N|_t - P^N|_t + I^N|_{t-} - P^N|_{t-}) + L^N|_{t+\Delta t/2} \quad (3.25)$$

Where $R^N|_{t+\Delta t/2}$ is set to a suitable portion of the forces that are acting in the dynamic system.

3.2.2 Frequency Dependent Eigenvalue Solutions

The natural frequencies and the corresponding eigenmodes are usually solved for by applying the classical eigenvalue problem [6]:

$$(-\omega^2[M] + i \cdot \omega[C] + [K])\{\phi\} = 0 \quad (3.26)$$

In Abaqus this equation set is solved by Lanczos Eigen Solver which is an augmented version of Inverse Power Method, where blocks of frequencies are evaluated incrementally.

$$[M] ([K] - \sigma[M]^{-1})[M]\{\phi\} = \theta[M]\{\phi\} \quad (3.27)$$

σ is a converging shift, $\{\phi\}$ is the eigenvector and θ is the eigenvalue. A new shift is created for after each convergence. Results from the analysis is converted to frequencies.

$$\omega^2 = \frac{1}{\theta} + \sigma \quad (3.28)$$

The Complex Eigenfrequency Analysis can be included as an extra step. The Complex Eigenvalue Procedure transforms the eigenmodes to diagonal form. The system is then solved for again, now with damping values included. This step is used when suitable damping ratios are estimated.

The added mass and added damping originating from the hydrodynamic effects caused by a water/structure interaction are both frequency dependent. The frequency dependent results from Wadam that are interpreted in Matlab are not compatible with the Abaqus software.

A frequency dependent added mass is therefore troublesome when obtaining the eigenfrequencies and eigenmodes, but also when doing a time domain evaluation. This can be further studied in formula 3.30, where $\mathbf{M}_{hd}(\omega_n)$ is a noncontinuous function, but a product of an iterative process with potential theory as its basis. The iterations for the estimation of the added mass are therefore done outside the Abaqus software for the eigenfrequency of interest.

$$[(\mathbf{K} + \mathbf{K}_{hd}) - \omega_2^2(\mathbf{M} + \mathbf{M}_{hd}(\omega))]\cdot \phi = \mathbf{0} \quad (3.29)$$

By considering one eigenmode at the time, the respective added mass can be modified, until the frequency results in Abaqus converge, and an accurate eigenfrequency is

obtained [13]. The process must be redone for each of the desired eigenmodes. This process is done in Matlab where a program containing the added mass and stiffness matrices for the current frequency.

Submitting the analysis will change the frequency, which then again can be evaluated in Matlab, so that the eigenfrequency can converge further.

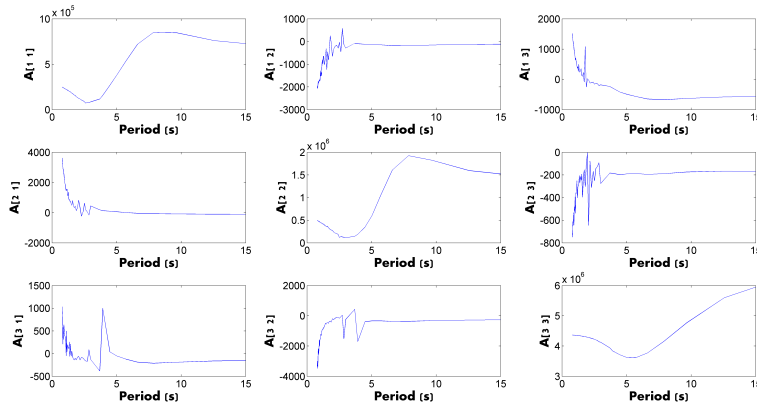


Figure 3.2: Example of added mass plot

3.2.3 Frequency Dependent Time Domain Forces

A frequency dependent mass and damping matrix, denoted as Added Mass and Added Damping is essential for the time domain solution for the global system to be accurate.

$$q(\omega, t) = \mathbf{M}_{hd}(\omega)\ddot{r}(t) + C_{hd}(\omega)\dot{r}(t) + K_{hd}r(t) \quad (3.30)$$

In a time domain analysis in Abaqus, the modal frequency solution for each step is not readily obtainable. Because of this was theory presented in “Prediction of Wave induced dynamic response in time domain using the finite element method” developed by the Department of Structural Engineering at NTNU used throughout the following two sections [13].

Since the external forces are broad banded, the movement will be irregular and a superposition of the Fourier Transformation of the motion will be essential for the implementation of frequency dependent effects.

$$\mathbf{G}_q(\omega) = \mathbf{F}_{hd}(\omega)\mathbf{G}_u(\omega) \quad (3.31)$$

Where $\mathbf{G}(\omega)$ is the Fourier transform and $\mathbf{F}_{hd}(\omega)$ is the hydrodynamic transfer function for the system obtained from Wadam. The transfer function is only frequency dependent and can thus be presented on the following form:

$$\mathbf{F}_{hd}(\omega) = -\omega^2 \cdot \mathbf{M}_{hd}(\omega) + i \cdot \omega \cdot \mathbf{C}_{hd}(\omega) + \mathbf{K}_{st} \quad (3.32)$$

\mathbf{M}_{hd} is the added mass, \mathbf{C}_{hd} is the added damping and \mathbf{K}_{st} is the hydrostatic stiffness. The inverse transform of the above equation is proposed:

$$\mathbf{q}(t) = \int_{-\infty}^{\infty} \mathbf{f}_{hd}(t - \tau)\mathbf{u}(\tau)d\tau \quad (3.33)$$

Where \mathbf{f}_{hd} is the discrete representation of \mathbf{F}_{hd} . The numerical analysis performed in Wadam creates noise for high frequency output because panel elements are flat which cause singularities. To avoid singularities and jumps a curve fitting procedure is applied:

$$\mathbf{F}_{hd}(\omega) = \mathbf{a}_1 + \mathbf{a}_2 i\omega - \mathbf{a}_3 \omega^2 + \sum_{l=1}^{N-3} \mathbf{a}_{l+3} \frac{i\omega}{i\omega + d_l} \quad (3.34)$$

The input values for the system can be determined by acknowledging that the fre-

quency independent term describes the hydrostatic restoring effect, the imaginary term describes the added damping input and real frequency dependent value is the signature of the added mass.

The response function describing hydrodynamic effects is defined as a Fourier transformation of equation (3.34), represented with the Dirac delta Function.

$$f_{hd}(\tau) = \mathbf{a}_1\delta(\tau) + \mathbf{a}_2\dot{\delta}(\tau) + \mathbf{a}_3\ddot{\delta}(\tau) + \sum_{l=1}^{N-3} \mathbf{a}_{l+3}(\delta(\tau) - d_l e^{-d_l \tau} H(\tau)) \quad (3.35)$$

By combining formula (3.35) and formula (3.33) the motion induced forces can be expressed in the following way:

$$\begin{aligned} q(t) &= \mathbf{a}_1 u(t) + \mathbf{a}_2 \dot{u}(t) + \mathbf{a}_3 \ddot{u}(t) + \sum_{l=1}^{N-3} \mathbf{a}_{l+3} \int_{-\infty}^{\infty} (\delta(t-\tau) - d_l H(t-\tau) e^{-d_l(t-\tau)}) \mathbf{u}(\tau) d\tau \\ &\quad \Downarrow \\ q(t) &= \mathbf{a}_1 u(t) + \mathbf{a}_2 \dot{u}(t) + \mathbf{a}_3 \ddot{u}(t) + \sum_{l=1}^{N-3} \mathbf{a}_{l+3} (\mathbf{u}(t) - d_l \int_{-\infty}^t e^{-d_l(t-\tau)} \mathbf{u}(\tau) d\tau) \end{aligned} \quad (3.36)$$

The motion induced forces are now purely denoted as a time domain function, and can be evaluated for each time step in Abaqus. This is achieved by running an external script in the FORTRAN engine. This gives us the ability to implement hydrodynamic effects incrementally. By shortening the equation, the expression becomes easier to comprehend:

$$\begin{aligned} q(t) &= \mathbf{a}_1 u(t) + \mathbf{a}_2 \dot{u}(t) + \mathbf{a}_3 \ddot{u}(t) + \mathbf{Z}(t) \\ &\quad \text{and} \\ Z &= \sum_{l=1}^{N-3} \mathbf{a}_{l+3} (\mathbf{u}(t) - d_l \int_{-\infty}^t e^{-d_l(t-\tau)} \mathbf{u}(\tau) d\tau) \end{aligned} \quad (3.37)$$

3.2.4 Implementation of the Frequency Dependent Time Domain Forces

Now that the transformation from the time and frequency domain to the purely time dependent domain is defined, a finite element implementation is desirable

$$\mathbf{M}\ddot{\mathbf{u}} + \mathbf{C}\dot{\mathbf{u}} + \mathbf{K}\mathbf{u} + \mathbf{q}(t) = \mathbf{P}(t) \quad (3.38)$$

Where \mathbf{M} , \mathbf{C} and \mathbf{K} are structural properties that are independent of the hydrodynamic effects, and $\mathbf{P}(t)$ is the wave action forces.

\mathbf{Z} contains an integration term that needs to be considered when creating the finite element presentation of the hydro dynamic effects.

$$\mathbf{Z} = \mathbf{Q}\mathbf{X}$$

$$\mathbf{Q} = [\mathbf{A}_4 + \mathbf{A}_5 \dots \mathbf{A}_N] \quad (3.39)$$

$$\mathbf{X} = [\mathbf{x}_1^T + \mathbf{x}_2^T \dots \mathbf{x}_{N-3}^T]$$

$$\dot{\mathbf{x}}_l = \mathbf{u} - d_l \mathbf{x}_l$$

Presenting the equation of motion and the derivative of the time history dependent term on matrix form yields the following expression:

$$\begin{bmatrix} (\mathbf{M} + \mathbf{a}_3) & 0 \\ 0 & 0 \end{bmatrix} \begin{bmatrix} \ddot{\mathbf{u}} \\ \ddot{\mathbf{X}} \end{bmatrix} + \begin{bmatrix} (\mathbf{C} + \mathbf{a}_2) & 0 \\ -\mathbf{E} & \mathbf{B} \end{bmatrix} \begin{bmatrix} \dot{\mathbf{u}} \\ \dot{\mathbf{X}} \end{bmatrix} + \begin{bmatrix} (\mathbf{K} + \mathbf{a}_1) & \mathbf{Q} \\ 0 & \mathbf{D} \end{bmatrix} \begin{bmatrix} \mathbf{u} \\ \mathbf{X} \end{bmatrix} = \begin{bmatrix} \mathbf{P} \\ 0 \end{bmatrix} \quad (3.40)$$

Where

$$\mathbf{E} = \begin{bmatrix} I \\ I \\ \vdots \\ I \end{bmatrix}, \mathbf{B} = \begin{bmatrix} I & & & \\ & I & & \\ & & \ddots & \\ & & & I \end{bmatrix}, \mathbf{D} = \begin{bmatrix} d_1 I & & & \\ & d_2 I & & \\ & & \ddots & \\ & & & d_{N-3} I \end{bmatrix} \quad (3.41)$$

To be able to use the Newmark β -method, the double derivation of \mathbf{Z} is desirable.

This results in the final equation for the equation of motion, where both hydrodynamic effects and structural properties are included:

$$\begin{bmatrix} (\mathbf{M} + \mathbf{a}_3) & 0 \\ -\mathbf{E} & \mathbf{B} \end{bmatrix} \begin{bmatrix} \ddot{\mathbf{u}} \\ \ddot{\mathbf{X}} \end{bmatrix} + \begin{bmatrix} (\mathbf{C} + \mathbf{a}_2) & 0 \\ 0 & \mathbf{D} \end{bmatrix} \begin{bmatrix} \dot{\mathbf{u}} \\ \dot{\mathbf{X}} \end{bmatrix} + \begin{bmatrix} (\mathbf{K} + \mathbf{a}_1) & \mathbf{Q} \\ 0 & 0 \end{bmatrix} \begin{bmatrix} \mathbf{u} \\ \mathbf{X} \end{bmatrix} = \begin{bmatrix} \mathbf{P} \\ 0 \end{bmatrix} \quad (3.42)$$

3.2.5 Rayleigh Damping

In Abaqus, the default method of adding damping to the structure is by the input of β and α , which decide which ratio of the mass and stiffness matrices to contribute to the total damping [2].

$$[C] = \alpha \cdot [M] + \beta \cdot [K] \quad (3.43)$$

High frequency modes will to a greater extent be damped by α , and β will contribute to the damping of lower frequency modes, which can be seen from (3.29). For a one degree of freedom system, the following applies:

$$C = 2\xi\omega = \frac{(\alpha m + \beta k)}{m} = \frac{(\alpha m + \beta \omega^2 m)}{m} \rightarrow \xi = \frac{(\alpha/\omega + \beta\omega)}{2} \quad (3.44)$$

By using two eigenfrequencies and its desirable damping values, α and β can be obtained

$$\alpha = 2 \cdot \omega_1 \omega_2 \frac{\xi_1 \cdot \omega_2 - \xi_2 \cdot \omega_1}{\omega_2^2 - \omega_1^2} \cup \beta = 2 \cdot \frac{\xi_2 \omega_2 - \xi_1 \omega_1}{\omega_2^2 - \omega_1^2} \quad (3.45)$$

If the two damping values are set to equal values, the equations render even simpler expressions:

$$\alpha = 2 \cdot \frac{\omega_1 \omega_2}{\omega_1 + \omega_2} \xi \quad (3.46)$$

$$\beta = 2 \cdot \frac{1}{\omega_1 + \omega_2} \xi$$

3.3 Cross-X

To develop a model which is both accurate and effective, sufficient stiffness due to the stiffening steel top is a necessity. As seen from figure 3.3a is the deck quite complicated and the need for different kinds of elements seems inevitable. Earlier models developed as a part of my project assignment used a combination of shell elements and beam elements to model the steel top.

Shear locking and demanding computational procedures renders an inadequate simulation [6]. The Cross-X software utilities basic beam theory [10], so that beam data can be extracted from an arbitrary cross section and the physical prospects of the whole plate can be merged into a single beam element, stiffeners included.

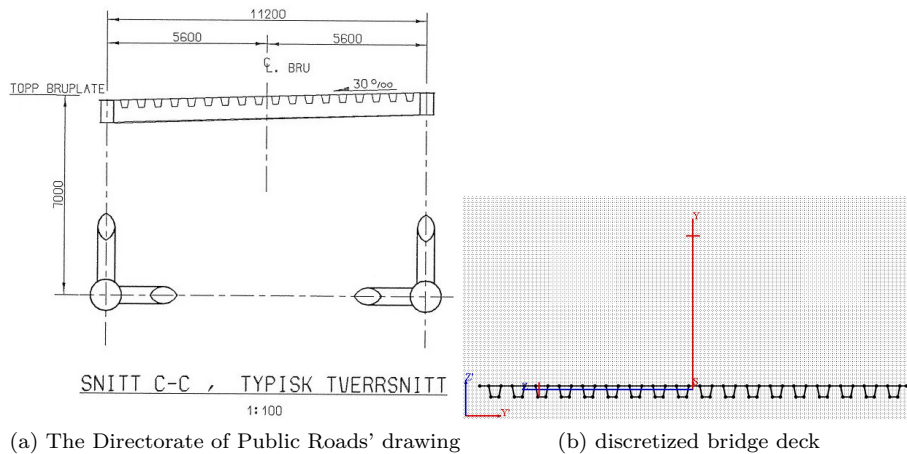


Figure 3.3: Bridge deck design

A shell element can be secured in position at both sides of the bridge way. The beam element is, on the other hand, only fixed to the middle node of the flipped T-cross-sections. This lessens the torsional stiffness, but shear locking is avoided. The first five eigenmodes are not dominated by twisting motion, which indicate that the lessened torsional stiffness properties for the bridge will affect the time series results in a negligible fashion.

Chapter 4

Signal processing

4.1 Fast Fourier Transform

To be able to study the time domain solution in the frequency domain, a fast Fourier transformation is used. The complex Fourier transformation and it's inverse is presented like this [12]:

$$\begin{aligned}\hat{f}(\omega) &= \int_{-\infty}^{\infty} f(t) \cdot e^{-i\omega t} dt \\ f(t) &= \int_{-\infty}^{\infty} \hat{f}(\omega) \cdot e^{i\omega t} dt\end{aligned}\tag{4.1}$$

Where the function is transformed from time dependent $f(t)$ to frequency dependent $\hat{f}(\omega)$.

The discrete Fourier approach is more relevant for a numerical discrete time series, and the leap from continuous domain to discrete is yet simple.

$$\begin{aligned}\hat{x}(\omega)_k &= \sum_{n=0}^{N-1} x(t_n) \cdot e^{-i\omega_k t_n} \\ x(t)_n &= \sum_{k=0}^{N-1} \hat{x}(\omega_k) \cdot e^{-i\omega_k t_n}\end{aligned}\tag{4.2}$$

Where the discrete Fourier transformation, DFT, calculate a frequency spectra for a noncontinuous time series.

The fast Fourier transformation is a much quicker and accurate take on the classical discrete Fourier transformation, where the spectrum is calculated directly from the signal input. For the DFT, the solution demands $O(N^2)$ calculations, as for the FFT, only $O(N)\log_2 N$ operations.

This is done by dividing the time series in smaller parts, as the contribution to the sum for a remote value is neglectable. Each sum then becomes smaller, and the process faster, without sacrificing accuracy of values in proximity of the step which is currently examined.

$$\hat{x}(k/N) = \frac{1}{N} \left| \sum_{n=0}^{N-1} x(n) e^{-i \frac{\omega_k t n}{N}} \right|^2 \quad (4.3)$$

Where $k = 0, 1, \dots, N - 1$. After each part is solved for, a combination of the results yields an accurate solution [5].

4.2 Welch's Method

As the FFT divides, in this case study, the time series into smaller bins, the Welch method secures continuity by allowing each bin to overlap. The lack of overlapping bins can cause spectral leakage. To secure clearer spectral densities, as the spectral leakage is minimized, a windowing function is used. A bell shaped windowing function is a common choice [5].

4.3 Histogramical Presentation

The histogramical presentation of the results which will be used later in the thesis makes use of a built in application in Matlab. The application creates a plot of a given number of bins and a normal density function that is fitted. The histogram is an easily accessible tool that displays the probabilistic distribution of amplitudes, which in this case are displacements, in an easily perceivable way.

Part II

Bridge Action Modeling

This part of the assignment describes how models were constructed and what kind of analysis that is submitted in Abaqus, Genie and Wadam. What parameters and inputs that are used will also be specified accordingly. A thorough review of the analysis architecture is essential for the troubleshooting and later use of the analysis procedures displayed in this thesis.

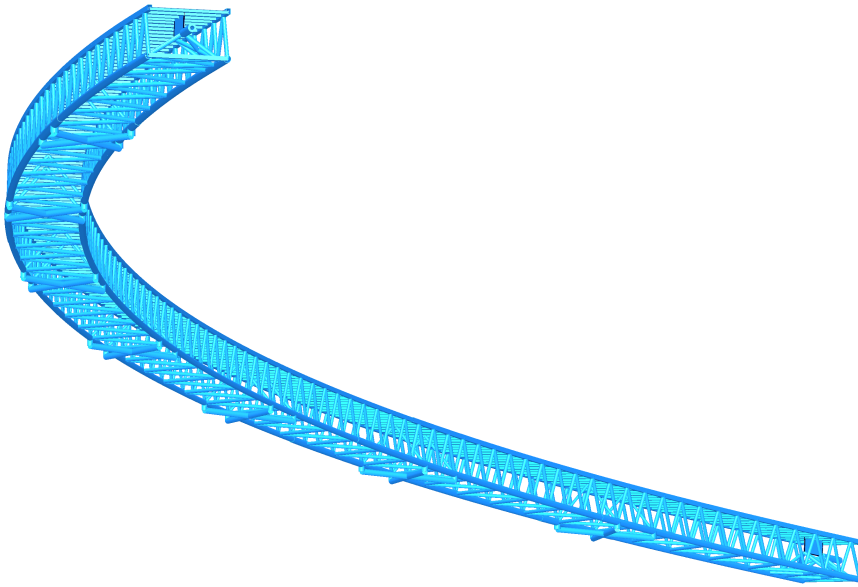


Figure 4.1: Complete FE-model of the Bergsøysund Bridge

Chapter 5

Pontoon Modeling

Two different pontoons are modeled. Pontoon number one and seven are both 0.9 meters taller than pontoon 2, 3, 4, 5 and 6 [16]. The design difference changes the restoring forces, the overall mass and the external forces. All of which are factors that should not be neglected. The concrete is described as light concrete and a density of $2000 \frac{kg}{m^3}$ was used. In appendix C ballast distributions is described. Each pontoon has a given ballast mass which is varying in placement and size for each of the seven pontoons. The ballast data was not used in the pontoon modeling.

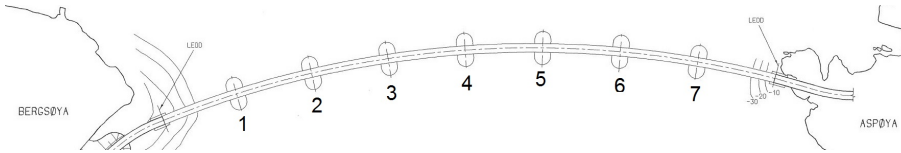


Figure 5.1: Pontoon numbering

The geometry of the pontoons are not included in the final time domain analysis, but are evaluated as nodes in Abaqus. Properties are extracted and implemented in the time domain and eigenfrequency analysis. Firstly were the inertia and mass values extracted, which are easily accessible in a separate Abaqus model describing the pontoons exclusively. The pontoon geometry has been designed in Abaqus with shell elements that have been later utilized to obtain the hydrodynamic properties. A more comprehensive Wadam analysis was completed later.

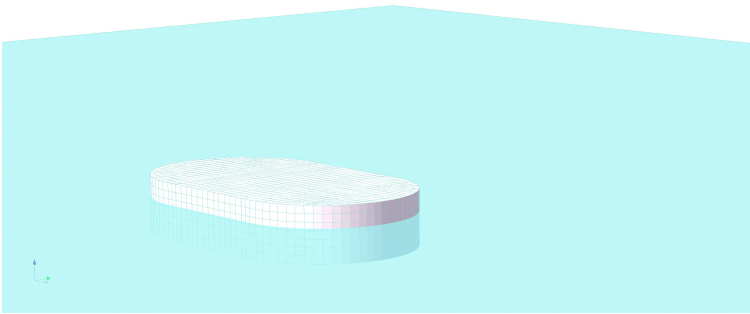
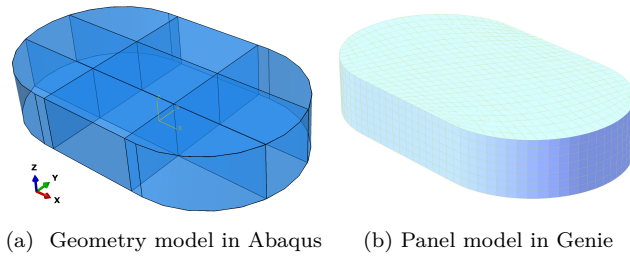
Table 5.1: Pontoon properties

		Pontoon 1 and 7	Pontoon 2-6
Height (m)	H	6.94	6.07
Water level (m)	H_{wl}	4.37	3.7
Mass (kg)	$M_{pontoon}$	1368893	1272540
Moment of inertia about x-axis	$I_{xx} (m^4)$	$8.48 \cdot 10^7$	$7.16 \cdot 10^7$
Moment of inertia about y-axis	$I_{yy} (m^4)$	$1.63 \cdot 10^8$	$1.42 \cdot 10^8$
Moment of inertia about z-axis	$I_{zz} (m^4)$	$1.85 \cdot 10^8$	$1.67 \cdot 10^8$

For the time domain analysis, the mass, stiffness and damping properties are condensed to one noded elements with six degrees of freedom for every pontoon. The data used to describe the rigid pontoon structures are listed above.

The procedure employed to obtain the water level estimations are described in Part III of the thesis.

To approximate the frequency dependent added mass and added damping, the Abaqus, HydroD and Genie software were used. The geometry is extracted from Abaqus. In the Genie engine, Panel models are created; consisting of 1342 panels for pontoon 1 and 7, 1286 panels for pontoon 2 to 6. Structural mass properties and water levels were extracted from a similar model in Abaqus. The final pontoon analysis is done in Wadam, where hydrodynamic parameters are extracted.



(c) Wadam, Panel model and sea state configurations included

Figure 5.2: The development of the Panel model analysis

5.1 Genie

The Genie software was used as a connecting link between the geometry created in Abaqus and the hydrodynamic Wadam analysis. The concrete permeability was set to zero. Appropriate wall thicknesses and concrete densities were applied. A mass model and a panel model were extracted from the software, which could be used in the HydroD software.

5.2 HydroD and Wadam

5.2.1 The Analysis

The hydrodynamic analysis was performed in HydroD with the Wadam software package for the two different types of pontoons that was earlier modeled in Abaqus, and further augmented in Genie. Both a panel model and a structural mass model were implemented in the Wadam analysis.

The internal walls are excluded for the panel model and included for the mass model. Because of symmetry, a set of wave directions ranging from 0 to 90 degrees, with 5 degree increments was used. Frequencies ranging from 0.2 to 8 radians per second with 0.1 rad/s increments were applied. This equals periods ranging from 0.8 s to 31 s. The water depth is set to 300 m since no information regarding the fjord was available. The water level is set to 4.37 meters for pontoon 1 and 7, and 3.7 meters for pontoon 2 to 6 reflecting on a static analysis done in Abaqus.

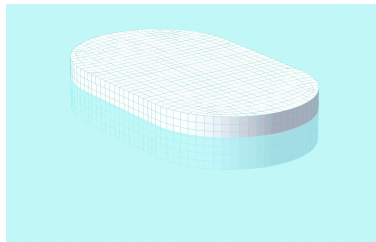


Figure 5.3: Loading conditions for Pontoon 2 to 6

5.2.2 Results

Hydrostatic data, which is the body mass matrix and the restoring force matrix, were obtained. The hydrodynamic parameters, added mass and potential damping, were also obtained. These values are frequency dependent, and each degree of freedom is therefore plotted as a period dependent variable. From the results, it is seen that some of the degrees of freedom are neglectable. The results are presented in a *.LIS file which is analyzed in Matlab.

Chapter 6

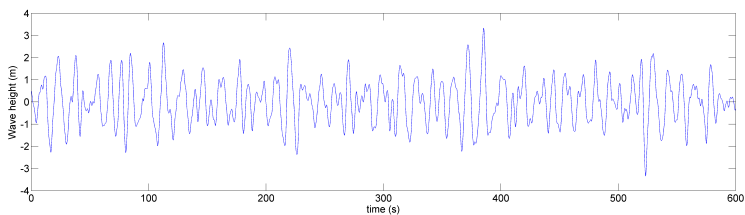
Wave Pattern and Stochastic Forces

The waves that are combined with the output from Wadam are two-dimensional long crested wave patterns developed by Ragnar Sigbjörnson. The occurrence of wave height uses the distribution developed by ITTC, where the typical wave period, T_0 , is set to 10 s, and the standard deviation of the wave elevation is set to 1. This causes a significant wave height of 4 meters. The directional distribution is varying between $\pm 60^\circ$ with increments of 3° . The incremental frequency step for the generation of the stochastic sea is 0.002 rad over a range of zero to two radians per second.

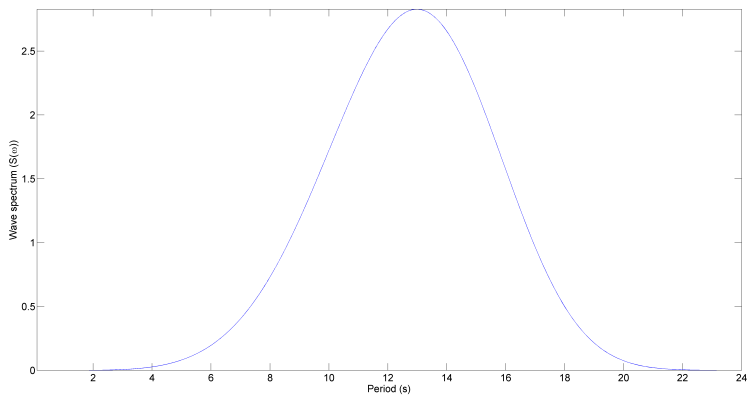
The simulation was set to endure for 10 to 100 minutes. Both nonlinear and linear analyses have been studied. This procedure was done multiple times to obtain a broad data basis. The main time series presented in the results is a composition of ten 3000 seconds long linear dynamic implicit time series with a maximum time step of 0.1 second. The extracted data file contains displacements in the system for every 0.5 second for each of the seven pontoons.

It should be pointed out that the sea developed is not describing the actual sea state at Bergsøysundet, and the forces employed due to the sea are much larger than any ordinary sea state at the site.

A one dimensional wave example with the data listed in this section is generated from the ITTC spectra is displayed below:



(a) A generic wave height plot



(b) The wave spectrum versus time

Figure 6.1: Wave action for one point

Chapter 7

Abaqus model

7.1 Earlier Model

The Begsøysund bridge was initially modeled as a part of my project assignment. The earlier model design was too comprehensive for an effective analysis to be reviewed. The model utilized shell elements to a greater extent which were used to model both cat walk and pontoons. Very coarse seeding was used for the shell elements because of the comprehensibility of the model. That simplification might render false results because coarse seeded shell elements cause shear locking and the stiffness of the structure might be exaggerated. To obtain the same stiffness in the simplified model is therefore not a goal.

The time step used for the old analysis was set to 0.02 seconds. This also prolonged the analysis time without rendering enhanced results. The analysis required 17 hours of computational time for a 600 second long time series to be solved for. A more suitable time step is therefore reviewed.

Real measurements from accelerometers on the Bergsøysund Bridge were supposed to be available, so that a correct model could be achieved by the process of system identification. Unfortunately were the real displacements attainable at a late stage of the master thesis course.

The improved model employed in the thesis has therefore been altered in a range of different ways for a more calculative effective FE-model. Because of a rather new design, a new assembly description is included.

7.2 Numerical Analysis

The time domain analysis and the frequency analysis were completed in Abaqus. Parameters obtained from Marine technical software and wave action forces are implemented node wise for each of the seven pontoons.

7.2.1 Eigenfrequency Analysis

To include gravity as a force contributor, the job submitted in Abaqus includes a static linear perturbation step, where masses and the restoring mass matrix are accounted for. Then a complex frequency step is employed. The complex frequency analysis was used, with Lanczos as the Eigen Solver algorithm. The complex frequency analysis is a necessity for the extraction of damping parameters. The iterative method described in chapter 3.2.2 was used to include hydrodynamic effects in the eigenvalue analysis. Every obtained eigenmode has been obtained by three iterative steps.

7.2.2 Time Domain Analysis

The time domain analysis is a linear dynamic implicit analysis where increment sizes between 0.02 s and 0.1 s have been tested. The dynamic implicit method is unconditionally stable, and the time step used is therefore only required to be half of the period of the frequencies of interest for its detection. To obtain high frequency responses, a small time step is required. The standard analysis lasts for 3000 seconds. The time domain analysis also starts out with a static step, where gravity is included, so the structure is able to settle before the dynamic aspects are commenced.

Since a linear analysis tend to be a quicker option than a nonlinear approach, both kinds of analysis have been studied under the same load conditions. Then can a

conclusion be rendered regarding the influence of nonlinear geometric effects and the necessity of the inclusion of these effects in the main time domain solution which will be presented in the results.

7.2.3 Meshing

The analysis is only supposed to supply accurate results for the overall dynamic tendencies for the model. Local stresses and strains are not to be studied and evaluated. A rather coarse mesh is therefore sufficient. A finer mesh would be required to study local stresses and strains, but the global displacements due to dynamic response are currently the main focus.

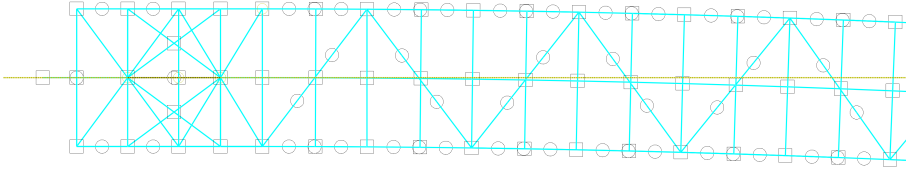


Figure 7.1: Seeding, west end of bridge

The node density is set to 5m, which means that most beams consist of two or three beam elements. For the truss work, the B31 element is used. The element is two noded with one Gaussian integration point, and each node contains six degrees of freedom.. The simple element is chosen for an effective analysis. The B31 element is not ideal for a curved beam, but since the beams in question have little curvature, the effects are neglectable. The built in seeding procedure in Abaqus regulate the mesh density according to maximum beam deviation ($h/L < 0.1$).

7.3 Structure

7.3.1 Coordinate System

The coordinate system has its center at the westernmost bridge end. The x-axis lays parallel with the cat walk at origin. This is important to act in accordance with when analyzing results from different pontoons.

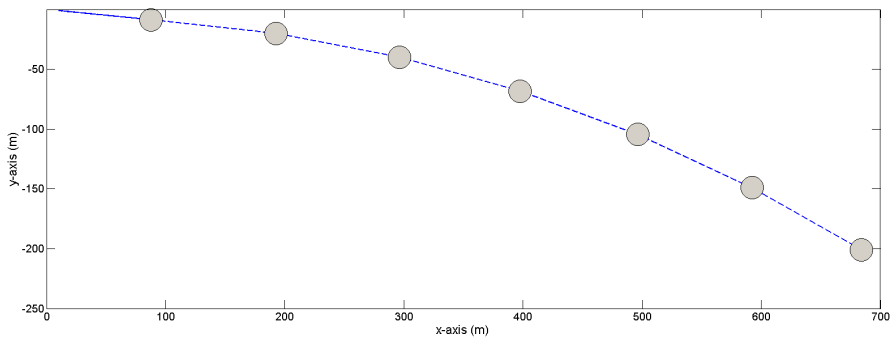


Figure 7.2: Coordinate system

7.3.2 Steel Structure

The steel structure is a three dimensional model consisting of 1763 wire elements that, because of stiff connections, are considered as beams. The connections are rigid, and do not include explicit details. All beams are straight, except for the beams that enclose the truss work.

The typical profiles are pipes and rectangular beams, with a wide range of dimensions. The diversity of profiles is displayed in figure 7.3 where every color indicates a different profile. The cross-sections used are available in appendix B. Material data for the steel is presented below.

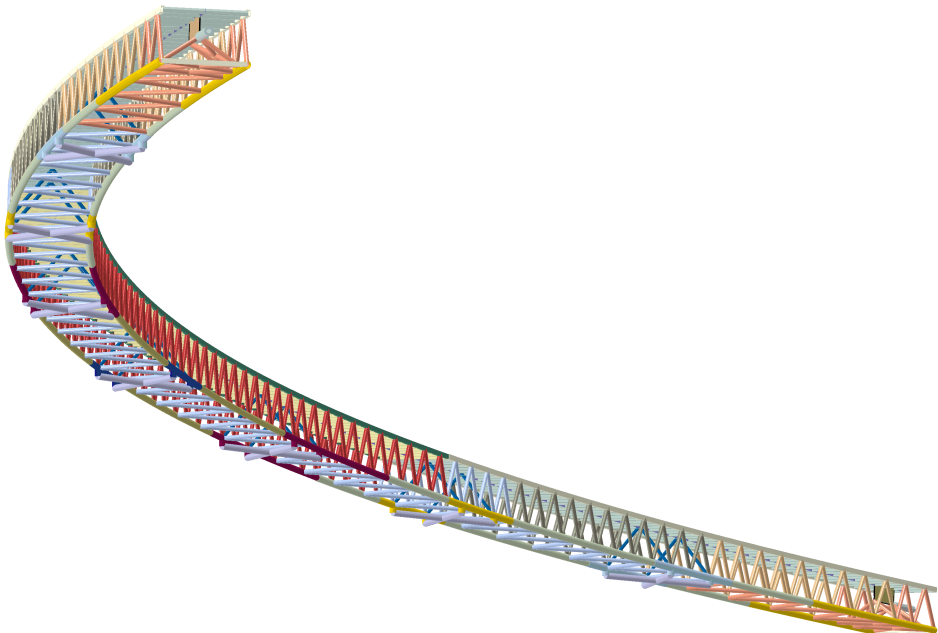


Figure 7.3: Profile illustration

Table 7.1: Steel Properties

Steel		property
Young's modulus	E_s	$210 \cdot 10^9 N/m^2$
Density	ρ_s	$7800 kg/m^3$
Poisson ratio	ν_s	0.3

7.3.3 Part Assembly

The Directorate of Public Roads drawings separate the structure in three parts due to differences in cross-sectional sizes, but owing to symmetry the bridge is modeled as one part in Abaqus, as cross sectional properties are included at a later stage. The steel top was modeled first as the floor beams could be assembled by utilizing the rotationally pattern tool.

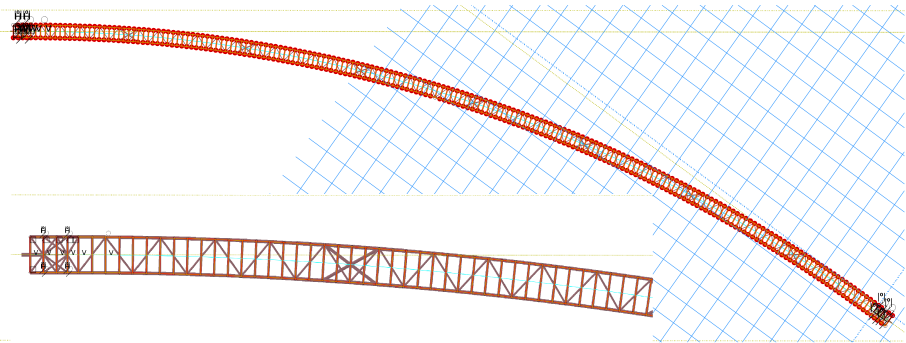


Figure 7.4: Bridge assembly of floor beams

The top is then copied and relocated, now representing the bridge chord. Lateral bracing is employed, and the two wire models are connected by using the wire tool.

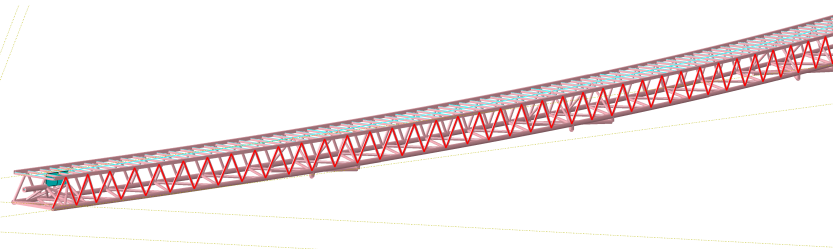
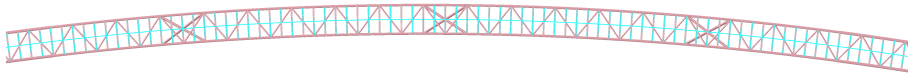
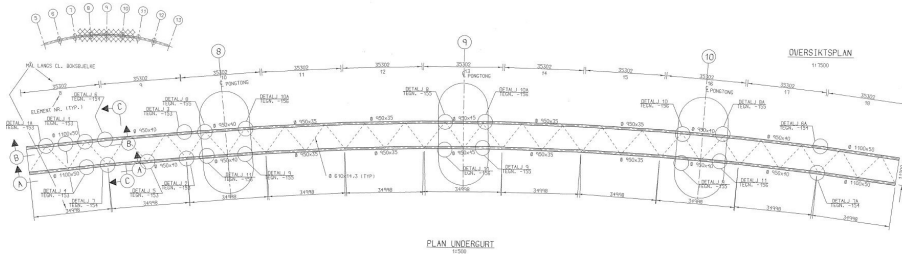


Figure 7.5: Wire tool



(a) Design in Abaqus



(b) Directorate of Public Roads drawings

Figure 7.6: Frame work, x-y-plane

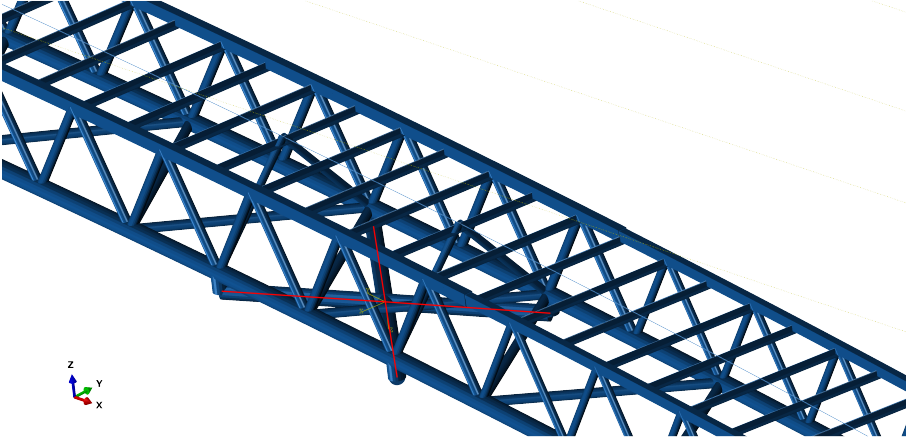
7.4 Pontoon Connectors

The pontoons were severely simplified in Abaqus, boiling down to seven single nodes with six degrees of freedom. Connecting each pontoon node to the four legs that tie the pontoons to the truss work was achieved by a simple truss work, making up a cross, where the pontoon node is located in the center.

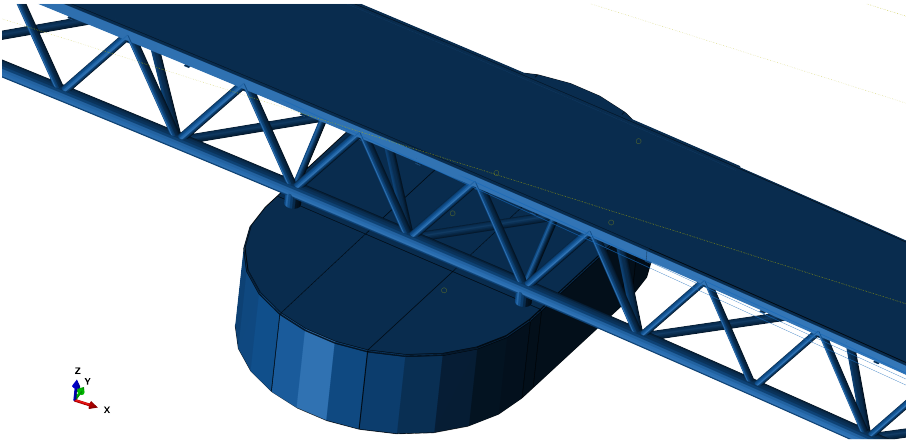
To limit displacements in these beams, an incredibly stiff material has been employed. The density is set low to avoid extra mass, but high enough for high pitch vibrations to be avoided.

Table 7.2: Material and cross-sectional properties

Pontoon Connections		Numerical values
Young's modulus	E_{pc}	$210 \cdot 10^{11} N/m^2$
Density	ρ_{pc}	$1000 kg/m^3$
Poisson ratio	ν_{pc}	0.3
Cross section	Type	Massive pipe
radius	r_{pc}	0.5 m



(a) Pontoon cross as modeled in the computational effective model



(b) Pontoon connection as modeled in the computational ineffective model

Figure 7.7: Pontoon connection

7.5 Boundary Conditions

The Bergsøysund Bridge is only anchored at its ends. There are two parts restricting movements. Firstly, there is a rod that connects the bridge truss work to a concrete slab on shore. This rod restricts movement in all axes, but mainly in the bridge deck direction.

Secondly, the truss work ends are held in place by rubber slabs, restricting movement in all directions except in the bridge deck direction. These rubber slabs does allow some movement so that tides and high sea doesn't cause an abundance of internal stress. As for this analysis, the movement is strictly prohibited [14].

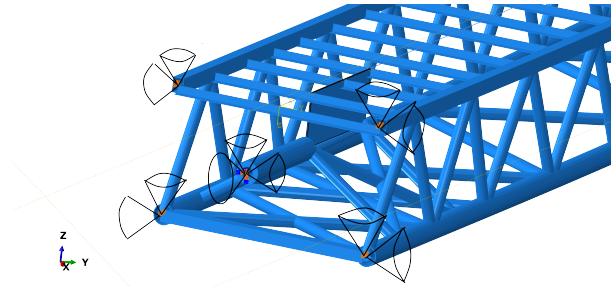


Figure 7.9: Boundary conditions in Abaqus

The cones on the illustration indicated that displacement is only restricted in the axis it is pointing. Angular movement is still allowed.

7.6 Combination of Input Data

To combine the different model data obtained in part II of this thesis, resulting in a fully functional Abaqus model, the external data must be included in either the keywords or as an external subroutine deployed in the job [2].

The sea loads are included by combining two scripts that are called upon in the dynamic implicit step in the keyword window, named “keyword.INP” and “CLOAD.INP”; the first script uses the *CLOAD command. The *CLOAD command employs concentrated point loads. The loads are applied at the centers of the pontoon crosses that were described earlier, by referring to Assembly sets created in the Abaqus interface. In combination with the *CLOAD command, an optional parameters is specified; amplitude. The amplitudes for each time step is stored in a keyword-file named CLOAD.

The mass of the pontoons is included in a script called “pontoonmass.txt”. The script generates seven one noded user elements with six degrees of freedom by using the following command (E.1.1):

```
*USER ELEMENT, LINEAR, NODES=1, UNSYM. TYPE='NAME', 1, 2, 3, 4, 5, 6
```

The user element uses the optional parameter *MATRIX, TYPE=MASS. Local coordinate systems are not generated. The pontoon masses have therefore been transformed prior to the analysis from their local coordinate systems to the global coordinate system.

The element also specifies damping values on Rayleigh damping form, as well as what element set the user element is associated with. This is achieved by using the *UEL PROPERTY and *ELEMENT command, and then specifying ALPHA and BETA.

In the time domain analysis is restoring stiffness, added mass and added damping implemented by first introducing a script denoted “HydroBergsoy.INP” in the keywords. The script generate elements in similar fashion as described above.

A FORTRAN script is implemented by including an “User subroutine file” called “Hydrodynamics.for”. The FORTRAN program will run as the Abaqus-job is running. The program will change and evaluate added mass and added damping matrices at every time step. To secure that the FORTRAN program is running Abaqus CAE must be started in the “Visual FORTRAN Intel” version of Abaqus Command.

Part III

Experimental Design

Chapter 8

Pre-analysis Considerations

This part of the thesis will discuss simplifications and design calculations that have been done to render an analysis that is realistic and effective. An issue that is neglected or emerges at a late stage in the process is discussed in the further work or the source of error part which can be found at the end of the thesis.

8.1 Water Level

The water level is obtained by doing a static analysis of the whole bridge with gravity as the only external load. The bridge rests solely on boundary conditions and springs calculated from the pontoon buoyancy. The static displacement at each pontoon in the vertical axis is an approximation of the water level. The water level information can then be used in the Wadam analysis, so correct hydrodynamic coefficients can be extracted.

This water level simplification was done because importing the FE-model of the whole bridge into the genie interface, and then importing the genie-extracted model into Wadam so that mass properties of the whole bridge can be considered to calculate the center of buoyancy is very time consuming. Sectional information needs to be retyped and geometrical errors regarding the combination of shell elements and beam elements turns out to be troublesome.

To allow for the bridge to have a level starting point in the time domain analysis and eigenfrequency analysis with gravity included, an opposite and equal force to the self-weight is calculated. The loads are sufficient for the bridge to initiate horizontally in the dynamic implicit analysis.

8.2 Cross-X

The bridge deck was analyzed in Cross-X software, so that the cross-sectional properties were obtained. The results from this analysis are listed below. The data was used to create a suitable beam-element for Abaqus. The “Augmented mass” is including the extra mass caused by a 5 cm thick asphalt layer was assumed. The asphalt density was set to $2500\text{kg}/\text{m}^3$. The inertia values are about the center of gravity of the cross section.

Table 8.1: Cross-sectional properties for the bridge deck

		Property
Area	A_{BD}	0.2638m^2
Augmented mass	ρ_{BD}	$11859\frac{\text{kg}}{\text{m}^3}$
2.nd moment of area		
	I_{11}	$3.313 \cdot 10^{-4}\text{m}^4$
	I_{12}	$-8.883 \cdot 10^{-4}\text{m}^4$
	I_{22}	$24558 \cdot 10^{-4}\text{m}^4$
St. Venant	I_t	$34.464 \cdot 10^{-4}\text{m}^4$

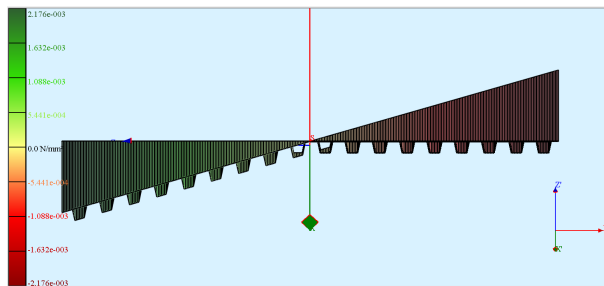


Figure 8.1: Cross-X example: σ_x due to M_y

As illustrated in figure 8.2, the augmented model is not as easy to interpret visually. The thin line, illustrating the beam, contains all of the data above.

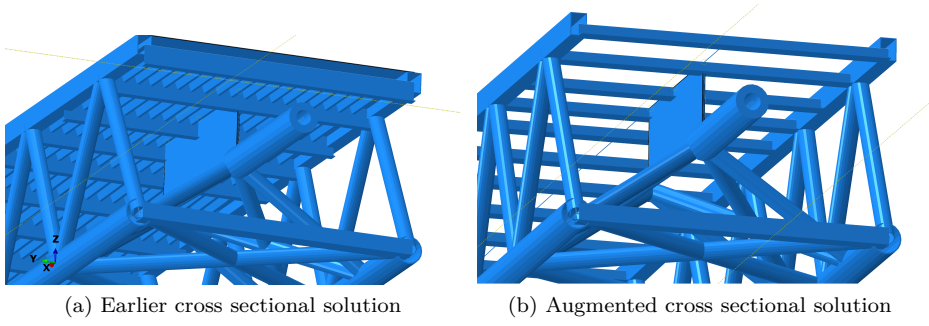


Figure 8.2: Implementation of the simplified bridge deck

Chapter 9

Analysis Considerations

To obtain information regarding the necessity of accuracy for aspects like detail level and time increment sizes, some analyses have to be done, not for the acquisition of results, but to weed out issues that need to be dealt with. Time step and seeding of the FE-model are examples studied and discussed in this part. One can save computational time and false results by doing these kinds of system identification procedures at an early stage in the assignment.

9.1 Damping

The damping used is the Rayleigh damping. According to equation 3.45, two eigenfrequencies are chosen as base points, where critical-damping ratios will be larger outside these limits. Since eigenfrequency one was the most prominent in early analyses, eigenfrequency one is chosen as the first value. The second eigenfrequency of interest was set to six. The one step method requires two desired damping values, which was set to 0.005 for both. For the procedure to work, all masses and stiffnesses need to have a defined damping value. The damping values were therefore also included in the external scripted user elements.

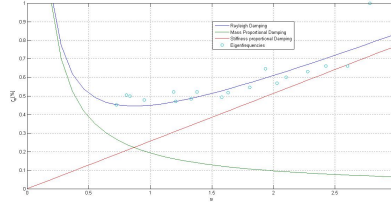


Figure 9.1: Illustrative presentation of α and β calculations

Table 9.1: Rayleigh Damping Coefficients

Coefficients	α	β
Values	0.0048633	0.0043309

The implicit dynamic analysis also has some numerical damping in its default settings. The standard value for α is -0.05, which was used for most of my time series. Analyses were also submitted with $\alpha = 0$ because of the time series implemented algorithm described in section 3.2.4 do recommend this value. This is due to the simplification of the iterative scheme, where:

$$\alpha = 0$$

$$\beta = \frac{1}{4}(1 - \alpha)^2 = \frac{1}{4} \quad (9.1)$$

$$\gamma = \frac{\alpha}{2} = 0$$

Which is commonly known as the Newmark- β method.

9.2 Mesh Seeding

The mesh seeding is crucial when doing comprehensive time domain analyses. The seeding density decides the size of the element matrices, which then again decide the amount of equations that are solved for at each iteration.

The seeding used in my project assignment was set to one, which means that a beam element was created for each meter of geometrical beam. This was one of the main problems when reviewing the model efficiency. The finite element model utilized in this thesis uses a seeding density of 5, which results in beam geometry divided in two or three beam elements. The bridge deck which is simulated as beam elements is also seeded in the same fashion. This simplification reduces the element count from 11 609 to 2 569. Further discussion of the chosen seeding is shown

9.3 Time Domain Analysis

To assure a both reliable and efficient time domain analysis, time domain analyses were evaluated with the toggling between different time steps and the inclusion/exclusion of nonlinearities. The dynamic implicit equational solver regime is supposed to be unconditionally stable, but as time increments increase, the solution ends up jagged, which also distorts the frequency spectra and very high frequency waves might be neglected all together. A good fit will require small enough increments to include all frequencies and peaks, without being too troublesome regarding computational time.

Because this is a temporary stage in the model development other Eigenfrequencies are described than what is being presented in the final results. This should not influence the arguments regarding analysis time step requirements.

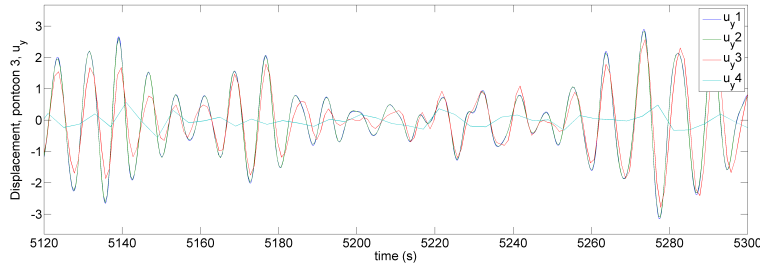
The results presented below are all inflicted with the same load pattern. It is not merely the same sea state, but the exact same incremental loads. The loads are specified for every 0.2 seconds for this exploration of the desired step size. Other load increments will be used in the final analysis. Abaqus will automatically linearly interpolate to obtain forces at any given point. That aspect may have an influence on results obtained from analyses using bigger than 0.2 seconds increments.

The time series tested lasts for 6000 seconds. Following step sizes are compared:

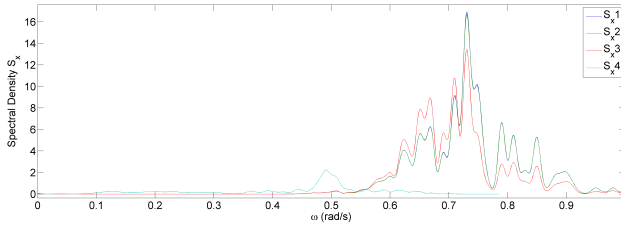
Table 9.2: Analysis description

Analysis no.	Time increment (s)	Computational time
1	0.02	30 hours
2	0.1	5 hours
3	1	34 minutes
4	4	10 minutes

As seen from above, it is important to find a suitable time step for the analysis to be effective, where a very small time step is time demanding. A small extraction from the time domain analysis and a spectral density plot, which utilizes Burgs method are presented on the next page:



(a) Time series



(b) Spectral density, view 1

Figure 9.2: Demonstration of time step influenced results

The time series display that a too large time step fails to include critical response patterns, both amplitudes and frequencies. It is seen that time series “4” is not corresponding to the rest of the results.

A dynamic analysis can’t register dynamic response with a period two times it’s time step. The first eigenperiod of the system is about 7.8 seconds, which means that a 4 second step is not sufficient for picking up any eigenfrequencies that might occur. This can be seen in the Spectral Density plot, where “4” abruptly stops at 0.7 rad/s .

It is also observed that time series “3” correspond to time series “1” and “2” for the lowest response peaks but doesn’t correspond adequately for higher frequencies. Time steps with a max value of 0.1 seconds are therefore chosen. The 0.02 second time step is rejected due to significantly longer computational time.

The half-increment residual algorithm described in chapter 3.2.1 was used. After a discussion with my supervisor, it was concluded that this process should be suppressed because of the use of residual error in the script that estimate hydrodynamic effects. The effects this change has on results will be discussed.

9.4 Nonlinearities

The bridge structure is built as a horizontal arch which causes geometric nonlinearities. This occurs because the beams will globally experience tension when moving upstream and compression when moving downstream. One of the main advantages of doing a time domain analysis to study dynamic response rather than committing to a purely frequency domain approach, is the accessibility of nonlinear effects.

The results from two time domain analysis are plotted below. As seen from the results, the movement is approximately identical when wave lengths are studied. The amplitude on the other hand is shifted due to these effects.

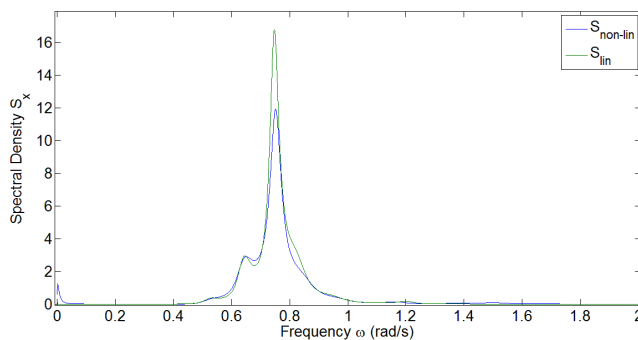


Figure 9.3: Nonlinear effects and linear effects compared, time domain

Since the results from this thesis will be compared to the results generated in Kvåle's thesis, the time domain analysis must be based on the same algorithms as Kvåle's spectral analysis. His analysis only include linear geometric effects, which means that this thesis will also focus on a linear time domain analysis. From a 6000 second time series, it is seen that the differences are minor. By studying the spectral density plot with Burgs algorithm employed it is seen that the same eigenfrequencies are present, but the peak in the spectral domain is lessened for the non linear analysis.

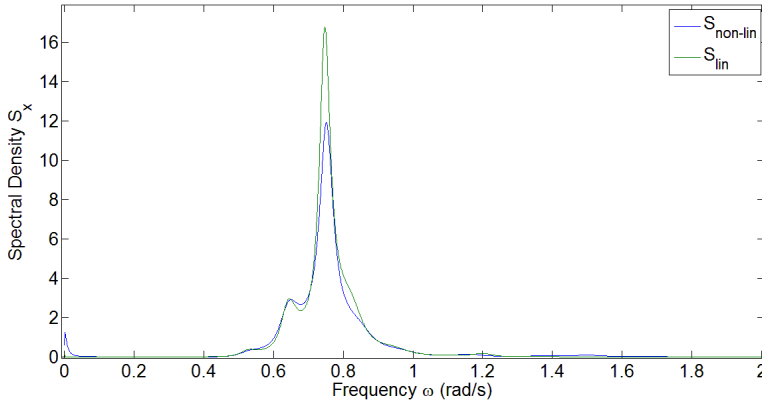


Figure 9.4: Nonlinear effects and linear effects compared for pontoon five, spectral density

The computational time is reduced significantly by only considering linear geometrical effects, and the possibility of doing longer time domain analyses is possible.

Table 9.3: Computational time

6000 seconds analysis	Computational time
Linear analysis	5 hours
Nonlinear analysis	11 hours

9.5 Differences in the Direct Implicit Method

The direct implicit method has a range of algorithmic settings. The main time series presented in the results uses the half-step residual increment setting and some numerical damping. A white noise analysis was submitted to assess the signification of these adjustments regarding the possibility of false results because of malimplementation of the FORTRAN-script.

Therefore were two identical stochastic white noise loads applied to two analyses, where one had these settings employed. The results show that the default settings has a marginal impact on the results for low frequency response. The difference in response become more apparent at higher frequencies, but the error is regarded as minor for my

final time series. The red plot indicate the time series without the half-step residual increment and the numerical damping. The difference in response can also be caused by the slightly lower numerical damping since the numerical damping is most effective on high frequency noise.

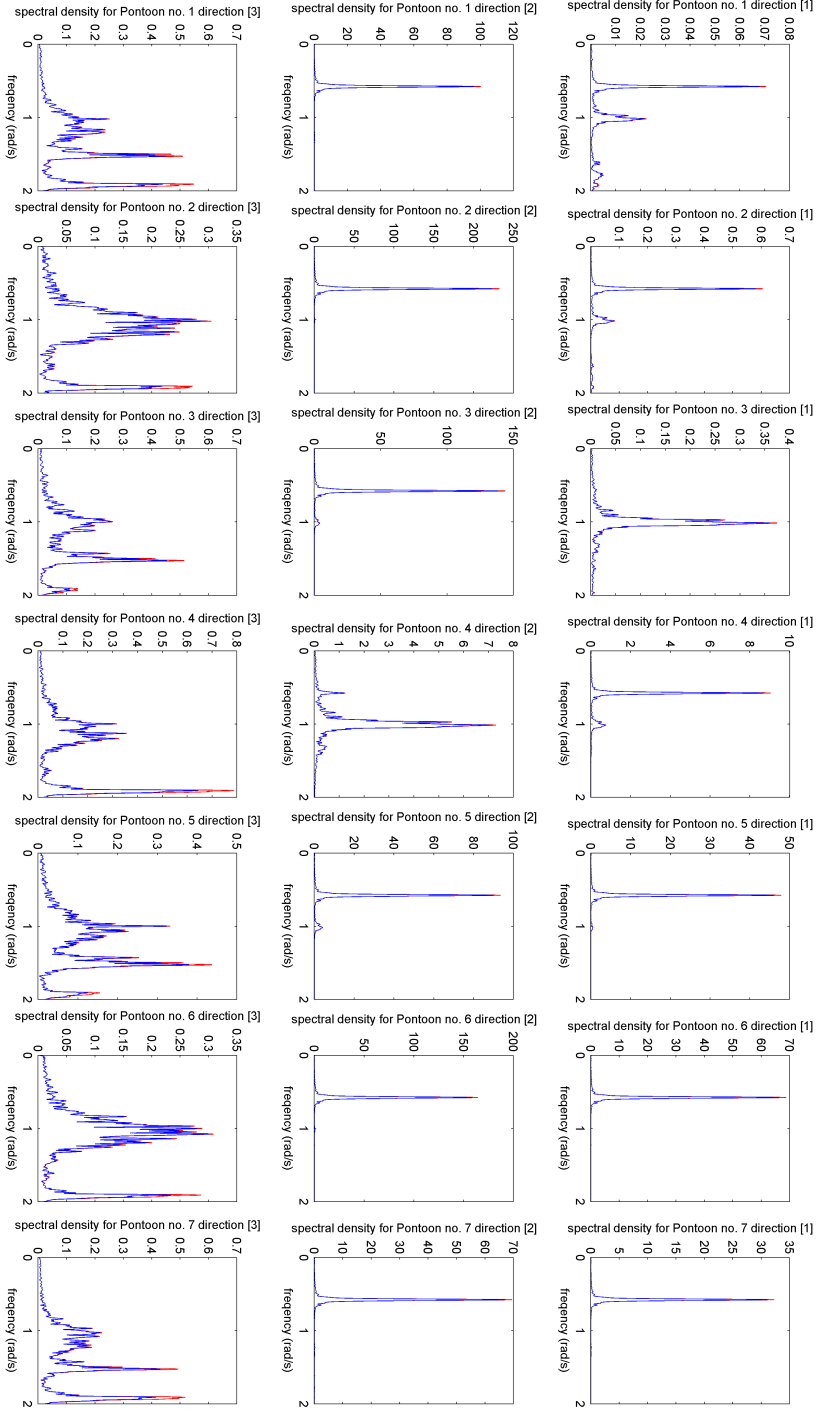


Figure 9.5: Direct implicit method with default and recommended setting

Part IV

Computational Results, Discussion and Conclusion

Chapter 10

Results

Results from the different analysis procedures will be presented in this part. Displacements are saved as field data in the ODB result file produced by Abaqus, and displacement information can be extracted from any given node.

The time domain analysis results are studied at the pontoon connection node for each of the seven pontoons. There are three reasons for using these nodes as reference points for extracting data. Firstly are the accelerometers that are employed at the Bergsøysund Bridge placed in proximity of the pontoons. Secondly because of Kvåle's calculations also originate from these points. The pontoon input nodes are also where the loads are applied.

The results will first be studied in the time domain, where plots of displacements, histogramical presentation of displacements and covariance between the pontoons will be examined. The time series that are examined, will be a combination of multiple time series, each lasting for 3000 seconds. The total of time series is ten, which means that the statistical foundation is based on 8 hours and 12 minutes of dynamic response due to a randomly generated sea state.

The time series will then be studied in the frequency domain. This is done to study which Eigenmodes are present, and to be able to compare the thesis results with Kvåle's results where coinciding results are welcome.

The illustration below is presented a second time because the different pontoons are often referred to due to varying results along the bridge. Making the overview easily accessible creates easier reviewable results. It is also noted that the pontoon design is different for pontoon one and seven, which explains the extra plots generated in the Wadam results.

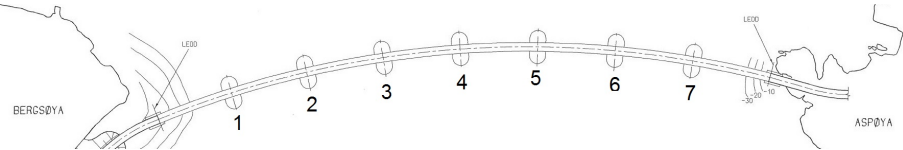


Figure 10.1: Pontoon numbering

10.1 Wadam Results

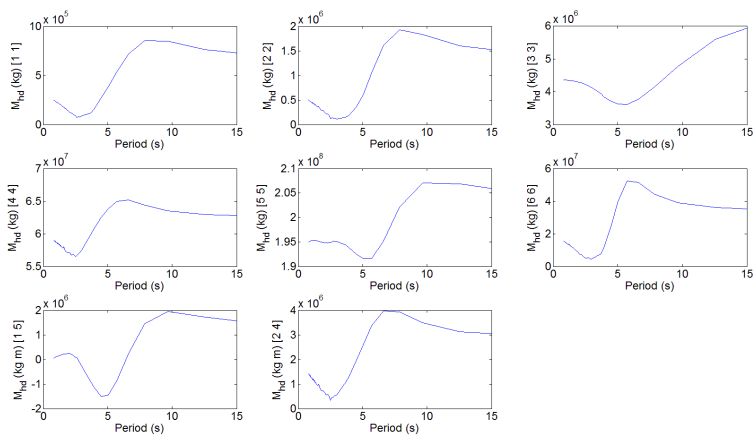
The Wadam analysis results are extracted as matrices, where each matrix is a discrete description of the added mass or added damping in a six degree of freedom system. The results are transformed from the center of gravity of the pontoon at hand to the pontoon-cross point that matches the location in the Abaqus FE-model within the Wadam software.

The transfer function which is developed from the added mass and damping according to equation 3.32 is also plotted. The results from the element analysis are presented below. A matrix is generated for each angular increment, but the angle of attack for the plots is set to zero. Specific results are shown, displaying degrees of freedom of considerable influence.

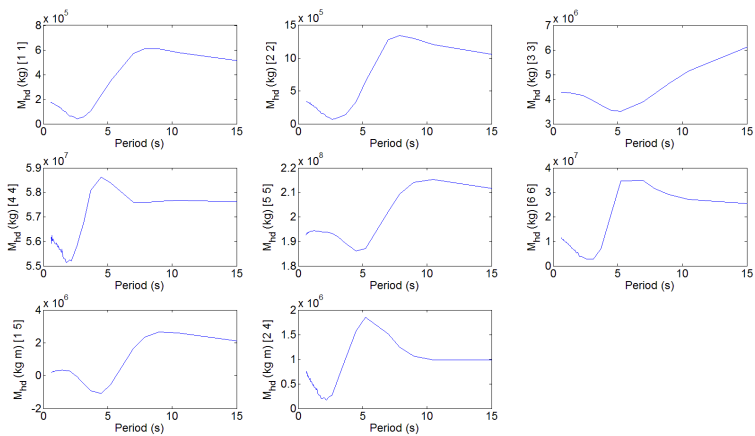
$$\mathbf{X} = \begin{bmatrix} X_{11} & 0 & 0 & 0 & X_{51} & 0 \\ 0 & X_{22} & 0 & X_{42} & 0 & 0 \\ 0 & 0 & X_{33} & 0 & 0 & 0 \\ 0 & X_{24} & 0 & X_{44} & 0 & 0 \\ X_{15} & 0 & 0 & 0 & X_{55} & 0 \\ 0 & 0 & 0 & 0 & 0 & X_{66} \end{bmatrix} \quad (10.1)$$

Where $X_{ij} = \{M_{hd,ij}, C_{hd,ij}\}$. The elements that are set to zero are small contributors that are not displayed here, but are included in the time domain analysis. The matrix is symmetric. The restoring force matrix is not frequency dependent, and is presented below for pontoon 2 to 6.

$$\mathbf{K}_{h,Pontoon\ 2-7} = \begin{bmatrix} 0 & 0 & 0 & 0 & 0 & 0 \\ 0 & 0 & 0 & 0 & 0 & 0 \\ 0 & 0 & 5.97 \cdot 10^6 N/m & -3.8 N & -8 Nm & 0 \\ 0 & 0 & 3.8 N & 1.4605 \cdot 10^8 Nm & -30 Nm & 0 \\ 0 & 0 & -8 Nm & -43.3 \cdot 10^6 Nm & 4.4 \cdot 10^8 Nm & 0 \\ 0 & 0 & 0 & 0 & 0 & 0 \end{bmatrix} \quad (10.2)$$

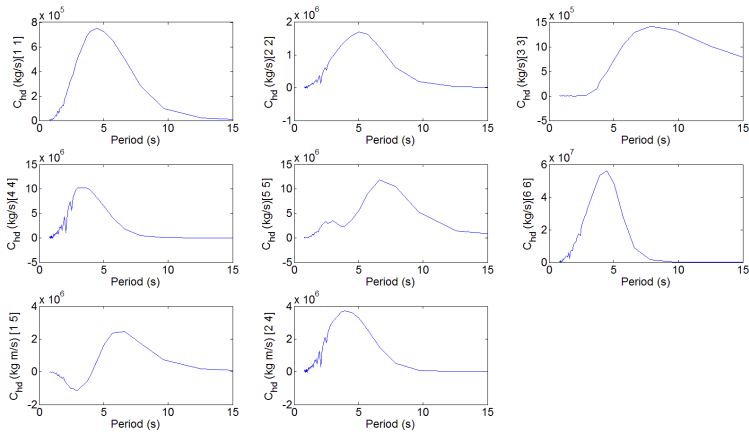


(a) Pontoon 1 and 7

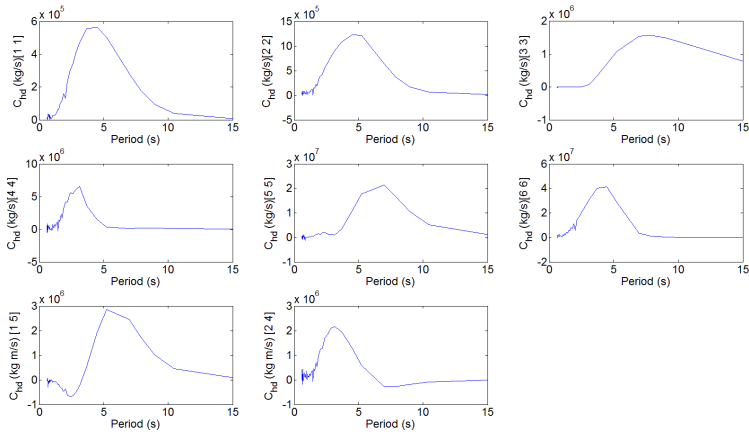


(b) Pontoon 2 to 6

Figure 10.2: Added Mass

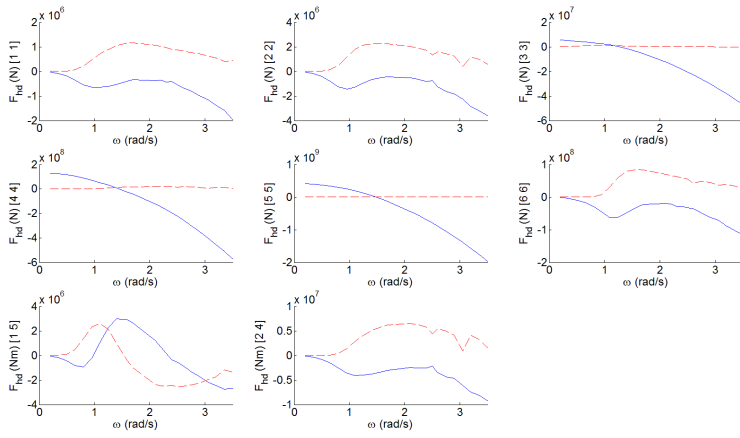


(a) Pontoon 1 and 7

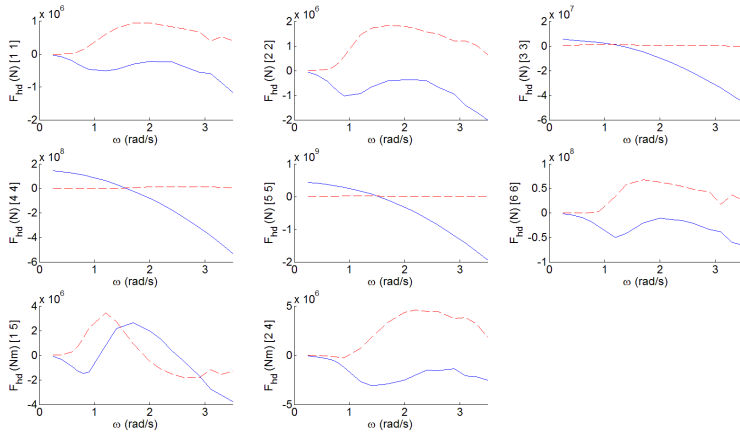


(b) Pontoon 2 to 6

Figure 10.3: Added Damping



(a) Pontoon 1 and 7



(b) Pontoon 2 to 6

Figure 10.4: Transfer function

10.2 Eigenfrequency and Eigenmode Results

An iterative routine that was described in equation 3.29 was completed, and the following results were extracted. This includes the manual iteration method where added mass for the eigenfrequency at hand is estimated.

These values are important when identifying which eigenmodes that are present in the time domain evaluation in this thesis. The frequency of the mode is also of interest, because a spectral analysis of the time domain results will tend towards one or more frequencies.

The frequency analysis has also been in use for the extraction of damping values and to effectively identify changes to mass and stiffness due to minor changes to the finite element model. The majority of the modes are generating eigenvectors in one plane and it is therefore noted that the results are presented in different axis. This is done for an easier grasping of the eigenmode at hand. The plane that the snap shots are taken from is illustrated with the small axis cross in each plot below.

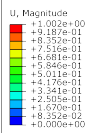
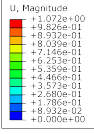
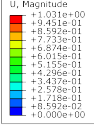
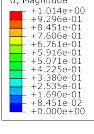
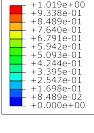
Mode no.	Frequency (cycle/s)	(rad/s)	Mode
1	0.0900	0.565	 <p>U, Magnitude +1.002e+00 +9.187e-01 +8.352e-01 +7.516e-01 +6.681e-01 +5.846e-01 +5.011e-01 +4.176e-01 +3.341e-01 +2.505e-01 +1.670e-01 +8.352e-02 +0.000e+00</p> <p>Y X ODB: freq.odb Abaqus/Standard 6.12-1 Sun Jun 02 11:49:53 W. Europe Daylight Time 2013 Step: Step 2 Mode 1: Value = 0.31975 Freq = 8.99963E-02 (cycles/time) Primary Var: U, Magnitude</p>
2	0.15116	0.949	 <p>U, Magnitude +1.072e+00 +9.822e-01 +8.932e-01 +8.039e-01 +7.146e-01 +6.220e-01 +5.339e-01 +4.460e-01 +3.572e-01 +2.680e-01 +1.786e-01 +8.932e-02 +0.000e+00</p> <p>Y X ODB: freq.odb Abaqus/Standard 6.12-1 Sun Jun 02 11:59:34 W. Europe Daylight Time 2013 Step: Step 2 Mode 2: Value = 0.89911 Freq = 0.15091 (cycles/time) Primary Var: U, Magnitude</p>
3	0.16127	1.013	 <p>U, Magnitude +1.031e+00 +9.451e-01 +8.552e-01 +7.733e-01 +6.874e-01 +6.011e-01 +5.153e-01 +4.296e-01 +3.437e-01 +2.578e-01 +1.718e-01 +8.582e-02 +0.000e+00</p> <p>Y X ODB: freq.odb Abaqus/Standard 6.12-1 Sun Jun 02 12:30:22 W. Europe Daylight Time 2013 Step: Step 2 Mode 3: Value = 1.0267 Freq = 0.16127 (cycles/time) Primary Var: U, Magnitude</p>
4	0.16556	1.040	 <p>U, Magnitude +1.014e+00 +9.296e-01 +8.451e-01 +7.506e-01 +6.761e-01 +5.916e-01 +5.071e-01 +4.227e-01 +3.380e-01 +2.535e-01 +1.690e-01 +8.451e-02 +0.000e+00</p> <p>Z X ODB: freq.odb Abaqus/Standard 6.12-1 Sun Jun 02 12:30:22 W. Europe Daylight Time 2013 Step: Step 2 Mode 4: Value = 1.0777 Freq = 0.16522 (cycles/time) Primary Var: U, Magnitude</p>
5	0.19019	1.195	 <p>U, Magnitude +1.019e+00 +9.338e-01 +8.489e-01 +7.540e-01 +6.791e-01 +5.942e-01 +5.093e-01 +4.244e-01 +3.395e-01 +2.547e-01 +1.698e-01 +8.489e-02 +0.000e+00</p> <p>Z X ODB: freq.odb Abaqus/Standard 6.12-1 Sun Jun 02 12:45:17 W. Europe Daylight Time 2013 Step: Step 2 Mode 5: Value = 1.4280 Freq = 0.19019 (cycles/time) Primary Var: U, Magnitude</p>

Table 10.1: Eigenfrequencies and Eigenmodes

Additional eigenfrequencies and eigenmodes are presented beneath. These modes are prominent in the white noise time domain example that is readily compared to the frequency domain analysis. The snap through mode is also included, due to concern regarding the possibility of the occurrence of snap through in the structure.

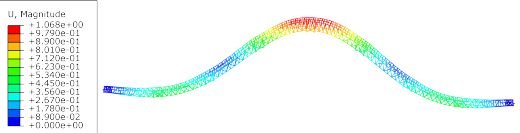
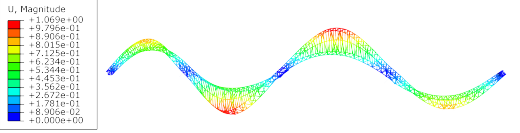
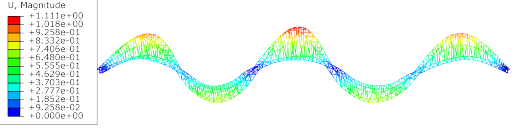
Mode no.	Frequency (cycle/s)	(rad/s)	Mode
6	0.20693	1.300	 <p>U, Magnitude +1.068e+00 +9.790e-01 +8.900e-01 +8.010e-01 +7.120e-01 +6.230e-01 +5.340e-01 +4.450e-01 +3.560e-01 +2.670e-01 +1.780e-01 +8.900e-02 +0.000e+00</p> <p>Y Z X QDB: freqny.odb Abaqus/Standard 6.12-1 Sun Jun 02 16:23:59 W. Europe Daylight Time 2013 Step: Step 2 Mode: 6; Value = 1.7508 Freq = 0.21059 (cycles/time) Primary Var: U, Magnitude</p>
8	0.23735	1.491	 <p>U, Magnitude +1.069e+00 +9.796e-01 +8.906e-01 +8.015e-01 +7.125e-01 +6.234e-01 +5.344e-01 +4.453e-01 +3.562e-01 +2.672e-01 +1.781e-01 +8.905e-02 +0.000e+00</p> <p>Z X Y QDB: freqny.odb Abaqus/Standard 6.12-1 Sun Jun 02 16:23:59 W. Europe Daylight Time 2013 Step: Step 2 Mode: 8; Value = 2.2239 Freq = 0.23735 (cycles/time) Primary Var: U, Magnitude</p>
11	0.30363	1.908	 <p>U, Magnitude +1.111e+00 +1.018e+00 +9.288e-01 +8.332e-01 +7.408e-01 +6.489e-01 +5.575e-01 +4.629e-01 +3.703e-01 +2.777e-01 +1.852e-01 +8.258e-02 +0.000e+00</p> <p>Z X Y QDB: freqny.odb Abaqus/Standard 6.12-1 Sun Jun 02 16:23:59 W. Europe Daylight Time 2013 Step: Step 2 Mode: 11; Value = 3.7502 Freq = 0.30821 (cycles/time) Primary Var: U, Magnitude</p>

Table 10.2: Additional Eigenfrequencies and Eigenmodes

10.3 Time Domain Results

The time domain analysis was completed with the model described in figure 8.2 and parameters developed in Part III. Hydrodynamic and hydrostatic effects are included. Wave action forces are applied and the desired time steps are used. Firstly was the response for each pontoon node studied. It was observed that the movements were similar for pontoon one, two, three, five, six and seven. This group of pontoons moves mostly in the surge direction. Pontoon four moves in heave and yaw.

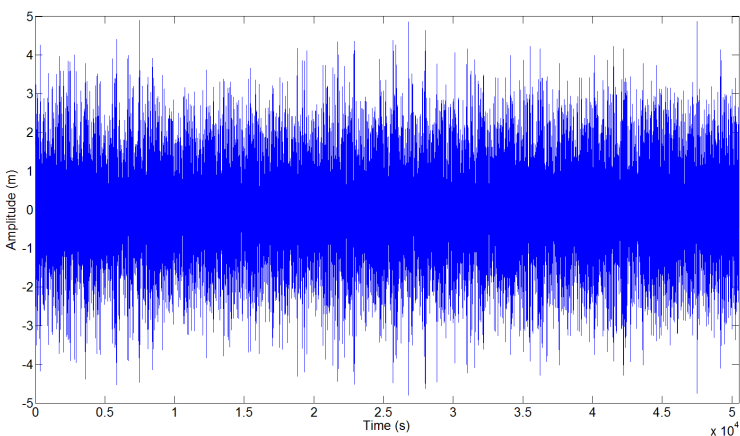
The results presented in big formats are from a data selection of the pontoon nodes. Variance will be presented, which support this choice.

10.3.1 Time Series Response

When evaluating the results in the frequency domain, auto spectral densities are artificially generated for frequencies approaching zero. The response is therefore presented in the time domain with only one configuration. To avoid the initial noise generated from the first, mainly static movement, a shift for each added time series is applied. The shift removes the initial 25 seconds of every time series.

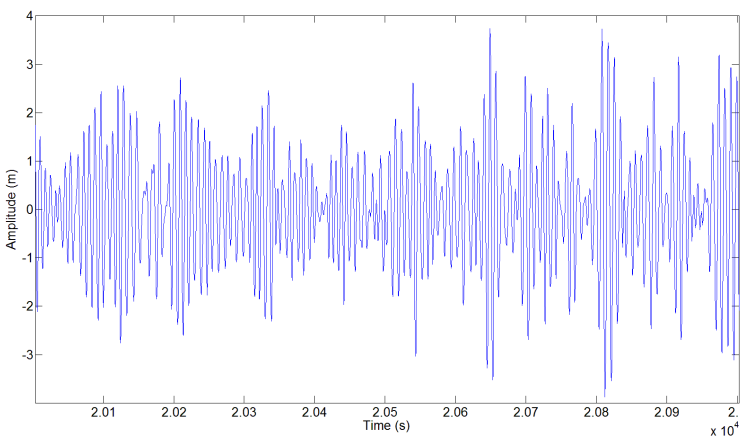
Time Series Plot

Figure 10.5 demonstrates that the time series response appears to be unrepetitive and that the response oscillate about zero. Figure 10.6 display typical response presented as a field output animation, where the color scheme gives easily interpretive results. The caption indicates a magnification factor of the displacements and the actual magnitude of the response is presented in the color scheme table.



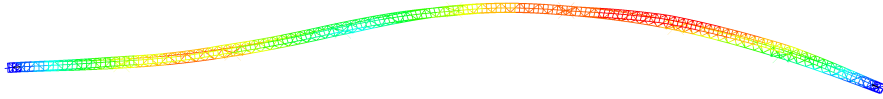
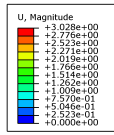
(a) Complete time series

mm

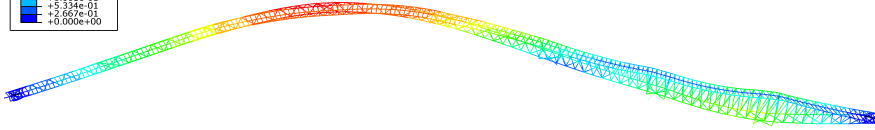
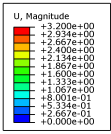


(b) 1000 seconds extraction

Figure 10.5: Time series, pontoon 1, y-direction



(a) 10x magnification

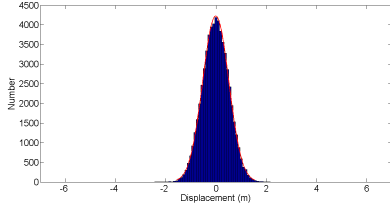


(b) 20x Magnification

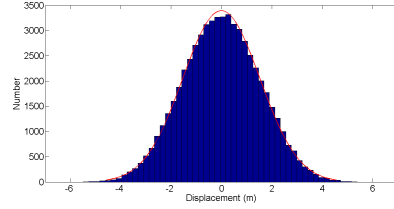
Figure 10.6: Snapshots from time series animation in the x-y-plane. Color coding describes displacements

Histogram Presentation

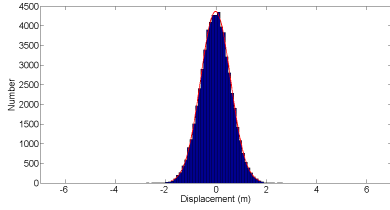
The histogram presentation is divided into 50 bins. The y-axis describes the number of time increments that gives the response for that specific bin. The histogram gives insight in the distribution of displacements in the time domain.



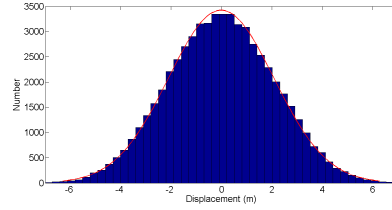
(a) Pontoon 4, sway



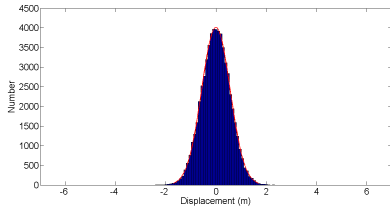
(b) Pontoon 6, sway



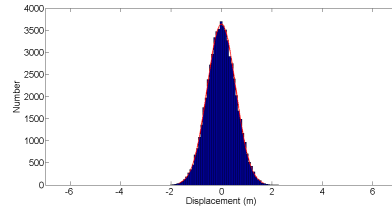
(c) Pontoon 4, surge



(d) Pontoon 6, surge



(e) Pontoon 4, heave



(f) Pontoon 6, heave

Figure 10.7: Histogram representation of displacements

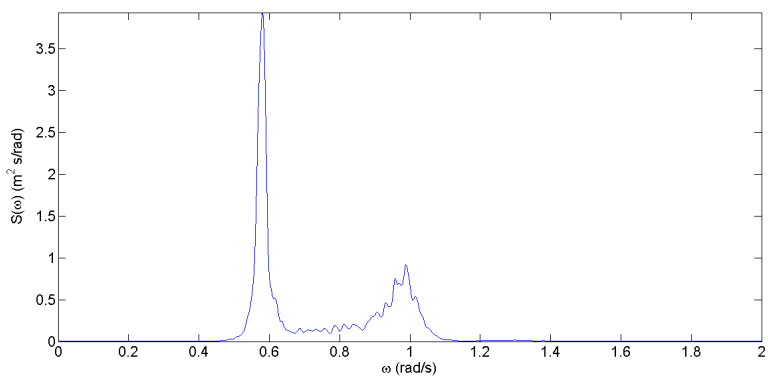
10.3.2 Auto Spectral Densities for the Time Domain Analysis

To evaluate which eigenfrequencies that are present in a time domain analysis a Fourier transformation to the frequency domain is essential. This allows for a more thorough interpretation of the results. The FFT tool that is used is Welch's method which is described at section 4.2. The time series is divided into 20 bins and a window function that include 50 time increments on either side of each bin is employed. The Auto Spectral Density describes the displacement in the frequency domain.

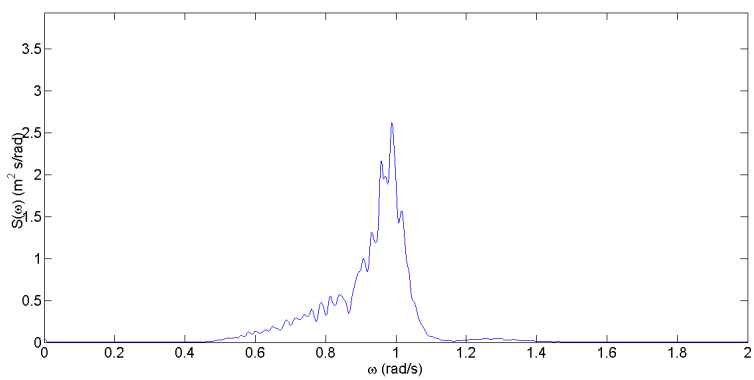
The coordinate system used in this thesis can be tedious to interpret when comparing the auto spectral densities for different points along the structure. Basic transformation procedures of the coordinate system display the results for each pontoon in its local coordinate system in sway, surge and heave.

Table 10.3: Displacement variance for time series

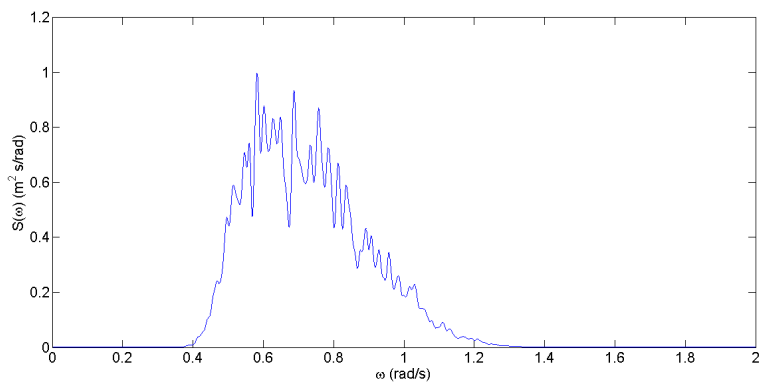
	Pontoon no.						
	1	2	3	4	5	6	7
Sway	0.681	1.325	0.564	0.268	1.867	2.327	0.955
Surge	1.648	4.268	2.880	0.350	2.924	4.396	1.775
Heave	0.174	0.311	0.318	0.317	0.317	0.317	0.181



(a) Sway

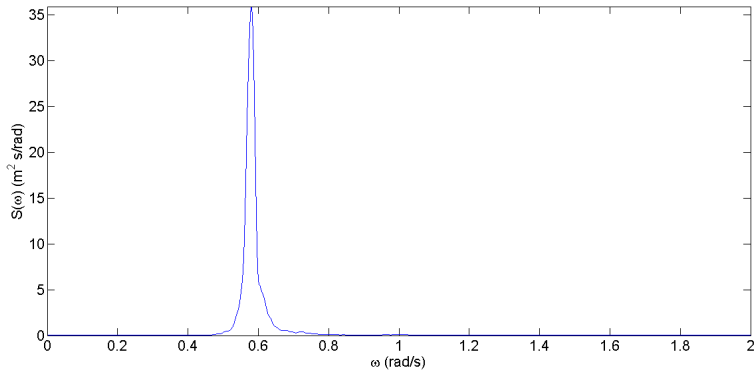


(b) Surge

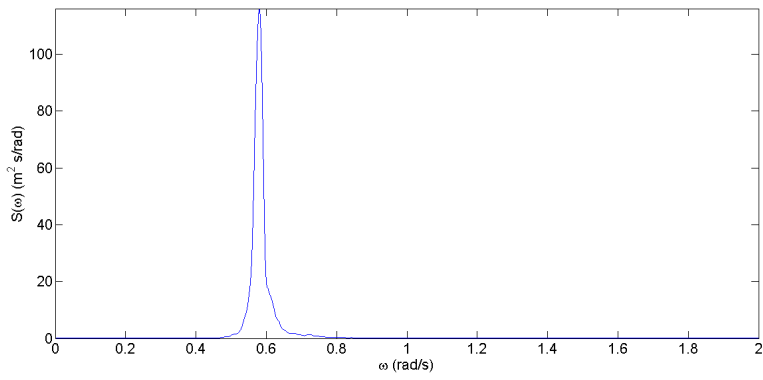


(c) Heave

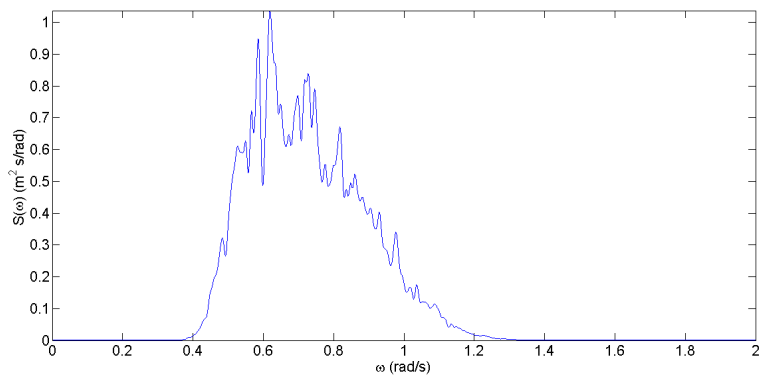
Figure 10.8: Auto Spectral Densities, Pontoon four



(a) Sway



(b) Surge



(c) Heave

Figure 10.9: Auto Spectral Densities, Pontoon two

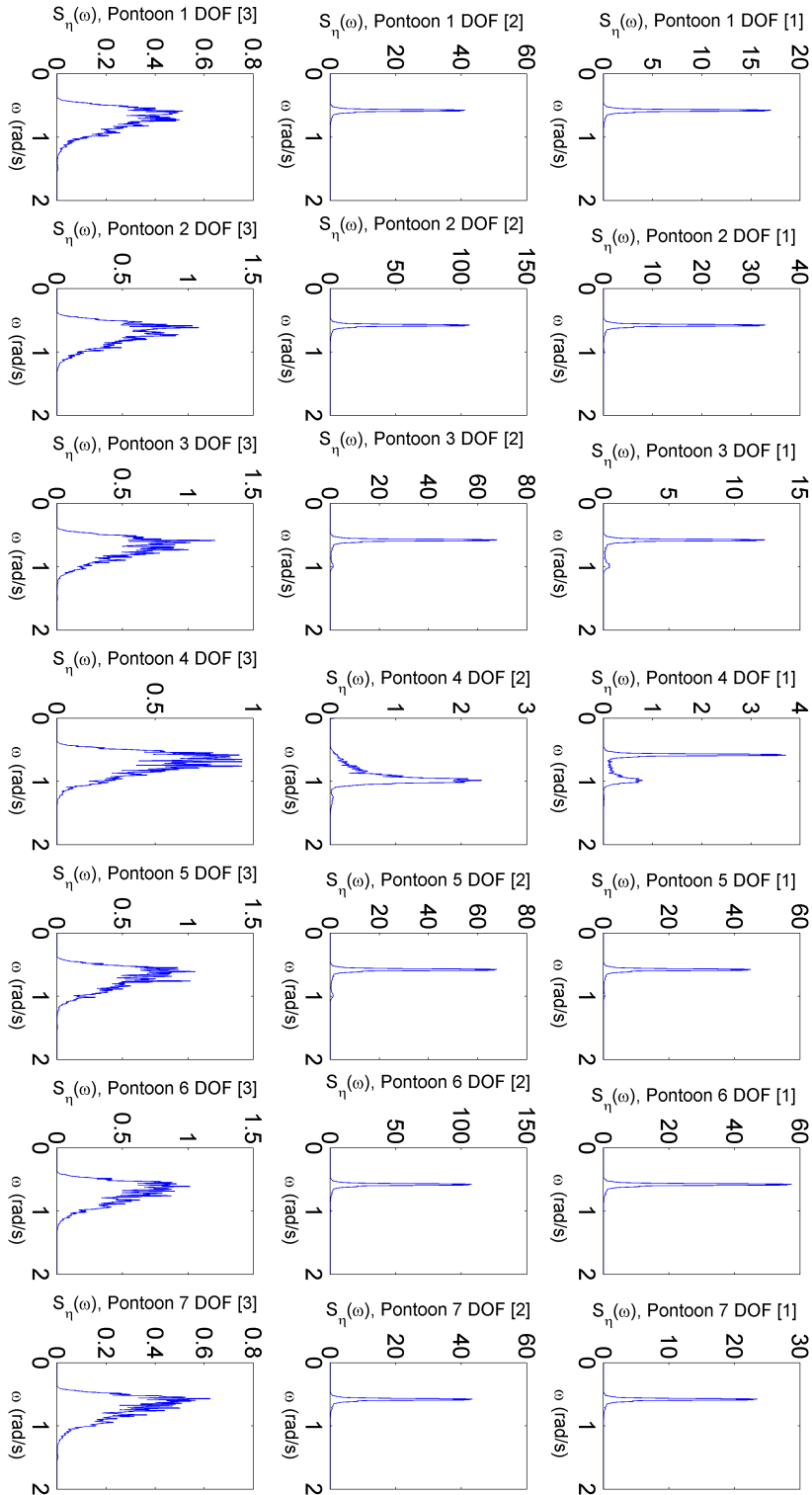


Figure 10.10: All Auto Spectral Densities regarding displacement

Covariance

Eigenmode one's presence in the time domain will be discussed. As seen in earlier results, Eigenmode one is an antisymmetrical mode, which fluctuates angularly about pontoon four. The response of pontoon two and its antisymmetrical counterpart, pontoon six, is plotted below.

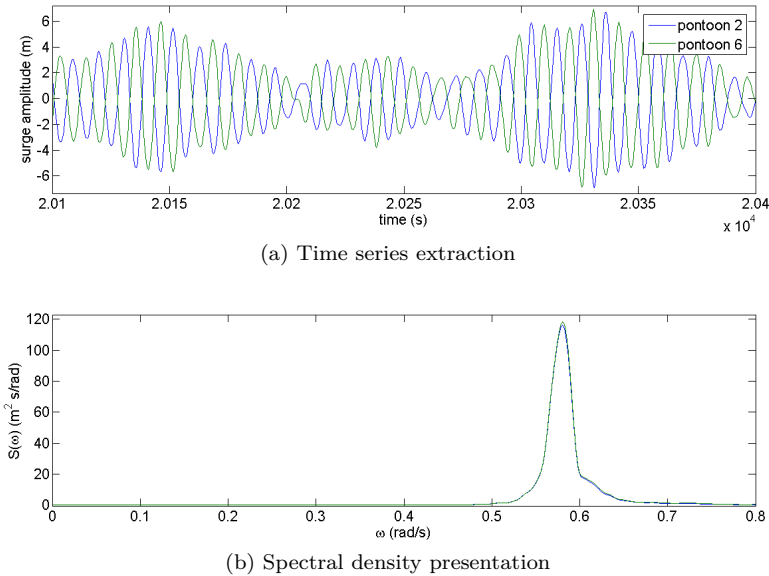


Figure 10.11: Presentation of covariance, pontoon two and six

10.3.3 White noise

It is observed in appendix A that the sea loads employed for Kvåle's frequency domain analysis and the time domain analysis presented in this thesis are not equal in magnitude. The analyses did render different response results as well and a white noise analysis was considered an appropriate approach for diminishing the incoherent input values.

The white noise used was developed according to chapter 2.3, and the following values were used:

Table 10.4: Values used for white noise

$\Delta\omega$	0.002 rad/s
ω_{max}	2 rad /s
F	$1 \cdot 10^6$ N (Nm)
Δt	0.1 s
t_{max}	3000 s

Results from our analyses are presented in 10.12. The red lines indicate results from the frequency domain analysis and the ragged blue line are results from the time domain analysis.

Table 10.5: Percentage difference between time domain and frequency domain analysis

Pontoon no.							
Variance	1	2	3	4	5	6	7
DOF 1	5.772 %	7.723 %	1.638 %	3.706 %	6.314 %	7.343 %	7.988 %
DOF 2	7.122 %	7.779 %	8.212 %	1.586 %	4.711 %	6.901 %	7.682 %
DOF 3	12.218 %	6.257 %	10.486 %	14.757 %	9.074 %	1.942 %	9.617 %

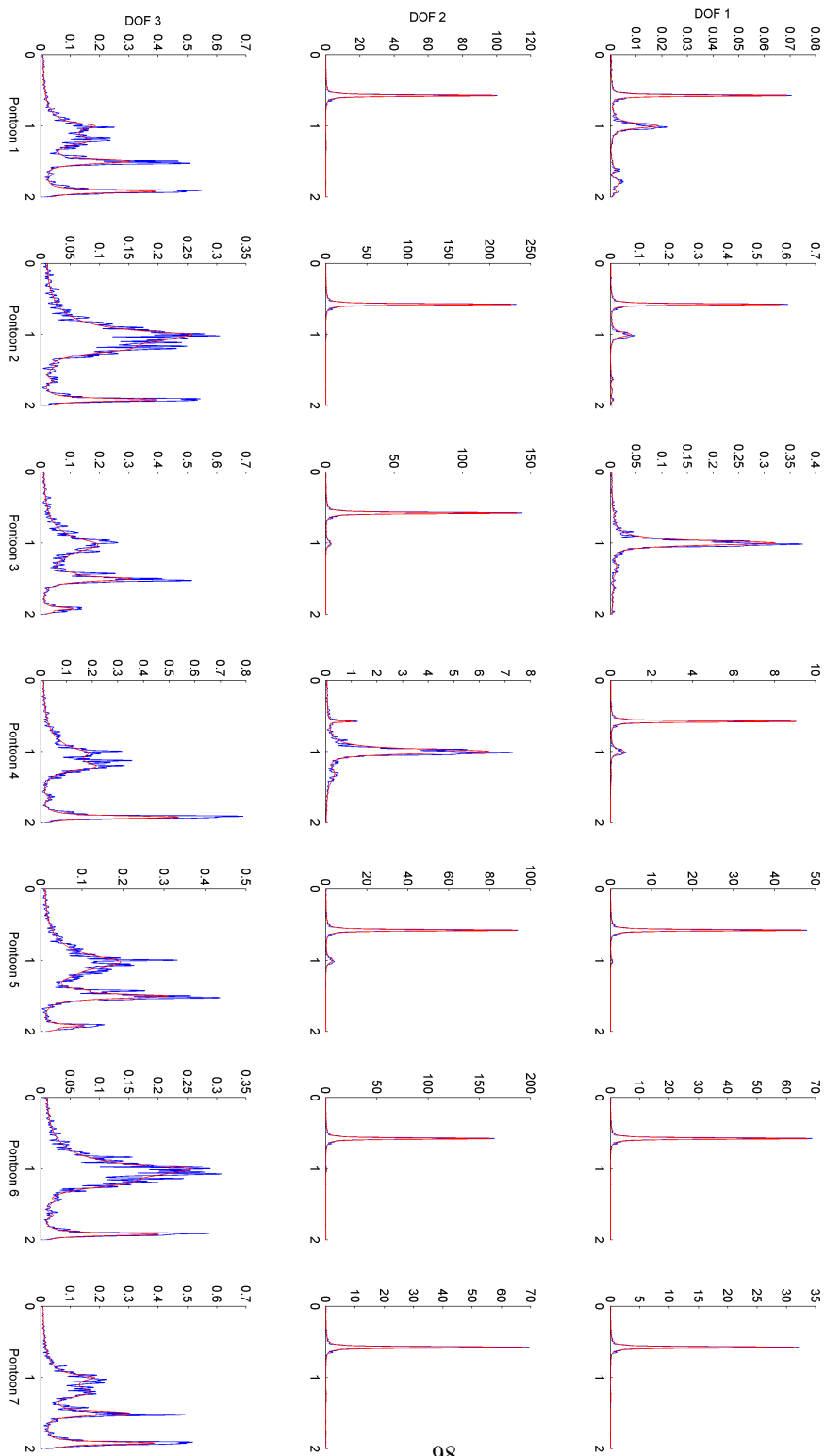


Figure 10.12: Auto Spectral Density of displacement

Chapter 11

Discussion

11.1 Wadam Discussion

The results generated from the Wadam software are able to display both the added mass and added damping in a reasonable fashion. The restoring stiffness in heave corresponds to hand calculations done in accordance with section 2.4.1. It can be seen from the results in chapter 10.1 that the modeling of two pontoons was necessary because of noticeable differences in added mass and damping. For the most prominent frequency value in the time domain analysis (0.09 cycles/s) the added mass difference in surge is 33% larger for the bigger pontoons.

Skepticism towards the FE-analysis describing the pontoon effects is present due to high frequency noise for added mass and damping. The noise appears in the period range of 1 and 2.5 seconds. The corresponding frequencies are $\frac{4}{5}\pi \text{ rad/s}$ and $2\pi \text{ rad/s}$. There are no eigenfrequencies for the system at this range, and it is also readily seen from the spectral density plot that there is neglectable response at this range of frequencies. Results obtained from the time domain analysis indicate where the response is most prominent in the frequency interpretation of the results. A new Wadam analysis with smaller increments in the range of dominant response would be preferable to assure accurate hydrodynamic transfer functions for this given system.

This extra ballast mass was not included in the final analysis because the ballast for each pontoon was only between 2% and 10% of the total mass of the pontoon in

question and there is no data available concerning the ballast in the finished bridge. Compared to the added mass for critical frequencies, the extra ballast discussed in chapter 5 is regarded as neglectable.

11.2 Wave Action Discussion

The waves that are developed for this thesis does seem to display long crested waves in a reasonable fashion. As noted earlier, the sea state is not an accurate reproduction of the sea in the Tingvoll fjord. With a third of the wave amplitudes peaking at more than 4 meters the external forces are assumed larger than a normal sea state at Tingvoll. The incorporation of significant wave forces permits for dynamic response, but the response in heave is mostly a static response to the forces than a dynamic response.

The bridge structure is symmetric about pontoon four, and from the response results in section 10.3 indicated that the response should be antisymmetric for pontoon three and five. There is a notable difference in auto spectral densities and variance in sway for the two antisymmetrical pontoons. This can indicate an unsymmetrical load or model. By comparing auto spectral densities for surge, which is the direction of most prominent response, there are coterminous results in the antisymmetrical pontoons, regardless of the slight difference in sway.

The wave action time domain input has been compared to Kvåle's wave action spectral densities. Our input values do not seem to mach perfectly, and there is reason for questioning the legitimacy of the wave action coherence between our simulations. Since the source of error is unidentified it would be recommended to do a study of the difference in input. The force amplitude is the major difference, and becomes especially apparent in surge. The greater surge forces in my analysis can cause the difference in auto spectral densities.

Because of uncertainty regarding input, white noise was also employed. By this simplification, there should be neglectable difference in force input and the results can verify the legitimacy of the correlation between the models and analysis methods used in our master thesis.

11.3 Abaqus Time Domain Analysis Discussion

The Eigenfrequency analysis in this thesis display results that indicate the proper implementation of frequency dependent properties. A major indication of correct implementation of hydrodynamics is that the iterative method described in section 3.2.1 influence the extractable eigenvalues and eigenfrequencies. The analysis done in the thesis produces lower eigenfrequencies compared to project assignment results. The results indicate bigger mass due to the implementation of added mass. Restoring forces which stiffen the structure are also included, but are not considered to cause significant shifts in eigenfrequency values due to the mostly horizontal eigenvector where restoring forces are lacking.

The implementation of the FORTRAN-script which includes hydrodynamics in the time domain analysis is of special interest. Ideally can a nonlinear implicit dynamic analysis with frequency dependent effects give crucial information about nonlinear dynamic response. The spectral analysis of the time series should indicate whether the data extracted from Wadam is properly implemented.

For an ordinary dynamic analysis where dynamic response is dominating the results, there should be a perfect concurrence between Eigenfrequencies and response frequencies if the loading and damping conditions allow for it. Due to identical mass and stiffness matrices is this result anticipated.

In this thesis the hydrodynamics are implemented with two different methods. In the eigenvalue analysis the correct added mass and damping is calculated for a given frequency with an iterative and straight forward process described in chapter 3.2.2. For the time domain analysis are the hydrodynamics calculated from residual error at each time step. Corresponding results between the two methods are therefore crucial. Particularly important is it for the legitimacy of the residual based method because it is the method most prone to malimplementation due to its complexity .

The spectral peaks in the time series correspond adequately with the estimated Eigenfrequencies one and three. These results support that the external scripts in the dynamic implicit analysis are running properly. To illustrate this further, figure 11.1 has the combination of eigenvalues from the eigenfrequency analysis and the spectral response from time series plotted. Pontoon four in sway is used in the illustration bellow because of different modal contributors.

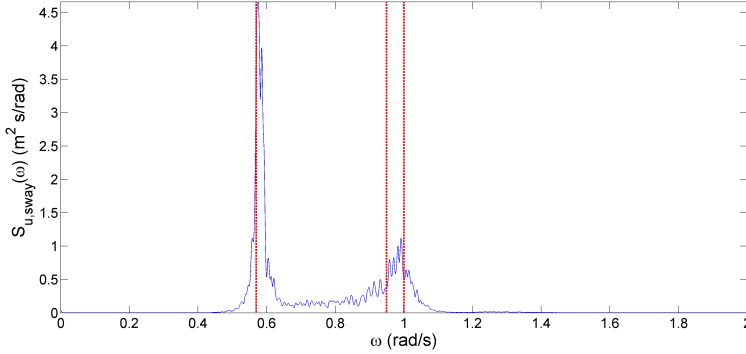


Figure 11.1: Spectral Density and Eigenfrequencies, Pontoon 4, sway

Observations indicate a correspondence between the two methods, although the auto spectral tops are not synonymous with the lines indicating Eigenfrequencies. The frequency differences are ranging between 1-2% and can appear due to numerical simplifications or damping in the system.

Kvåle has used the same FE-geometry as presented in this thesis. The compared white noise analysis results should therefore yield similar results given that the external forces or the method of implementing hydrodynamics do not differ. Insufficient data basis or misinterpretation of results can cause differing results. The results correspond excellently without much considerable error. Slight differences in variance can emerge due to the short time series of 3000 seconds.

The time domain analysis and the frequency domain analysis are showing the same tendencies which indicate that the methods are giving similar results. The small differences in the spectral domain can come from numerical differences since Kvåle uses a definite spectral value, $S_{Force} = 10^{12}$, and the time series is based on random values. The implications of the start up period in the time domain can also cause slight differences. The numerical dynamic implicit method can also add to the cumulative difference. But the results are satisfactorily and the comparison is regarded as a success.

The analysis method presented and utilized in this thesis will forth most be used in analyses with nonlinear geometry. The first problem to be addressed in the initial design possess of the Bergsøysund Bridge was the probability of snap through. Snap through is a nonlinear geometric process where a typical arch can be pushed in,

causing radical changes in stress distribution. The occurrence of such an event for the Bergsøysund Bridge, or in a future floating bridge will be disastrous, and correct assessment of the issue is vital.

The application described in this thesis is able to perform an analysis with geometric nonlinearities. This is seen from chapter 9.4, where the linear and nonlinear analysis have matching tendencies where differences in response are assumed to be due to the geometric nonlinearities which are being studied.

Chapter 12

Conclusions

This master thesis has been addressing the problem description presented in chapter 1.3 and results obtained from a range of analyses have been discussed. Concluding remarks regarding my findings are presented below.

The time domain analysis of the Bergsøysund Bridge has been rewarding in regard of the study of the possibility of doing nonlinear analyses in the time domain for new structures. The implementation of hydrodynamic effects in Abaqus can become a crucial tool for the study of dynamic response when geometric nonlinearities must be considered.

The simplifications in the FE-model which is developed in Part III are deemed necessary. When developing new methods for calculating hydrodynamic response an effective and uncomplicated model is recommended. Simulating a real structure, like the Bergsøysund Bridge, is an advantage even if it complicates the implementation of the newly developed methods. This is desirable due to the emergence of issues that will appear at some step in the progress can be assessed early on in the development process. The modeling of an existing structure also opens for system identification procedures when measured data can be used as a basis.

The nodal approach representing the pontoons has turned out to be an effective way for implementing effects caused by the structure-water interaction. The sea loads were

implemented to the Abaqus time domain analysis by this approach. The FORTRAN-script developed at The Department of Structural Engineering at NTNU, which is mathematically described in chapter 3.2.4, transform the frequency dependent effects to a purely time dependent input that utilizes incremental information regarding residual error which then opens up for the possibility for doing frequency dependent time series.

The legitimacy of the analysis method is verified by considering the comparison of the eigenvalue solution and the frequencies which the structure oscillates in the time domain. This is illustrated in figure 11.1 where the first eigenfrequency from the eigenvalue analysis coincide with a response peak in the auto spectral domain.

Dynamic response solutions in the frequency domain presented in section 10.3.3 does also exhibit the same tendencies as my time domain analysis when white noise loads are used. This is an important achievement that will simplify the further work. The coinciding results support that the correct implementation of pontoon mass and hydrodynamic effects was employed.

Difference in sea loads is identified as the source of error when results are compared. Apart from the difference in the sea spectra used by Kvåle and me, the sea loads have been shown to display reasonable sea characteristics as coherent sea loads on the structure are implemented. The results from the Wadam-software have appeared to be implementable in the Abaqus software and as transfer functions for the sea load development.

The analysis with nonlinear geometric effects yields satisfactory results. Difficulties with nonlinearities in the frequency domain solution can be assessed by comparing results with the nonlinear time domain analysis in future work.

Chapter 13

Further Work and Source of Error

When the data from the accelerometers deployed at the bridge has been interpreted a new verification process of the FE-model should be done. Stiffness and mass properties should then be compared with measured data. The bridge deck developed in Cross-X software might render a too slack structure and should be studied closer to verify its properties. The wave action forces used in this thesis did not give the same results as in Kvåle's thesis. The spectrum used for the two types of analysis should be compared and similar force spectra should be attained.

Because similar results were obtained in this thesis compared to the results in Knut Andreas Kvåle's thesis further development of a frequency domain algorithm with nonlinear geometric tendencies is possible. The methods illustrated in this thesis can be used as a comparison when this is being developed. To base this further work on the Bergsøysund Bridge can be recommended because of a numerically effective and accurate model.

Bibliography

- [1] *Abaqus 6.09 Abaqus Theory Manual*, 2009.
- [2] *Abaqus 6.11 Keyword Reference Manual*, 2011.
- [3] John J. Bertin. *Aerodynamics for Engineers*. Person Education, Inc, 2009.
- [4] E.O Brigham. *The fast Fourier transform*. Englewood Cliffs, N.J, 1974.
- [5] Y.T. Chan, Q. Ma, H.C. So, and R. Inkol. Evaluation of various fft methods for single tone detection and frequency estimation. In *Electrical and Computer Engineering, 1997. Engineering Innovation: Voyage of Discovery. IEEE 1997 Canadian Conference on*, volume 1, pages 211–214 vol.1, 1997.
- [6] D.S. Malkus Cook, R.D. and M.E. Plesha. *Concepts and applications of finite element analysis*. 1989.
- [7] O. M. Faltinsen. *Sea loads on Ships and Offshore Structures*. 1990.
- [8] Langen Ivar. *Frequency Domain Analysis of a Floating Bridge Exposed to Irregular Short-crested Waves*. SINTEF, 1980.
- [9] Langen Ivar and Sigbjörnson Ragnar. *Dynamisk Analyse av konstruksjoner*. Tapir, 1979.
- [10] O.V. Bleie K. Bell and L. Wollebæk. *Cross-X, User manual*. 2000.
- [11] Kvåle Knut Andreas. *Dynamic Analysis of the Bergsøysund Bridge in the Frequency Domain*. NTNU, 2013.
- [12] Erwin Kreyszig. *Advanced engineering mathematics- 9th ed*. Laurie Rosatone, 2006.

- [13] Øiseth Ole, Suyuthi Abdillah, Kjell Magne Mathisen Bernt, Leira, Rönquist Anders, Sigbjörnson Ragnar, and Svein Remseth. Prediction of wave induced dynamic response in time domain using the finite element method. 2013.
- [14] Øiseth Ole, Suyuthi Abdillah, Mathisen Kjell Magne, Sigbjörnson Ragnar, and Kvåle Knut Andreas. Meeting at tyholt, marinteknisk senter, otto nielsens vei 10, 2013.
- [15] E. VanMarcke. *Random Fields: Analysis and Synthesis*. MIT Press, Cambridge MA, 1983.
- [16] Statens Vegvesen. *Concrete drawings*. 1991.
- [17] Statens Vegvesen. *Steel drawings*. 1991.

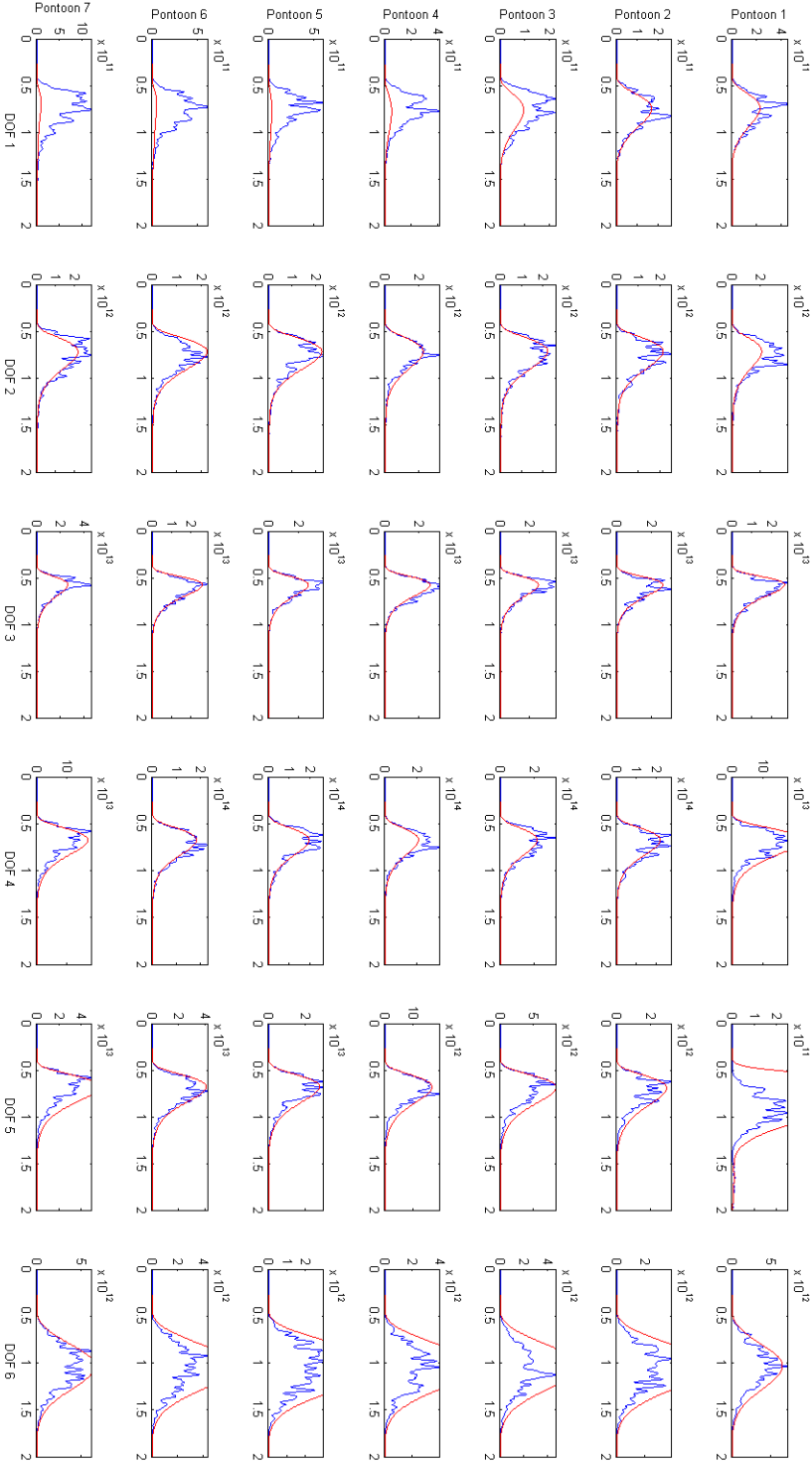
Part V

Appendix

Appendix A

Comparison of Sea Loads

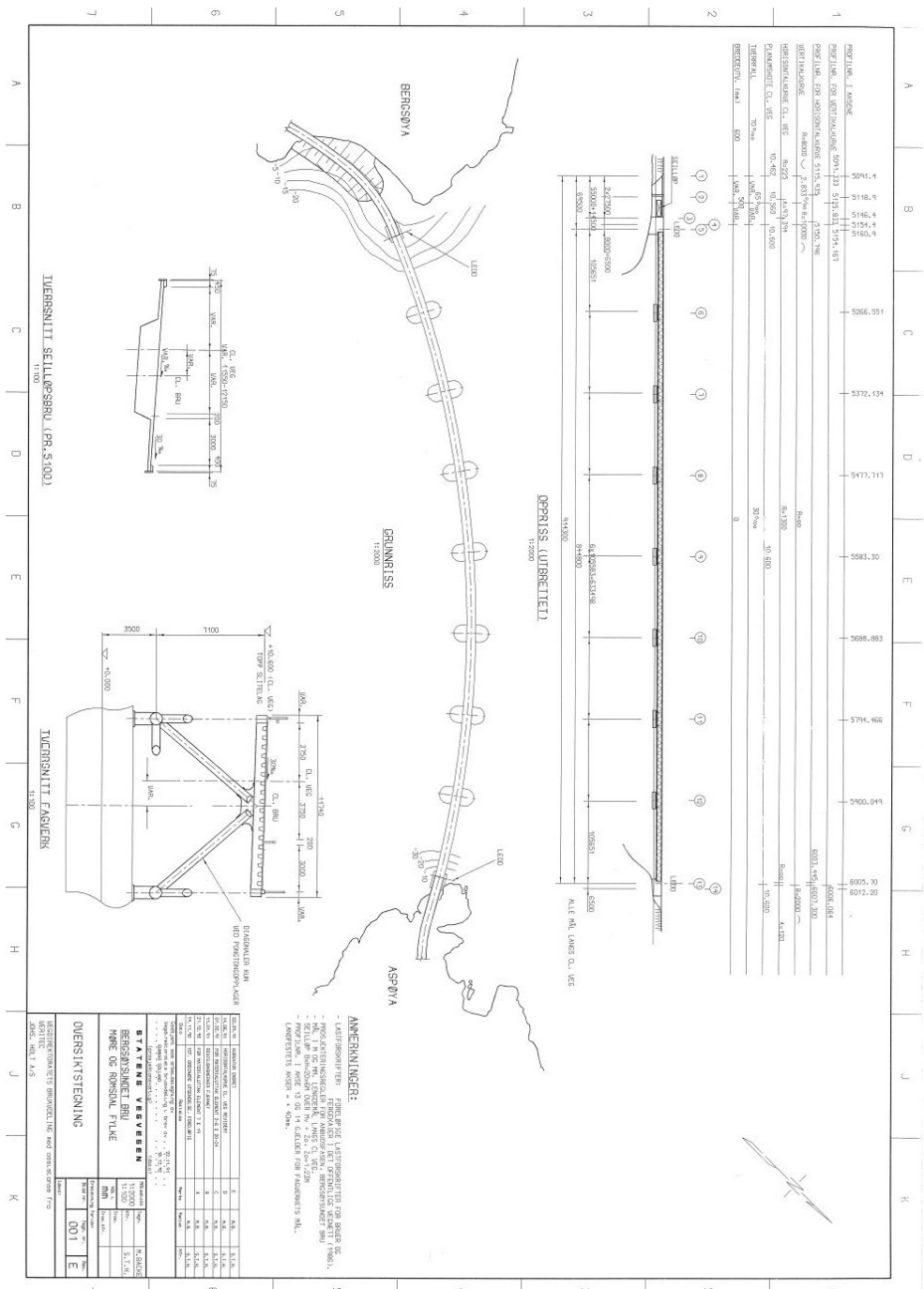
Loads developed for the frequency domain and time domain are plotted.

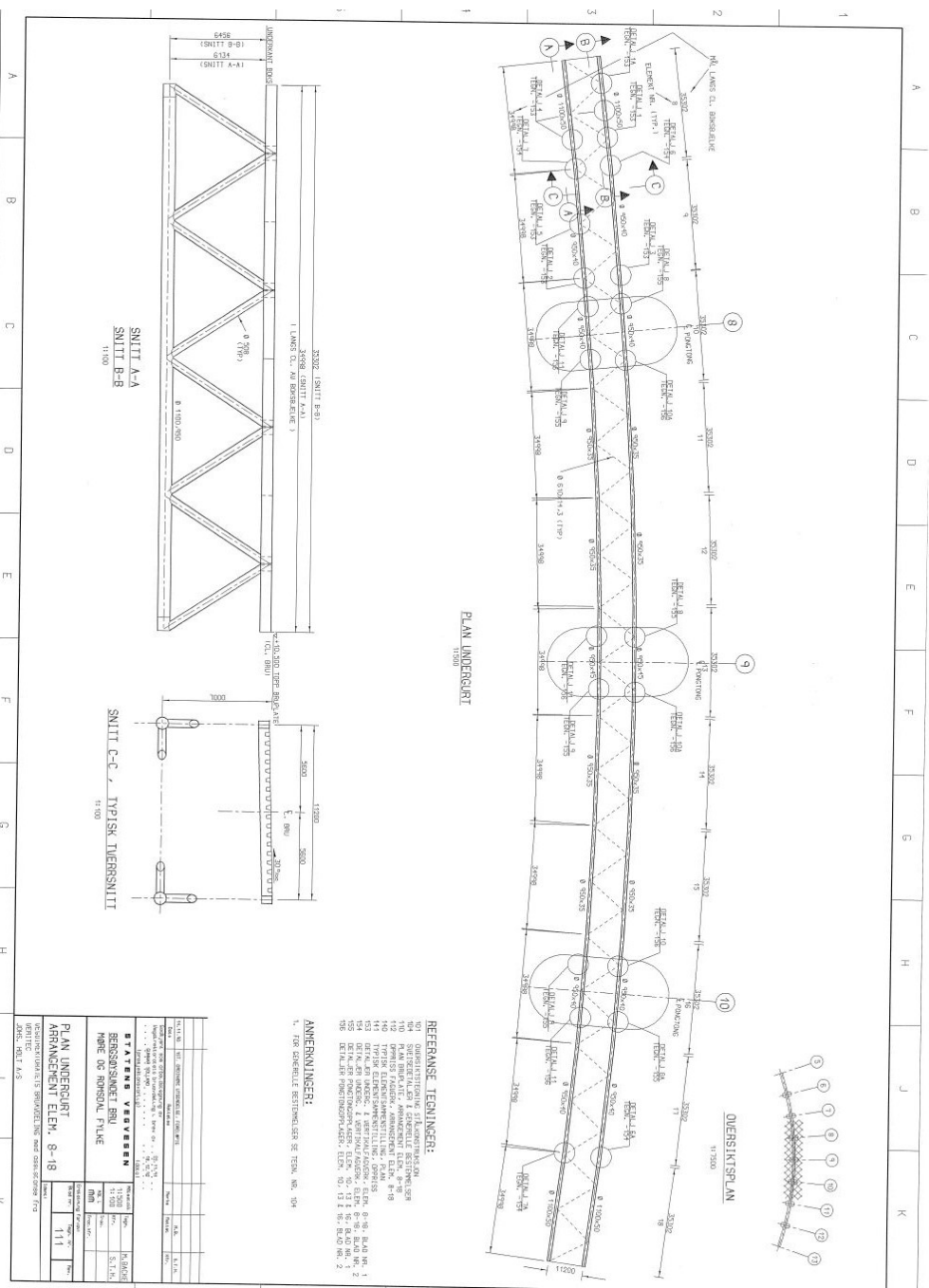


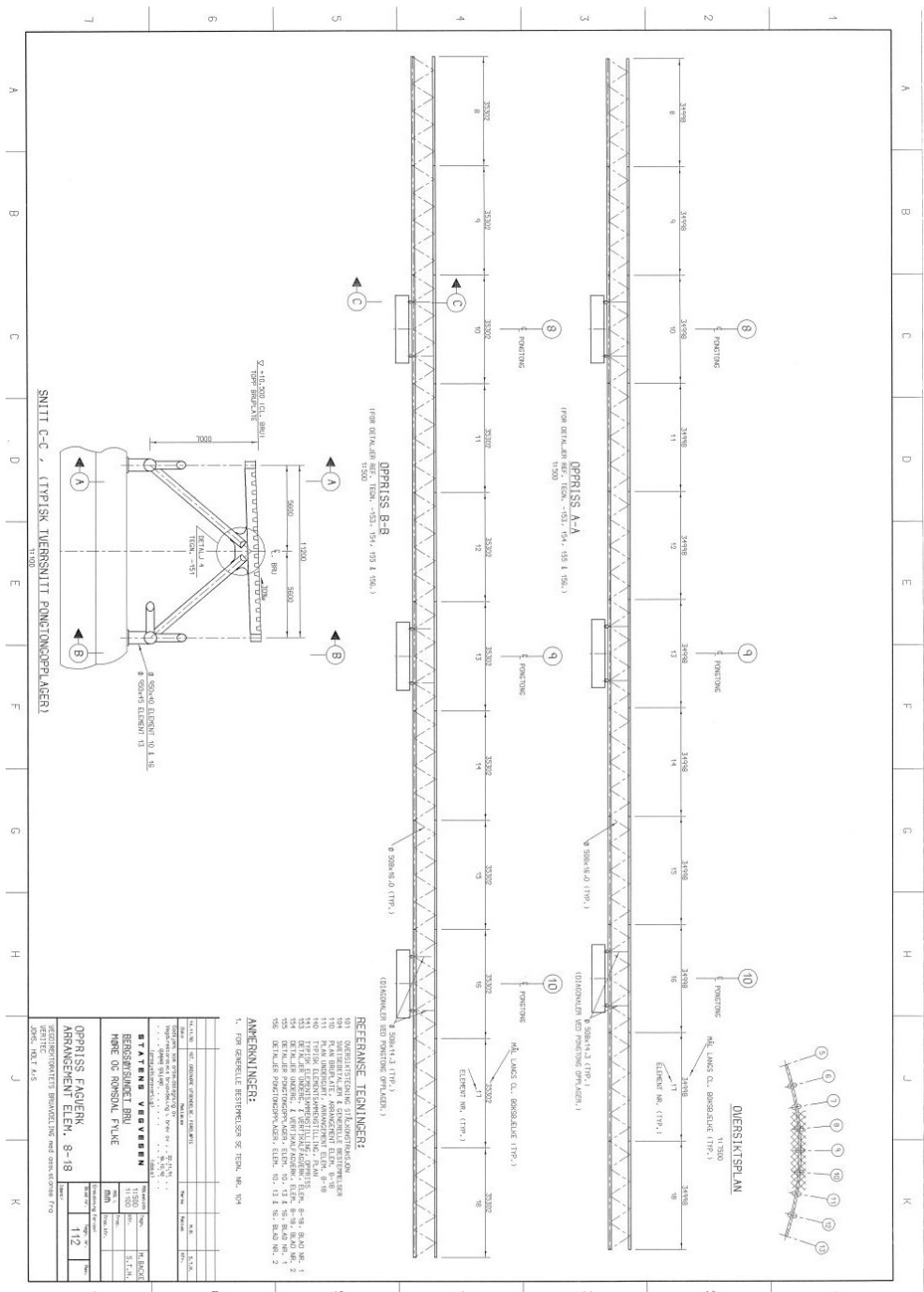
Appendix B

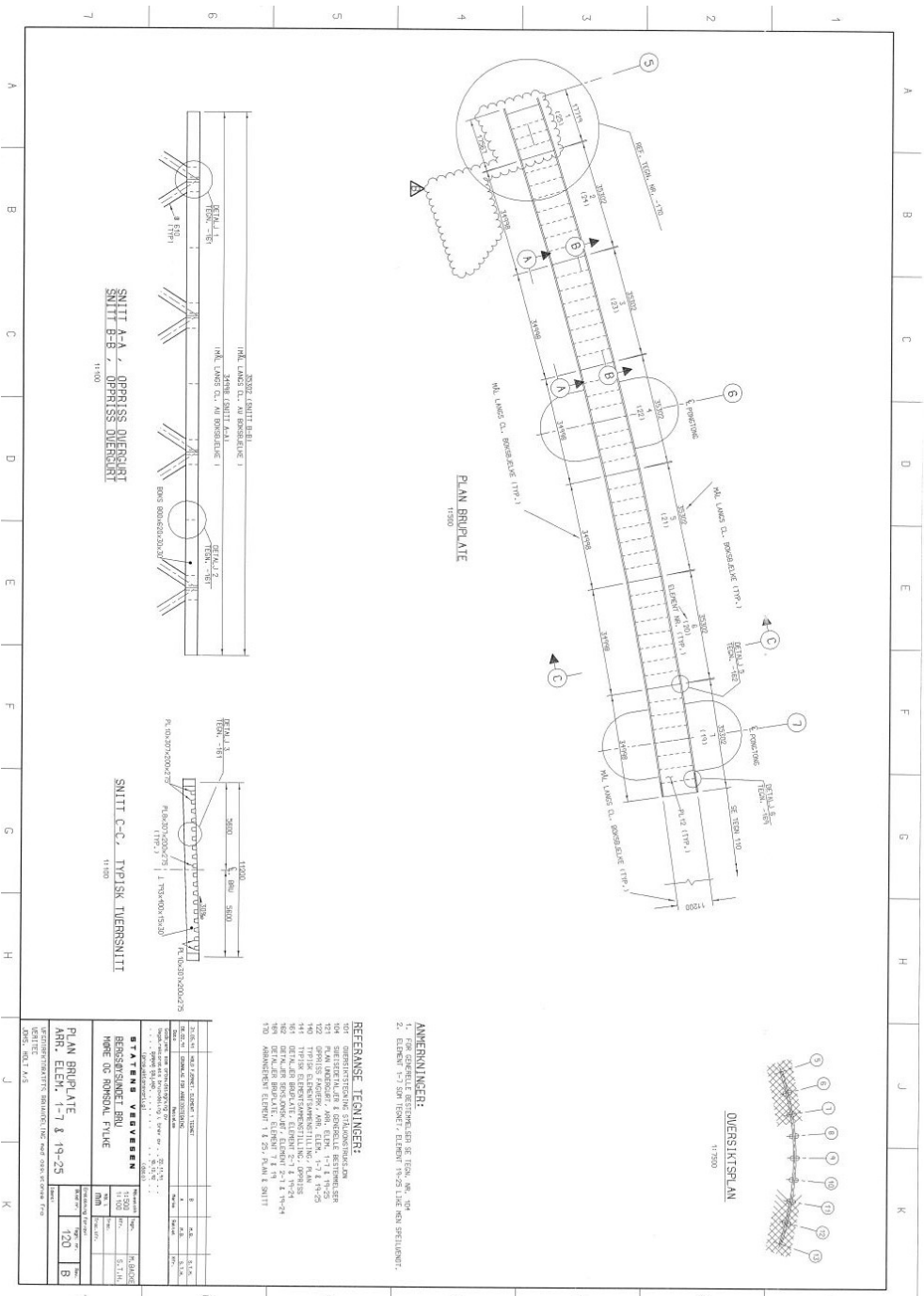
Steel structure

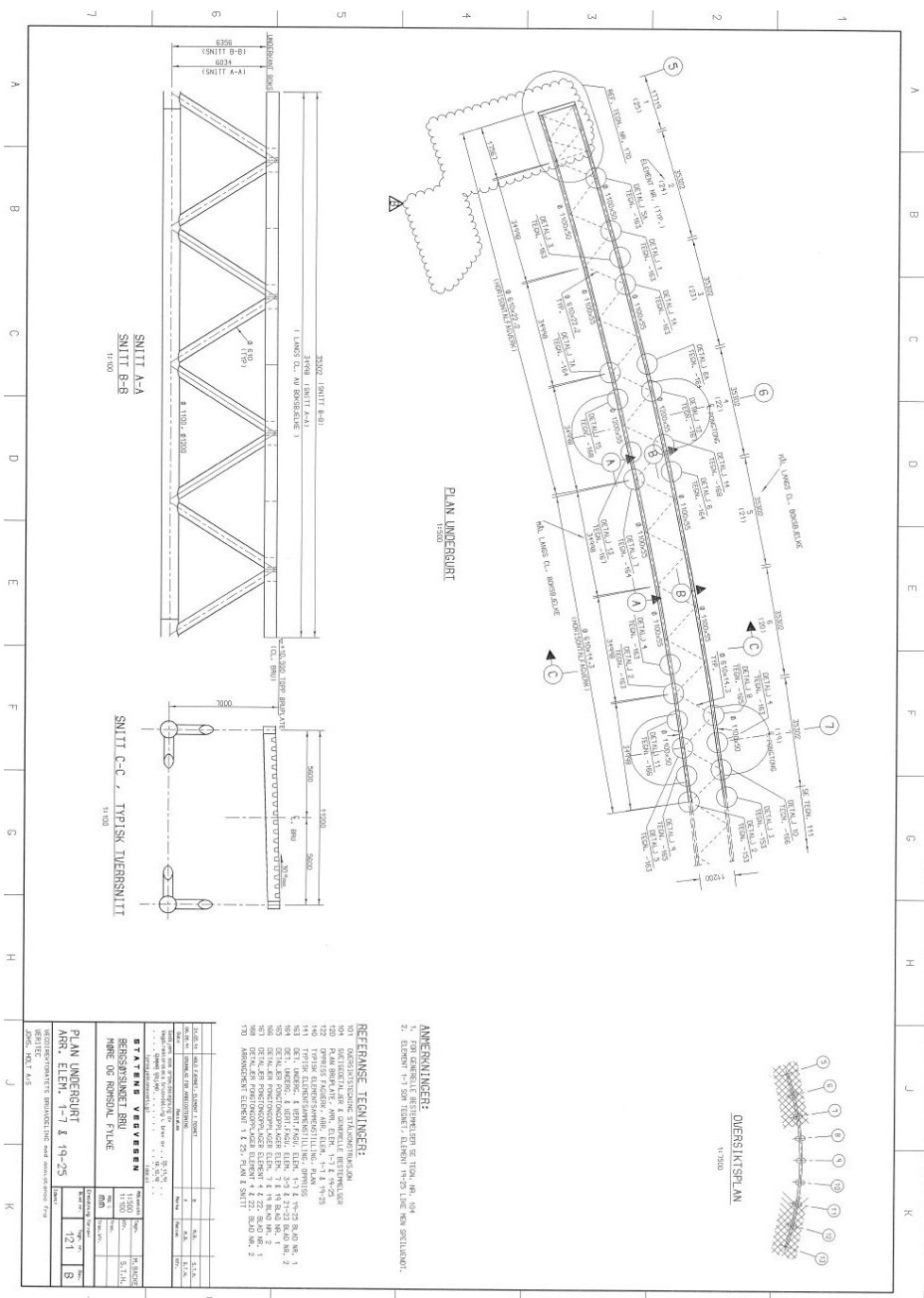
The following drawings are from The Directorate of Public Roads which describe the Bergsøysund Bridge steel structure. Only the technical drawings that were used for the modeling of the bridge are included. Notice that cross sectional information from technical drawings are used.

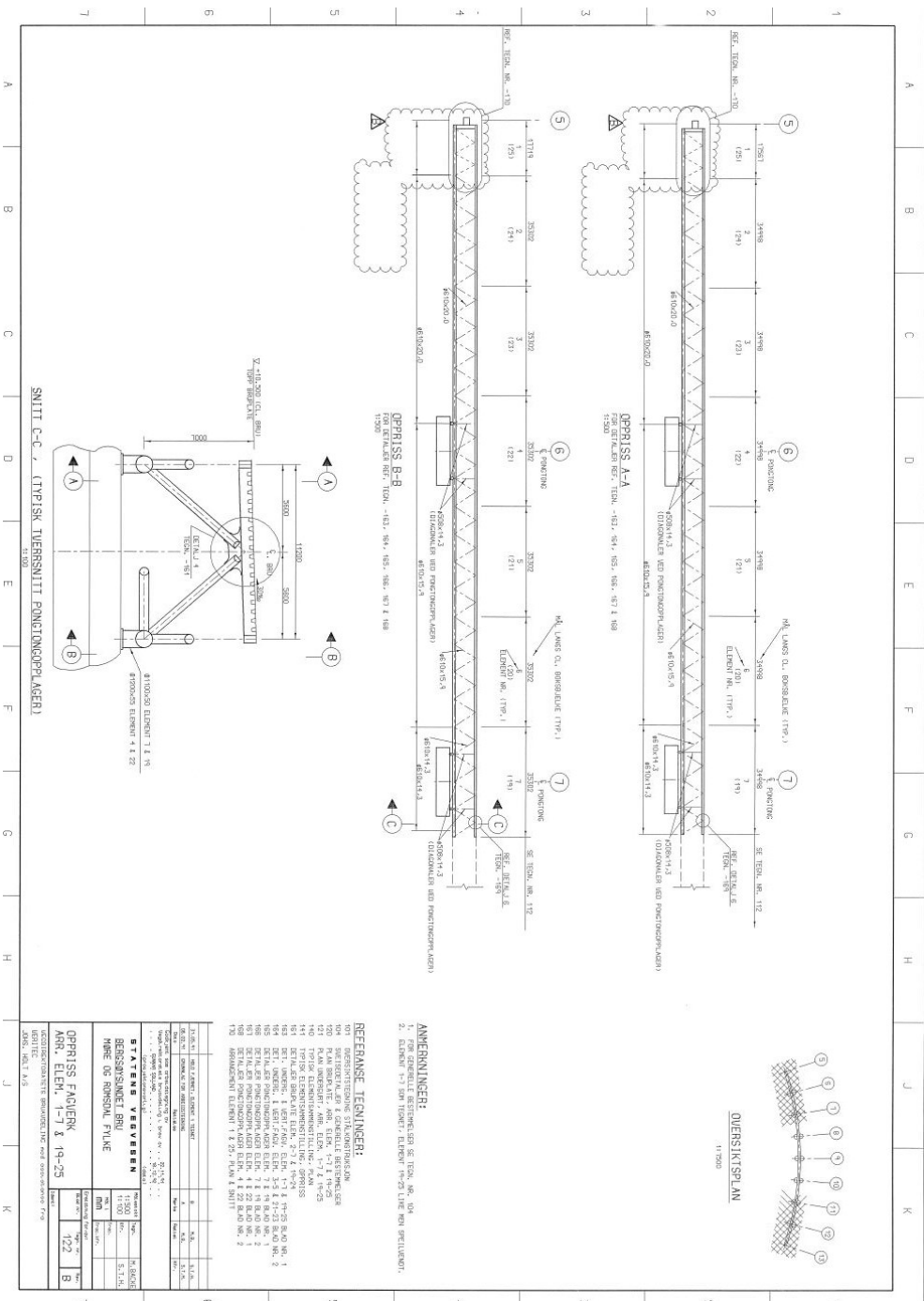


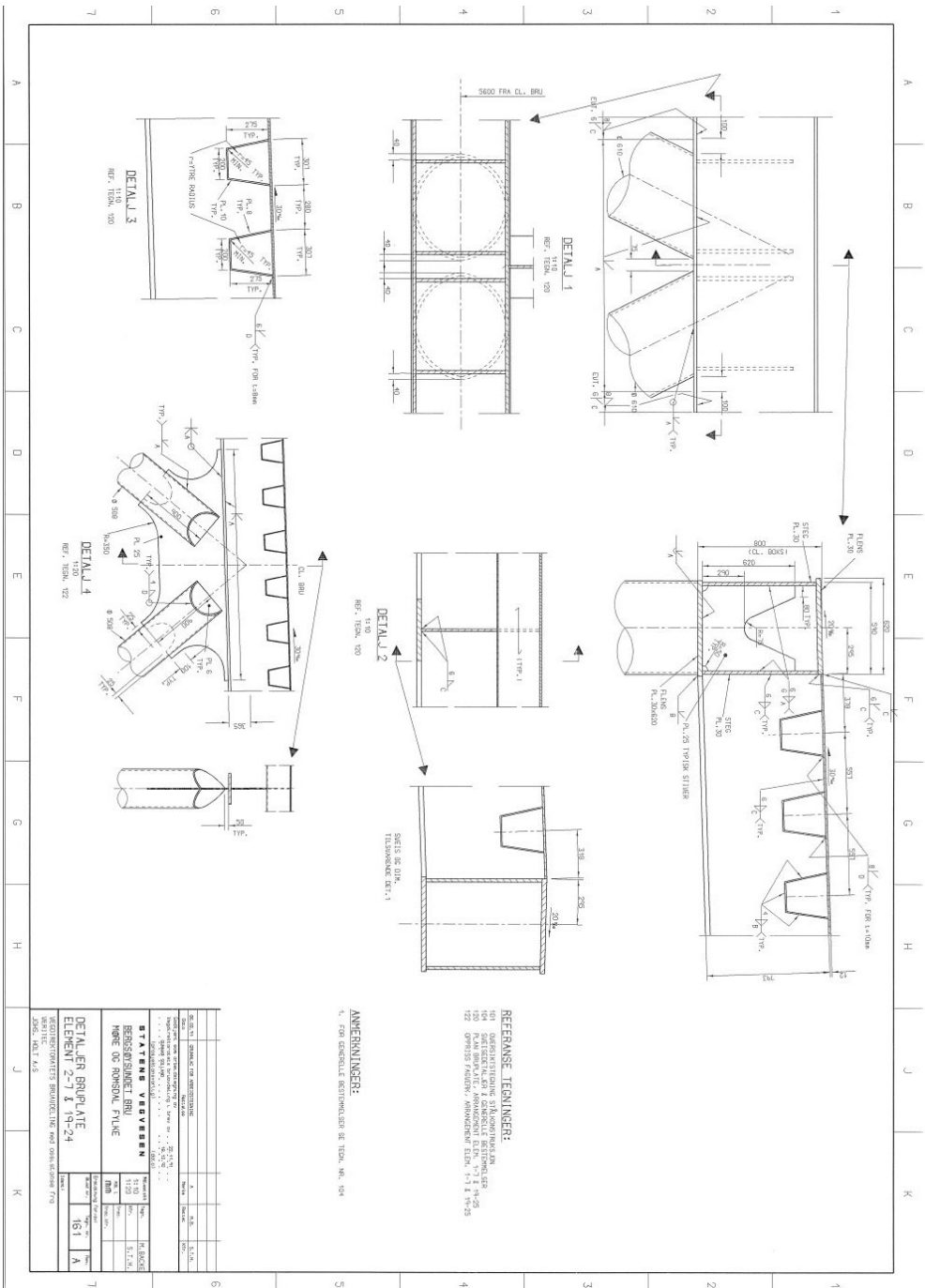


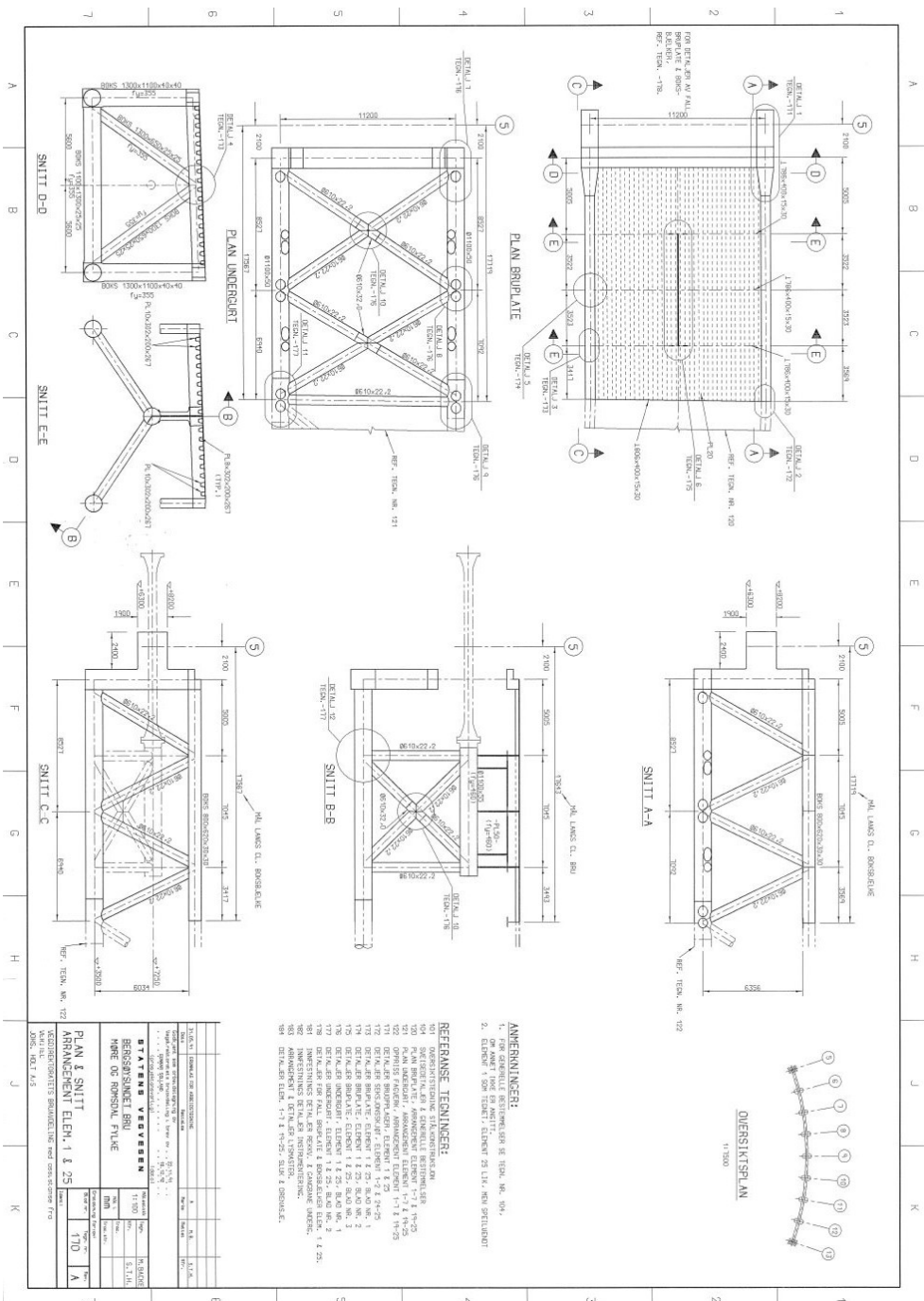


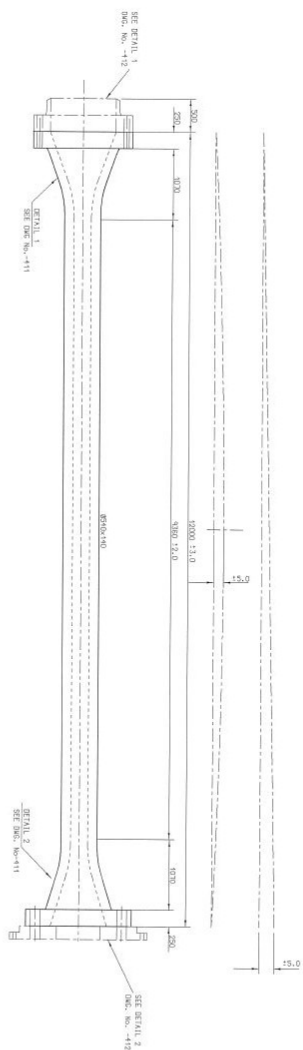












FLEXIBLE ROD (2 No. OFF)
STEEL GRADE B (fy=550MPa)

STEEL GRADE 0.7G (Y_T=550MPa)

NOTES

TOLERANCES
AS SPECIFIED ON DRAWING.

OUTSIDE SURFACE: MACHINING TO Rq 6.3, THEN
SANDBLASTED TO Sa 3.0
INSIDE SURFACES: MACHINING TO Rq 6.3

CONTACT AREAS BETWEEN FLANGES:
MACHINING TO Pd 1.6

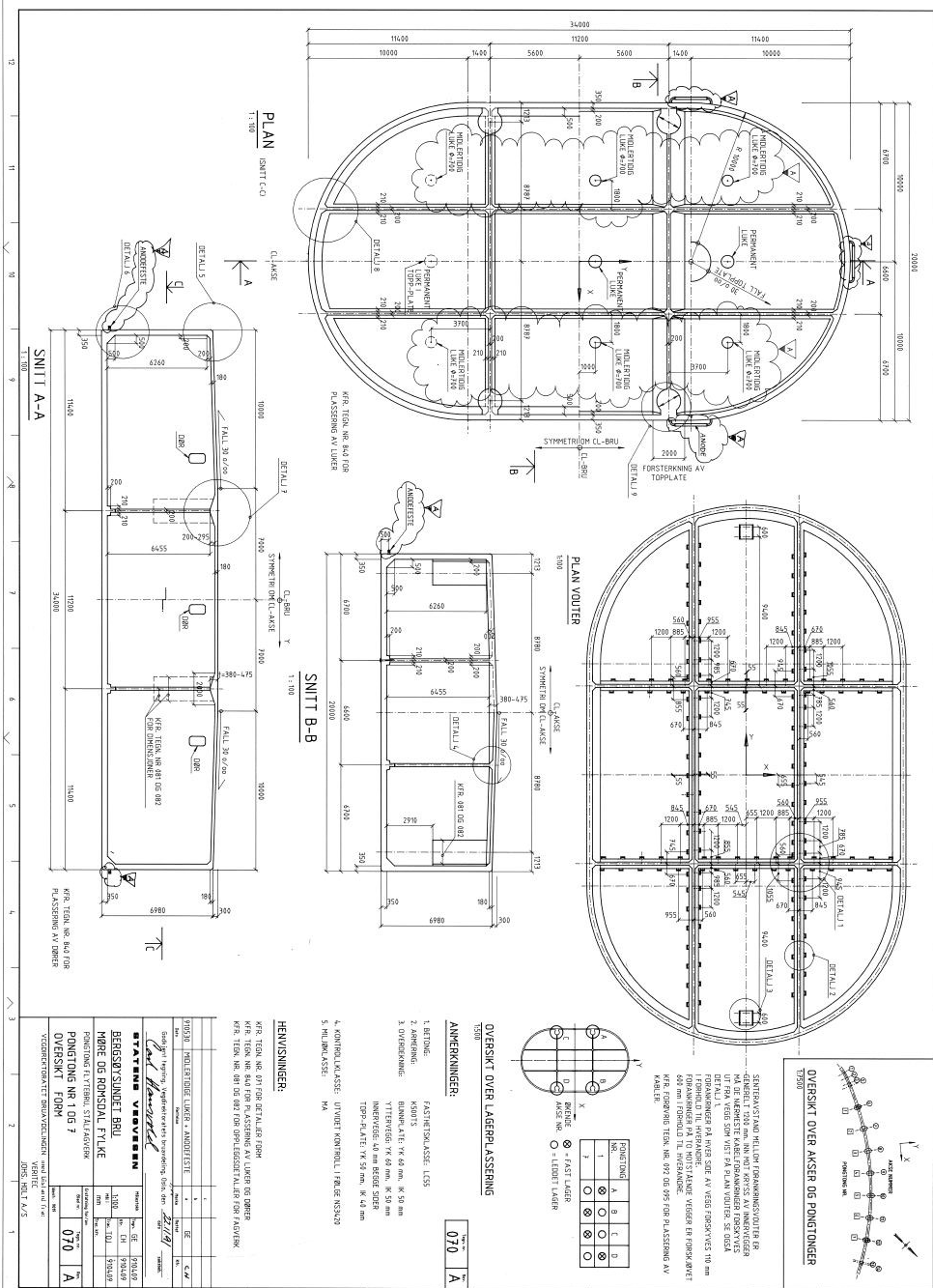
ALL DIMENSIONS IN MILLIMETRES.

[illegible]

Appendix C

Concrete structure

The following drawings are from The Directorate of Public Roads which describe the Bergsøysund Bridge concrete structure. Only the technical drawings that were used for the modeling of the bridge are included. Notice that wall thicknesses information from technical drawings are used. Drawing no. 880 describing ballast was not used in the modeling of the pontoons.



Appendix D

Matlab scripts

D.1 AddedMassAndDampingAbaqus.m

Iterative eigenvalue script to be used parallel with Abaqus eigenvalue solver developed by Ole Andre Øiseth

```

clc
clear all
close all
%% Settings
fi=0.089;
%% Load the geometry
Geometri=load('Geometri.txt');
for i=1:7
    Geometritemp(i,:)=Geometri(8-i,:); %#ok<*SAGROW>
end
Geometri=Geometritemp;
[~, pos]=sort(Geometri(:,2));
Geometri=Geometri(pos,:);

x(1,:)=Geometri(:,2)';
x(2,:)=Geometri(:,3)';
x(3,:)=Geometri(:,4)';

x0(1,1)=0;
x0(2,1)=-1300.6;
x0(3,1)=-7.8250;
%% Calculate the direction vectors for the pontoons
[e1 e2 e3]=DirVectors(x,x0); %#ok<*NCOMMA>
%% Load Wadam results
[ADD_MASS1, ADD_DAMP1, HYD_KK1,T1,~]=Import('Pontoon1and7.txt');
[ADD_MASS2, ADD_DAMP2, HYD_KK2,T2,~]=Import('Pontoon2to6.txt');
%% Build matrices
ADD_MASSi1=zeros(6,6);
ADD_DAMPi1=zeros(6,6);
ADD_MASSi2=zeros(6,6);
ADD_DAMPi2=zeros(6,6);

for n=1:6
    for m=1:6
        ADD_MASSi1(n,m)=interp1(T1,squeeze(ADD_MASS1(n,m,:)),1/fi);
        ADD_DAMPi1(n,m)=interp1(T1,squeeze(ADD_DAMP1(n,m,:)),1/fi);
        ADD_MASSi2(n,m)=interp1(T2,squeeze(ADD_MASS2(n,m,:)),1/fi);
        ADD_DAMPi2(n,m)=interp1(T2,squeeze(ADD_DAMP2(n,m,:)),1/fi);
    end
end

```

```

for n=2:size(e1,2)-1

    TT=[e1(:,n)'; e2(:,n)'; e3(:,n)'];
    TT=blkdiag(TT,TT);
    ADD_MASS_ABAQUS(:, :, n)=TT'*ADD_MASSi1*TT;
    ADD_STIFFNESS_ABAQUS(:, :, n)=TT'*HYD_KK1*TT;
    ADD_DAMP_ABAQUS(:, :, n)=TT'*ADD_DAMPi1*TT;

end

for n=1:6:7

    TT=[e1(:,n)'; e2(:,n)'; e3(:,n)'];
    TT=blkdiag(TT,TT);
    ADD_MASS_ABAQUS(:, :, n)=TT'*ADD_MASSi2*TT;
    ADD_STIFFNESS_ABAQUS(:, :, n)=TT'*HYD_KK2*TT;
    ADD_DAMP_ABAQUS(:, :, n)=TT'*ADD_DAMPi2*TT;

end

%% The nodes where mass and stiffness will be added
Nodes=Geometri(:,1)';

%% Create an input file that can
%be Included just before END PART in the edit keywords

fw = fopen('PointMassFreq.inp','wt');
for EL=1:length(Nodes)
    fprintf(fw,['PONTOON NUMBER ' num2str(EL) '\n']);
    fprintf(fw,['USER ELEMENT, LINEAR, NODES=1, UNSYM, TYPE=U'
               num2str(EL) '00' '\n']);
    fprintf(fw,['1, 2, 3, 4, 5, 6' '\n']);
    fprintf(fw,['*MATRIX, TYPE=MASS' '\n']);
    teller=0;
    for n=1:size(ADD_MASS_ABAQUS,1)
        for m=1:size(ADD_MASS_ABAQUS,1) ...
    end

    fprintf(fw,['*MATRIX, TYPE=STIFFNESS' '\n']);
    teller=0;
    for n=1:size(ADD_MASS_ABAQUS,1)
        for m=1:size(ADD_MASS_ABAQUS,1) ...
    end

    fprintf(fw,['*ELEMENT, TYPE=U' num2str(EL) '00, ELSET=PONTONG'
               num2str(EL) '\n']);
    fprintf(fw,['800' num2str(EL) ' ', ' num2str(Nodes(1,EL)) '\n']);
    fprintf(fw,['* UEL PROPERTY, ELSET=PONTONG' num2str(EL) '\n']);
end
fclose(fw);

```

Appendix E

Wadam extracts

Static data extracted from Wadam-software.

E.0.1 General

h

```
*****      *****      *****      *****      ** *** *****
*****      *****      *****      *****      *****
**   **   **   **   **   **   **   **   **   **   **   **
**   **   **   **   **   **   **   **   **   **   **   **
*****      *****      *****      *****      **   **   **
*****      *****      *****      *****      **   **   **
**   **   **   **   **   **   **   **   **   **   **   **
**   **   **   **   **   **   **   **   **   **   **   **
*****      *****      *****      *****      **   **   **
*****      *****      *****      *****      **   **   **
```

```
*****
*****
**
**
**   *   *   *****   *****   *   *   **
**   *   *   *   *   *   *   *   *   *   **
**   *   *   *   *   *   *   *   *   *   **
**   *   *   *****   *   *****   *   *   **
**   *   *   *   *   *   *   *   *   *   **
**   *   *   *   *   *   *   *   *   *   **
**   *   *   *   *   *   *   *   *   *   **
**   *   *   *   *   *****   *   *   *   **
**
**
**   Wave Analysis by Diffraction and Morison Theory   **
**
**
*****
*****
```

Marketing and Support by DNV Software

Program id	: 8.2-02	Computer	: 586
Release date	: 6-APR-2011	Impl. update	:
Access time	: 03-MAY-2013 10:32:14	Operating system	: Win NT 6.2 [9200]
User id	: Sindre Hermstad	CPU id	: 1181277782
		Installation	: , SINDRESPC

Copyright DET NORSKE VERITAS AS, P.O.Box 300, N-1322 Hovik, Norway

Sifttool version 8.3-07 29-NOV-2010

INDICES:

1	INDICATES	SURGE	AND	X-COMPONENT OF FORCE
2	INDICATES	SWAY	AND	Y-COMPONENT OF FORCE
3	INDICATES	HEAVE	AND	Z-COMPONENT OF FORCE
4	INDICATES	ROLL	AND	ROLL MOMENT
5	INDICATES	PITCH	AND	PITCH MOMENT
6	INDICATES	YAW	AND	YAW MOMENT

1

COMMENTS ON SOME RESULTS:

ALL RESULTS IN THIS SECTION (4.) ARE NONDIMENSIONALIZED AS DESCRIBED ABOVE

TOTAL RESTORING, ADDED MASS AND EXCITING FORCES/MOMENTS	ARE THE SUMS OF RESULTS FOR THE PANEL MODEL AND THE MORISON MODEL. IF A DUAL MODEL IS DEFINED THE RESULTS FOR THE MORISON PART OF THE DUAL MODEL ARE SUBTRACTED.
TOTAL DAMPING	IS THE SUM OF POTENTIAL DAMPING AND VISCOUS DRAG FROM MORISON'S THEORY.
MEAN DRIFT FORCES	INCLUDE THE EFFECTS OF MOTION.
SUM OF DISTRIBUTED LOADS	IS A SUM OF ALL DISTRIBUTED LOADS CALCULATED INCLUDING FLUCTUATING HYDROSTATIC FORCES DUE TO MOTION, AND INERTIA FORCES/MOMENTS FROM BODY ACCELERATIONS. IF EXACTLY CALCULATED, THIS SUM SHOULD BE ZERO FOR A FLOATING STRUCTURE.
LOAD DISTRIBUTION ON THE	MORISON MODEL INCLUDES ALL DISTRIBUTED LOADS CALCULATED INCLUDING FLUCTUATING HYDROSTATIC FORCES DUE TO MOTION. IF A DUAL MODEL IS DEFINED THE MORISON LOADS DUE TO ADDED MASS ARE REPLACED BY THE PRESSURES FROM PANELS COUPLED TO EACH SUBELEMENT. IF DISTRIBUTED MASS IS GIVEN INERTIA FORCES/MOMENTS FROM BODY ACCELERATIONS ARE INCLUDED.
PRESSURE DISTRIBUTION	INCLUDE PRESSURES FROM BOTH THE RADIATION- AND DIFFRACTION VELOCITY POTENTIALS. NO FLUCTUATING HYDROSTATIC PRESSURES DUE TO MOTION ARE INCLUDED.
FLUID PRESSURES AND FLUID VELOCITY	INCLUDE THE EFFECT OF MOTION.
SECTIONAL LOADS ON THE PANEL MODEL	INCLUDE FLUCTUATING HYDROSTATIC FORCES DUE TO MOTION, AND INERTIA FORCES/MOMENTS FROM BODY ACCELERATIONS. (MASS DISTRIBUTION FROM THE MASS MODEL).
MORISON MODEL	INCLUDE FLUCTUATING HYDROSTATIC FORCES DUE TO MOTION, AND INERTIA FORCES/MOMENTS FROM BODY ACCELERATIONS. (MASS FROM THE DISTRIBUTED MASS ON THE MORISON MODEL).

E.0.2 Pontoon one and seven

1

4. PRESENTATION OF RESULTS =====

4.1 EXPLANATION OF THE RESULTS -----

NON-DIMENSIONAL DEFINITIONS: -----

		I=1-3 J=1-3	I=1-3 I=4-6 J=4-6 J=1-3	I=4-6 J=4-6
MASS INERTIA MATRIX	NON-DIMENSIONALIZED BY:	RO*VOL,	RO*VOL*L	RO*VOL*L*L
ADDED MASS MATRIX	NON-DIMENSIONALIZED BY:	RO*VOL,	RO*VOL*L	RO*VOL*L*L
DAMPING MATRIX	NON-DIMENSIONALIZED BY:	RO*VOL*SQRT(G/L)	RO*VOL*SQRT(G*L)	RO*VOL*L*SQRT(G*L)
RESTORING MATRICES	NON-DIMENSIONALIZED BY:	RO*VOL*G/L,	RO*VOL*G	RO*VOL*G*L
		I=1-3	I=4-6	
EXCITING FORCES	NON-DIMENSIONALIZED BY:	RO*VOL*G*WA/L	RO*VOL*G*WA	
MOTIONS	NON-DIMENSIONALIZED BY:	WA	WA/L	(4-6 IN RADIANs)
SECTIONAL LOADS	NON-DIMENSIONALIZED BY:	RO*VOL*G*WA/L	RO*VOL*G*WA	
DRIFT FORCES	NON-DIMENSIONALIZED BY:	RO*G*L*WA*WA	RO*G*L*L*WA*WA	
		I=1-3		
PRESSURES	NON-DIMENSIONALIZED BY:	RO*G*WA		
VELOCITIES	NON-DIMENSIONALIZED BY:	WA*SQRT(G/L)		
ACCELERATIONS	NON-DIMENSIONALIZED BY:	WA*G/L		
2ND-ORDER FORCES	NON-DIMENSIONALIZED BY:	RO*G*L	RO*G*L*L	
2ND-ORDER PRESSURE	NON-DIMENSIONALIZED BY:	RO*G/L		
		I=1,2	I=6	
WAVE DRIFT DAMPING MATRIX	NON-DIMENSIONALIZED BY:	RO*G*L*WA*WA	RO*G*L*L*WA*WA	

NON-DIMENSIONALIZING FACTORS: -----

THE OUTPUT IS NON-DIMENSIONALIZED USING -

RO = DENSITY OF THE FLUID
G = ACCELERATION OF GRAVITY
L = CHARACTERISTIC LENGTH, AS GIVEN IN THE INPUT
VOL = DISPLACED VOLUME OF BODY 1 (COMBINED MORISON AND PANEL MODEL)
WA = WAVE AMPLITUDE OF THE INCOMING WAVES

RO = 0.1025E+04
G = 0.9807E+01
VOL = 0.2715E+04
L = 0.1000E+03
WA = 1.0 (IF NOT GIVEN AS INPUT)

4.2 STATIC RESULTS

MASS INERTIA COEFFICIENT MATRIX

	1	2	3	4	5	6
1	5.0021E-01	0.0000E+00	0.0000E+00	0.0000E+00	-1.9656E-02	-1.5918E-05
2	0.0000E+00	5.0021E-01	0.0000E+00	1.9656E-02	0.0000E+00	8.7408E-05
3	0.0000E+00	0.0000E+00	5.0021E-01	1.5918E-05	-8.7408E-05	0.0000E+00
4	0.0000E+00	1.9656E-02	1.5918E-05	3.0822E-03	8.3848E-08	3.3694E-06
5	-1.9656E-02	0.0000E+00	-8.7408E-05	8.3848E-08	5.8646E-03	6.5071E-07
6	-1.5918E-05	8.7408E-05	0.0000E+00	3.3694E-06	6.5071E-07	6.6348E-03

HYDROSTATIC RESTORING COEFFICIENT MATRIX

	1	2	3	4	5	6
1	0.0000E+00	0.0000E+00	0.0000E+00	0.0000E+00	0.0000E+00	0.0000E+00
2	0.0000E+00	0.0000E+00	0.0000E+00	0.0000E+00	0.0000E+00	0.0000E+00
3	0.0000E+00	0.0000E+00	2.1869E+01	6.9368E-04	-3.9716E-03	0.0000E+00
4	0.0000E+00	0.0000E+00	6.9368E-04	4.8006E-02	2.1833E-06	-8.6774E-05
5	0.0000E+00	0.0000E+00	-3.9716E-03	2.1833E-06	1.5575E-01	-1.6974E-05
6	0.0000E+00	0.0000E+00	0.0000E+00	0.0000E+00	0.0000E+00	0.0000E+00

E.0.3 Pontoon two to six

NON-DIMENSIONALIZING FACTORS:

THE OUTPUT IS NON-DIMENSIONALIZED USING -

RO = DENSITY OF THE FLUID
G = ACCELERATION OF GRAVITY
L = CHARACTERISTIC LENGTH, AS GIVEN IN THE INPUT
VOL = DISPLACED VOLUME OF BODY 1 (COMBINED MORISON AND PANEL MODEL)
WA = WAVE AMPLITUDE OF THE INCOMING WAVES

RO = 0.1025E+04
G = 0.9807E+01
VOL = 0.2197E+04
L = 0.1000E+03
WA = 1.0 (IF NOT GIVEN AS INPUT)

RESULT-REFERENCE POINT:

THE OUTPUT OF GLOBAL RESULTS ARE GIVEN IN
THE USER-SPECIFIED POINT (X,Y,Z) IN THE
GLOBAL SYSTEM:

X = 0.0000E+00
Y = 0.0000E+00
Z = 0.2370E+01

INDICES:

1	INDICATES	SURGE	AND	X-COMPONENT OF FORCE
2	INDICATES	SWAY	AND	Y-COMPONENT OF FORCE
3	INDICATES	HEAVE	AND	Z-COMPONENT OF FORCE
4	INDICATES	ROLL	AND	ROLL MOMENT
5	INDICATES	PITCH	AND	PITCH MOMENT
6	INDICATES	YAW	AND	YAW MOMENT

4.2 STATIC RESULTS

MASS INERTIA COEFFICIENT MATRIX

	1	2	3	4	5	6
1	5.6490E-01	0.0000E+00	0.0000E+00	0.0000E+00	-1.9866E-02	4.0870E-13
2	0.0000E+00	5.6490E-01	0.0000E+00	1.9866E-02	0.0000E+00	3.4138E-10
3	0.0000E+00	0.0000E+00	5.6490E-01	-4.0870E-13	-3.4138E-10	0.0000E+00
4	0.0000E+00	1.9866E-02	-4.0870E-13	3.1797E-03	-7.8000E-14	1.0362E-11
5	-1.9866E-02	0.0000E+00	-3.4138E-10	-7.8000E-14	6.3038E-03	-1.2989E-11
6	4.0870E-13	3.4138E-10	0.0000E+00	1.0362E-11	-1.2989E-11	7.4223E-03

HYDROSTATIC RESTORING COEFFICIENT MATRIX

	1	2	3	4	5	6
1	0.0000E+00	0.0000E+00	0.0000E+00	0.0000E+00	0.0000E+00	0.0000E+00
2	0.0000E+00	0.0000E+00	0.0000E+00	0.0000E+00	0.0000E+00	0.0000E+00
3	0.0000E+00	0.0000E+00	2.7027E+01	-1.7238E-07	-4.0495E-07	0.0000E+00
4	0.0000E+00	0.0000E+00	-1.7238E-07	6.6111E-02	-1.3813E-08	3.5184E-08
5	0.0000E+00	0.0000E+00	-4.0495E-07	-1.3813E-08	1.9922E-01	9.4248E-09
6	0.0000E+00	0.0000E+00	0.0000E+00	0.0000E+00	0.0000E+00	0.0000E+00

E.1 Scripts used in Abaqus

E.1.1 Pontoonmass.inp

A script that includes mass from the pontoons.

```

** *****PONTON NUMBER 1*****
*USER ELEMENT, LINEAR, NODES=1, UNSYM, TYPE=U1000
1, 2, 3, 4, 5, 6
*MATRIX, TYPE=MASS
1392022.0000,      0.0000,      0.0000,      -0.0000
-5470019.0000,    0.0000
-0.0000,      1392022.0000,      0.0000,      5470019.0000
-0.0000,      0.0000
0.0000,      0.0000,      1392022.0000,      0.0000
0.0000,      0.0000
0.0000,      5470019.0000,      0.0000,      162848785.1291
-5236002.8658,    0.0000
-5470019.0000,    0.0000,      0.0000,      -5236002.8658
86129474.8709,    0.0000
0.0000,      0.0000,      0.0000,      0.0000
0.0000,      184638190.0000
*ELEMENT, TYPE=U1000, ELSET=PONTONG1
8021, 791
* UEL PROPERTY, ALPHA=0.0045279, BETA=0.0051766, ELSET=PONTONG1
** *****PONTON NUMBER 2*****
*USER ELEMENT, LINEAR, NODES=1, UNSYM, TYPE=U2000
1, 2, 3, 4, 5, 6
*MATRIX, TYPE=MASS
1272112.0000,      0.0000,      0.0000,      -0.0000
-4473674.0000,    0.0000
0.0000,      1272112.0000,      0.0000,      4473674.0000
-0.0000,      0.0000
0.0000,      0.0000,      1272112.0000,      0.0000
0.0000,      0.0000
0.0000,      4473674.0000,      0.0000,      140400630.8694
-10347066.3080,    0.0000
-4473674.0000,    0.0000,      0.0000,      -10347066.3080
73160676.1306,    0.0000
0.0000,      0.0000,      0.0000,      0.0000
0.0000,      167144629.0000
*ELEMENT, TYPE=U2000, ELSET=PONTONG2
8022, 786
* UEL PROPERTY, ALPHA=0.0045279, BETA=0.0051766, ELSET=PONTONG2
** *****PONTON NUMBER 3*****
*USER ELEMENT, LINEAR, NODES=1, UNSYM, TYPE=U3000
1, 2, 3, 4, 5, 6
*MATRIX, TYPE=MASS
1272112.0000,      0.0000,      0.0000,      0.0000
-4473674.0000,    0.0000
0.0000,      1272112.0000,      0.0000,      4473674.0000
0.0000,      0.0000
0.0000,      0.0000,      1272112.0000,      0.0000
0.0000,      0.0000
0.0000,      4473674.0000,      0.0000,      138278677.0536
-15660114.0391,    0.0000
-4473674.0000,    0.0000,      0.0000,      -15660114.0391
75282629.9464,    0.0000
0.0000,      0.0000,      0.0000,      0.0000
0.0000,      167144629.0000
*ELEMENT, TYPE=U3000, ELSET=PONTONG3
8023, 781
* UEL PROPERTY, ALPHA=0.0045279, BETA=0.0051766, ELSET=PONTONG3

```